

# O<sub>3</sub>-Type Cathodes for Sodium-Ion Batteries: Recent Advancements and Future Perspectives

Xinghan Li,<sup>[a]</sup> Yameng Fan,<sup>\*[a]</sup> Bernt Johannessen,<sup>[a, b]</sup> Xun Xu,<sup>[a]</sup> Khay Wai See,<sup>[a]</sup> and Wei Kong Pang<sup>\*[a]</sup>

Over recent decades, rapid advancements in energy technology have transformed human life. Lithium-ion batteries (LIBs) have played a pivotal role nevertheless concerns about limited lithium resources and price fluctuations underscore the need for sustainability. Sodium-ion batteries (SIBs), operating on principles akin to LIBs, have emerged as promising candidates for rechargeable batteries in the next generation of energy storage systems, primarily due to their cost-effectiveness and sustainable attributes. Analogous to LIBs, the cathode in SIBs assumes a critical role in dictating the electrochemical performance of the battery. Therefore, the research and development of cathode materials for SIBs take on paramount significance. O<sub>3</sub>-type SIB cathodes, inspired by the successful O<sub>3</sub>-type LIB

cathodes (e.g., LiCoO<sub>2</sub> and NMC variants), hold promise for commercial applications. This comprehensive overview offers an in-depth exploration of various unary-metal oxide cathode materials characterized by an O<sub>3</sub>-layered structure. Subsequently, nickel (Ni), manganese (Mn), and Ni/Mn-based O<sub>3</sub> cathode materials are conducted a comprehensive study, assessing the effects of element substitution and doping on capacity, phase transitions, and cycle life. In light of the current challenges, advancing SIB cathode materials of future directions will propose, addressing key considerations in the pursuit of enhanced performance and sustainable energy storage solutions.

## 1. Introduction

The globe is currently confronted with numerous daunting issues of energy and the environment. As the demand of human development for diverse energy resources escalates, the imperative shift from conventional fossil fuels to clean energy alternatives like solar, wind, and tidal power gains paramount significance,<sup>[1]</sup> which led to a growing need for advanced technology in the storage of intermittent and localized energy. Driven by the global imperative of sustainable development, there is an urgent requirement to develop high-stability, high-safety, high-power, and high-energy storage systems.<sup>[2,3]</sup> Accordingly, rechargeable batteries have emerged as highly competitive technologies in the field of Energy Storage Systems (ESSs) because of their exceptional conversion efficiency and environmental friendliness. They play an increasingly pivotal role in energy discharge during peak periods and energy storage during off-peak periods.<sup>[4–6]</sup> Since its inception in the early 1970s and subsequent commercialization by Sony Corp in 1992,

lithium-ion batteries (LIBs) have experienced remarkable advancements regarding energy density, cycle life, cost, capacity, and safety, igniting a revolutionary transformation in commercial energy storage.<sup>[7–10]</sup> Over the ensuing decades, LIBs have gradually permeated the realm of electric vehicles (EVs), portable electronic devices, and various energy storage systems, profoundly enhancing human productivity and quality of life.<sup>[11–14]</sup> Presently, rechargeable LIBs are heralded as a pivotal technology for mitigating carbon dioxide emissions across the transportation, power, and industrial sectors, while simultaneously facilitating the progression toward low-carbon or zero-carbon societies.<sup>[15,16]</sup> Notwithstanding its extensive dispersion within the Earth's lithosphere and hydrosphere, lithium (Li) is not deemed an abundant element. Scientific investigations propose that the average mass fraction of Li is a mere 20 parts-per-million (ppm) in the crust of Earth, as shown in Figure 1a.<sup>[17]</sup> Additionally, as a result of the burgeoning demand for Li resources in recent years, which soared to a staggering consumption rate of 49,000 tons per annum in 2019,<sup>[18]</sup> coupled with a current annual growth rate of 5%, the lithium reserves in the Earth's crust can only endure for a maximum of 65 years.<sup>[19]</sup> This is incongruent with the strategic imperatives for sustainable development outlined by the United Nations. Hence, the availability and prices of Li resources have emerged as pivotal apprehensions in contemporary times.<sup>[20,21]</sup> Furthermore, LIB manufacturing significantly depends on imported Li due to the disparate distribution of Li resources across various regions. This constraint hinders its extensive implementation in large-scale ESSs.<sup>[22]</sup>

In contrast, Sodium (Na) resources are plentiful and widely distributed, with an abundance exceeding that of Li by 1,180 times, making it the 4<sup>th</sup> most abundant element on Earth.

[a] X. Li, Y. Fan, Dr. B. Johannessen, Dr. X. Xu, Dr. K. W. See, Dr. W. K. Pang  
Institute for Superconducting & Electronic Materials, University of Wollongong, NSW 2500, Australia  
E-mail: yfan@uow.edu.au  
wkpang@uow.edu.au

[b] Dr. B. Johannessen  
Australian Nuclear Science and Technology Organization, Clayton Victoria 3168, Australia

© 2024 The Authors. *Batteries & Supercaps* published by Wiley-VCH GmbH. This is an open access article under the terms of the Creative Commons Attribution Non-Commercial License, which permits use, distribution and reproduction in any medium, provided the original work is properly cited and is not used for commercial purposes.

Moreover, Na belongs to the alkali-metal family with lithium, the second smallest and lightest alkali element.<sup>[23]</sup> Table 1 demonstrates a juxtaposition of the characteristics of Na and Li elements. Notably, the lower redox potential of the  $\text{Na}^+$  brings about better safety and feasibility with electrolytes of lower voltage during the operation.<sup>[24]</sup> Consequently, the charging and discharging mechanism of sodium-ion batteries (SIBs) resembles that of LIBs, and Na ions possess analogous physical and chemical properties to Li ions.<sup>[25–27]</sup> Besides, Na ions, like Li ions, exhibit the capability of intercalation and deintercalation in suitable materials. In Figure 1b, an exemplary SIB configuration comprises a cathode, an anode, an electrolyte, a diaphragm (known as a separator), and a metallic collector. SIBs operate on a comparable principle to LIBs and can also be called “rocking-chair”, such as alkali metal-ions bidirectional shuttling between the cathode and anode by intercalation and deintercalation.<sup>[28]</sup> During the charging process, the cathode experiences an oxidation reaction, relinquishing electrons, whereas the anode undergoes a reduction reaction, acquiring electrons. Inside the battery cell, the sodium ions deintercalated from the cathode materials and intercalated into the anode materials, facilitated by the electrolyte and diaphragm. Simultaneously, in the external circuit, electrons flow from the cathode to the anode. Conversely, the direction of both electron and ion movement is reversed during the discharging process.<sup>[29]</sup> In the development of SIBs, due to their similarity to LIBs in principles, a significant amount of mature LIB technology has been adopted and applied in SIBs. Currently, unprecedented achievements have been made in the anode,<sup>[30–36]</sup> electrolyte,<sup>[37–39]</sup> and aluminum collectors,<sup>[40–43]</sup> in SIBs. Therefore, SIBs have been widely regarded as promising candidates for next-generation EESs,<sup>[20,44–47]</sup> not only due to their comparable energy density but also their extensive elemental resources, economical, excellent safety, and environmentally friendly.<sup>[48–51]</sup> With these advantages, SIBs hold great potential to become substitutes for LIBs in commercial energy storage.<sup>[20,24,52–55]</sup> Furthermore, it is well known that in SIBs, the cathode assumes a crucial role in determining the sodium kinetics, reversibility, energy density and cycle life.<sup>[56–60]</sup> Among the investigated cathode materials



Dr. Wei Kong Pang is currently an associate professor at the University of Wollongong, Australia. He specializes in the characterization of atomic-level structure and dynamics. He is particularly interested in constructing the structure-function relations of electrode materials for metal-ion batteries using neutron and synchrotron X-ray techniques. His work revolves around utilizing state-of-the-art techniques and facilities, e.g., neutron and synchrotron sources, to advance the understanding of energy storage materials. He received recognition as an ARC Future Fellowship (2016), the Australian Synchrotron Research Award (2020), the prestige Australian Neutron and Deuteration Impact Award (2021), and the ARC Discovery Project funding grant (2022).

**Table 1.** comparison of properties for sodium and lithium. Data derived from.<sup>[265]</sup>

Properties	Sodium	Lithium
Ionic radius (nm)	0.102	0.076
Atomic weight (g.mol <sup>-1</sup> )	22.99	6.94
Density (g.cm <sup>-3</sup> )	0.534	0.971
Standard electrode potential (V)	-2.71	-3.04
Specific capacity (mAh.g <sup>-1</sup> )	1166	3862
Abundance (% & ppm)	2.83 & 23600	0.0065 & 20

for SIBs, O3-type layered transition metal oxides are widely acknowledged as the most promising cathode candidates, thanks to their superior performance in terms of synthesis methods, cost-effectiveness, and electrochemical performance. The main emphasis of this review lies in providing a comprehensive overview of the electrochemical performance and structural evolution of O3-type layered transition metal oxides utilized as cathode materials for SIBs and extensively covers the latest research progress in the area. This review categorizes materials based on their composition in layered form as follows: Unary, binary, and ternary  $\text{Na}_x\text{TMO}_2$  refers to materials containing only one, two, and three transition metal or redox elements. Additionally, materials with more than three transition metal elements are classified as multinary or high-entropy  $\text{Na}_x\text{TMO}_2$ . The review also addresses the challenges associated with O3-type cathode materials and concisely summarizes the recent developments pertaining to element doping and substitution. Furthermore, it offers valuable insights into future advancements in exceptional-performance layered oxide cathode materials for SIBs.

## 2. Structure Classification and Progress

In contrast to LIBs, SIBs exhibit a more stable functional structure and a consistent diffusion path for Na ions. For SIBs, this can be attributed to the unique “rich chemistry” characteristics of the electrode materials, which arise from the considerable difference in size between Na ions and transition metal ions.<sup>[61]</sup> The research community for SIBs has predominantly concentrated on investigating cathode materials, such as polyanionic compounds,<sup>[62,63]</sup> conversion-type materials,<sup>[64]</sup> transition metal oxide,<sup>[40]</sup> organic compounds,<sup>[65]</sup> and Prussian blue-like cathode materials.<sup>[66]</sup> Figure 2a illustrates the advantages and disadvantages associated with these five cathode materials,<sup>[67]</sup> and Figure 2b compares the capacity and working voltage of such cathode materials.<sup>[68]</sup> Compared with other cathode materials, layered transition metal oxides, such as  $\text{NaMn}_{0.25}\text{Fe}_{0.25}\text{Co}_{0.25}\text{Ni}_{0.25}\text{O}_2$ ,<sup>[69]</sup> have a higher initial sodium content,<sup>[70]</sup> smaller electrode polarization and stabler Na<sup>+</sup> diffusion,<sup>[71,72]</sup> satisfactory cycling stability, high reversible capacity,<sup>[73–75]</sup> and relatively higher specific capacities.<sup>[76]</sup> Hence, greater energy-density performance, approaching the performance of counterparts in LIBs.<sup>[69]</sup> Owing to the similarity to LIB technology, the adoption of such SIB layered oxides presents

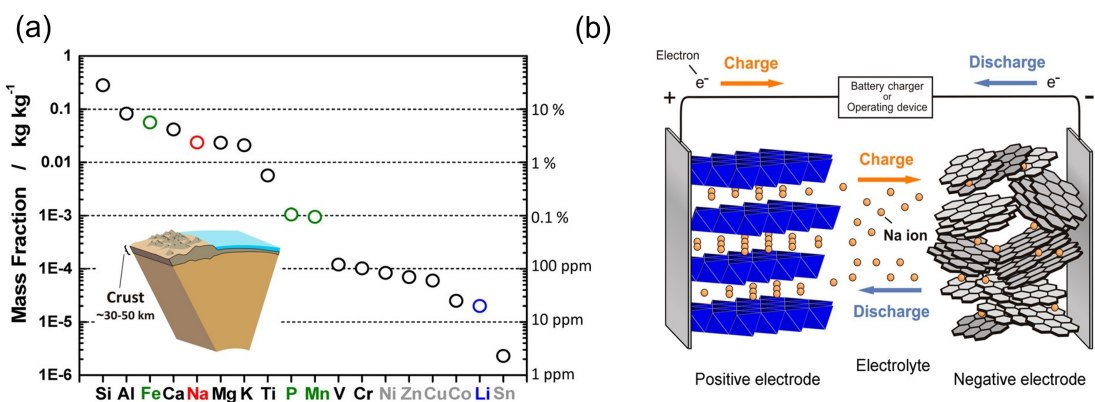


Figure 1. (a) The abundance of major elements in globe.<sup>[147]</sup> (b) Schematic diagram of a sodium-ion battery.<sup>[147]</sup>

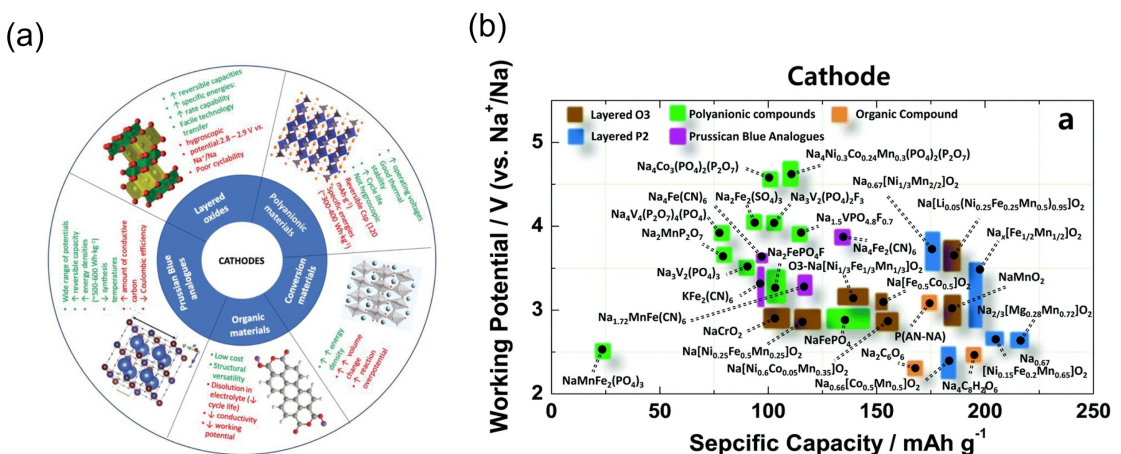


Figure 2. (a) Existing five main kinds of sodium ion battery cathode materials.<sup>[67]</sup> (b) The relationship between theoretical capacity and voltage of cathode materials for SIBs.<sup>[68]</sup>

higher industrial feasibility, as they can leverage established technologies from mature LIBs.<sup>[68,77,78]</sup> Therefore, layer-structured transition metal oxides are poised to assume a pivotal role as next-generation cathode materials for SIBs.<sup>[79]</sup>

The chemical formula for the layered oxide cathode material is denoted as  $\text{Na}_x\text{TMO}_2$  ( $0 < x \leq 1$ , TM = one or more transition metal elements), where the TM can be various types of combinations of transition metal ions and alkaline-earth metal ions (such as Cr, Fe, Ni, Mn, Co, V, Ti, Zn, Cu, Ru, Sn, Ir, Li, Mg, etc.),<sup>[79–88]</sup> which demonstrates substantial advantages, encompassing compositional flexibility, higher capacity, and easy synthesis.<sup>[41,68,89]</sup> Notably, the various combinations of TMs and the changes in  $\text{Na}^+$  content can induce pronounced disparities in TM–O bond strengths, electronic configurations, and oxidation states, leading to distinct structural differences in the  $\text{Na}_x\text{TMO}_2$ . Considering the diverse stacking sequences of oxygen layers,  $\text{Na}_x\text{TMO}_2$  can be further categorized into various types, including O2, O3, P2, P3, etc.,<sup>[90]</sup> as shown in Figure 3a, where P and O denote prismatic and octahedral coordination of sodium ions, respectively, and the number after the letter indicates the number of oxygen layers stacked in the minimum repetitive unit.<sup>[91,92]</sup> The structural difference leads to notable distinctions in the electrochemical characteristics of these materials. Pres-

ently, the predominant architectures observed in layered oxide cathode materials for SIBs are primarily P2-type and O3-type.<sup>[93]</sup>

When  $x \leq 0.7$ ,  $\text{Na}_x\text{TMO}_2$  typically forms a P2 phase with an ABBAAB oxygen stacking array (oxygen packing), and a space group is  $P6_3/mmc$ .<sup>[80,94,95]</sup> P2-type cathode materials have a larger Na layer spacing that can enhance the transport rate of  $\text{Na}^+$  and sustain the wholeness of the layered structure, leading to admirable rate performance, cycling, and air stability.<sup>[77,96,97]</sup> While P2-type materials exhibit wider  $\text{Na}^+$  transport channels and lower sodium ion migration barriers, enabling faster diffusion kinetics, they undergo a phase transformation from P2 to O2 as sodium ions deintercalate during deep sodium extraction. This transformation not only diminishes the ionic diffusion rate but also induces volume expansion and structural instability, leading to compromised rate performance and cycling stability.<sup>[98–100]</sup> Moreover, P2-type oxides have high  $\text{Na}^+$  defects and poor initial charge capacity, which poses challenges for practical applications.

In contrast, when  $0.8 \leq x \leq 1.0$ ,  $\text{Na}_x\text{TMO}_2$  preferentially forms an O3 phase with an oxygen stacking array of ABCABC. There are two variants, O3 and O'3 (Figure 3b). The former belongs to the hexagonal crystal system with a space group of  $R-3m$ ,<sup>[94]</sup> and the latter has a space group  $C2/m$ , which is classified as a

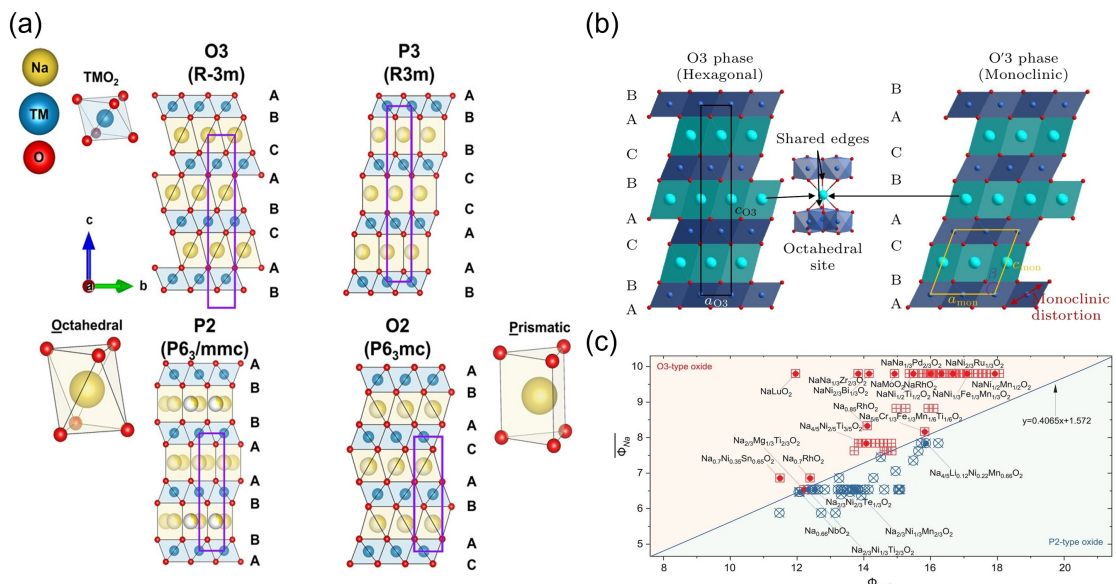


**Figure 3.** (a) Illustration of P2/O2 and O3/P3 structures.<sup>[266]</sup> (b) Crystal structure of O3 and O'3 phases.<sup>[267]</sup> (c) Comparison for the cationic potential of P2 and O3 type cathodes.<sup>[268]</sup>

monoclinic crystal system. Remarkably, almost all cathode materials used in LIBs have an O3-type structure.<sup>[101,102]</sup> Given that the O3 cathodes have a higher initial Na content compared to the Na-deficient P2-type ones, they can release more sodium ions (Figure 3c), providing higher initial specific capacity during charging and discharging.<sup>[88,103,104]</sup>

However, O3-type cathodes still face some problems and challenges. The poor symmetry of the crystal structure and the Jahn-Teller effect of transition metals, such as Mn<sup>3+</sup>, contribute to multiple and complicated phase transitions from O3 to O'3, P3, P'3, and P3'', which bring about an adverse effect on the cycling performance.<sup>[79,104–109]</sup> During sodium extraction, the O3-phase generates an increasing number of prismatic vacancies,<sup>[110]</sup> resulting in the sliding of TMO<sub>2</sub> layers and the transformation of oxygen packing into a new "ABBCCA" arrays, forming a thermodynamically stable P3-type phase.<sup>[111]</sup> The interlayer spacing of the transition metal in the P3 phase is relatively larger than that of the O3 phase, making it more conducive to the diffusion of Na<sup>+</sup>.<sup>[112]</sup> Although the O3 structure provides a larger diffusion space for Na<sup>+</sup>, its phase transition product, P3, exhibits a relatively lower Na<sup>+</sup> diffusion barrier.<sup>[113]</sup> The complex phase transitions and the ordered arrangement between the larger Na<sup>+</sup> ions and vacancies at different Na contents can lead to irreversible phase transitions, resulting in capacity degradation and structural instability.<sup>[114,115]</sup>

Currently, researchers have dedicated to enhancing the lattice structure stability and ion conductivity of O3-type materials, which is crucial for the extraction/insertion processes of Na<sup>+</sup>. To overcome these obstacles, it has been proven that element doping and substitution are effective means to alleviate these negative effects.<sup>[80,97,104,107,116–118]</sup> For instance, expensive Ni and Co are applied to partially replace Fe and Mn, which increases the specific capacity and prolongs the cycling life of the material.<sup>[119]</sup> In the following sections, we systemati-

cally summarized the O3-type cathode materials based on their chemical composition.

### 3. Unary Metal System

In a unary system, the O3-Na<sub>x</sub>TMO<sub>2</sub> consists of one 3d transition metal element, such as Cr, Mn, Fe, Co, Ni, V, Ti, etc.<sup>[29]</sup> In this section, the O3-type unary cathodes such as NaCrO<sub>2</sub>, NaMnO<sub>2</sub>, NaFeO<sub>2</sub>, NaCoO<sub>2</sub>, and NaNiO<sub>2</sub> will be comprehensively discussed to demonstrate the characteristics of a single redox center and its associated mechanistic behavior, forming the foundation for the multi-metal system.

#### 3.1. O3-NaCrO<sub>2</sub>

In 1982, Braconnier et al. first studied NaCrO<sub>2</sub> as a cathode material for SIBs.<sup>[120]</sup> This material possesses an  $\alpha$ -NaFeO<sub>2</sub>-type layered structure with an R3-m space group.<sup>[121,122]</sup> O3-NaCrO<sub>2</sub> exhibits a satisfactory reversible capacity of 120 mAh.g<sup>-1</sup> (~0.5 Na) in the voltage range of 2.5–3.6 V, with a long plateau at around 3 V.<sup>[121]</sup> In O3-NaCrO<sub>2</sub>, Cr is in the form of Cr<sup>3+</sup> with an electronic configuration of [Ar] 3d<sup>3</sup> and without J-T distortion. Upon charging, the extraction of ~0.5 Na will bring about the formation of Cr<sup>4+</sup> ([Ar] 3d<sup>2</sup>, with weak J-T distortion). Moreover, Cr has different ionic radii 0.615 and 0.55 Å, respectively, at octahedral coordination. Moreover, mean Cr–O bond lengths (1.976 and 1.950 Å) at 3+ and 4+. In other words, the valence changes in Cr induce a nearly negligible shrinkage in CrO<sub>6</sub> octahedra, despite the shorter ionic radius. Due to the significant difference in the radii of Na<sup>+</sup> (0.102 Å) and Cr<sup>4+</sup>, when Na<sup>+</sup> is extracted, Cr<sup>4+</sup> can be retained within the transition metal layer without undergoing migration.<sup>[123]</sup> As

shown in Figure 4a, there is only a tiny irreversible capacity of  $8 \text{ mAh.g}^{-1}$  in the first cycle at  $1/20 \text{ C}$  ( $12.5 \text{ mA.g}^{-1}$ ). However, as researchers delved deeper into  $\text{NaCrO}_2$ , the Na intercalation/deintercalation processes were revealed at different upper cutoff voltages (3.7, 3.8, and 4.5 V).<sup>[123]</sup> It was found that the discharge capacity ( $9 \text{ mAh.g}^{-1}$ ) sharply decreased when the charging cutoff voltage was increased to 4.5 V. The phase evolution behavior of  $\text{NaCrO}_2$  has been revealed (Figure 4b).<sup>[123]</sup> During Na extraction, the structure of  $\text{NaCrO}_2$  cathode undergo a series of transformation, from O3-type (1.0 Na) to the monoclinic O'3-type ( $0.9 \geq x \geq 0.7 \text{ Na}$ ), to the monoclinic P'3-type ( $\sim 0.5 \text{ Na}$ ), and to the hexagonal O3'-type ( $\sim 0.16 \geq x \geq 0 \text{ Na}$ ) structures. During the complex transitions, the Cr–Cr bond lengths decreased, while the interslab distance increased, hindering the transportation of  $\text{Na}^+$  ions and affecting the specific capacity performance.<sup>[109,123,124]</sup> Ceder et al.<sup>[125]</sup> found that after complete sodium deintercalation, the layered P'3- $\text{Na}_{0.4}\text{CrO}_2$  transforms into the rock-salt structure  $\text{CrO}_2$  phase, which may be the reason for the capacity decrease of  $\text{NaCrO}_2$  when charging is completely finished. At high voltages,  $\text{Cr}^{4+}$  may undergo a disproportionation mechanism and into  $\text{Cr}^{3+}$  and  $\text{Cr}^{6+}$  ([Ar]), as well as soluble  $\text{Cr}^{5+}$  ions,<sup>[126–128]</sup> forming the origin of the irreversibility of  $\text{Na}^+$  extraction in the following cycles.

### 3.2. O'3- $\text{NaMnO}_2$

Due to its relatively abundant reserves and non-toxicity, Mn-based layered transition metal oxides have become a promising SIB cathode material.<sup>[129]</sup> Parant et al.<sup>[130]</sup> first reported the properties of  $\text{NaMnO}_2$  cathode material with a monoclinic O'3 structure (space group:  $C2/m$ ). It is noteworthy that  $\text{NaMnO}_2$  and the well-known layered  $\text{LiMnO}_2$  exhibit distinct differences. The former can maintain its structure without transforming into a spinel structure during  $\text{Na}^+$  deintercalation. At the same time,

the latter, due to the high migration rate of  $\text{Mn}^{2+}$  ions,<sup>[131]</sup> undergoes a transformation into a spinel structure upon the first deintercalation.<sup>[132–135]</sup> Compared to  $\text{Li}^+$  ions, the larger ionic size difference between Na and transition metals makes the  $\text{Na}_x\text{MO}_2$  system more likely to form layered structures.<sup>[136,137]</sup> Mn is in the form of  $\text{Mn}^{3+}$  within the O3-type layered oxide, with an electronic configuration of  $[\text{Ar}] 3d^4$ . Due to the strong J–T effect associated with  $\text{Mn}^{3+}$  ions, layered cathode materials like  $\text{Na}_x\text{MnO}_2$  often generate unstable monoclinic O'3 structure, leading to poor cycling stability. During charging, with the extraction of  $\text{Na}^+$  ions,  $\text{Mn}^{4+}$  ([Ar]  $3d^3$ , without J–T distortion) is formed. Additionally, Mn exhibits significantly different ionic radii (0.645 and 0.53 Å at octahedral coordination) and mean Mn–O bond lengths (2.031 and 1.903 Å) at  $3^+$  and  $4^+$ , respectively. Figure 5a reveals that, during Na extraction in the voltage range of 2.0 to 4.5 V, the O'3- $\text{NaMnO}_2$  undergoes a solution reaction at  $1.0 \geq x \geq 0.44 \text{ Na}$ , followed by a two-phase reaction (O'3 & O1) at  $0.48 \geq x \geq 0.2 \text{ Na}$ , and then another solid solution until the completed Na extraction.<sup>[138]</sup> Owing to the complexity of  $\text{Mn}^{3+}$ ,  $\text{Na}_x\text{MnO}_2$  can form in either monoclinic  $\alpha$ - $\text{NaMnO}_2$  ( $C2/m$ ) or orthorhombic  $\beta$ - $\text{NaMnO}_2$  ( $Pmm$ ), or the intergrown structure, as shown in Figure 5b.<sup>[139]</sup> At low temperatures, the J–T effect of  $\text{Mn}^{3+}$  ions induces a distortion of  $\text{Na}_x\text{MnO}_2$  into a layered O3 monoclinic structure. At high temperatures, the orthorhombic  $\beta$ - $\text{NaMnO}_2$  phase comprises double-layered  $\text{MnO}_2$  sheets, formed by sharing edges of  $\text{MnO}_6$  octahedra. In the early time, it is reported that merely 0.22 and 0.15 of  $\text{Na}^+$  ions, respectively, can be reversibly deintercalated and re-intercalated in  $\alpha$ - $\text{NaMnO}_2$  and  $\beta$ - $\text{NaMnO}_2$ .<sup>[79]</sup> With the improvement in particle and electrolyte engineering,  $\alpha$ - $\text{NaMnO}_2$  can deliver an initial discharge capacity of  $185 \text{ mAh.g}^{-1}$  ( $\sim 0.8 \text{ Na}$ ) at  $0.1 \text{ C}$  rate between 2.0 and 3.8 V (Figure 5c) and retained a discharge capacity of  $132 \text{ mAh.g}^{-1}$  after 20 cycles,<sup>[132]</sup> where the intergrown compound of  $\alpha$ - $\text{NaMnO}_2$  and  $\beta$ - $\text{NaMnO}_2$  exhibited a remarkable specific capacity of  $190 \text{ mAh.g}^{-1}$  at  $0.05 \text{ C}$  and  $142 \text{ mAh.g}^{-1}$  at  $2 \text{ C}$  (Figure 5d), with retaining

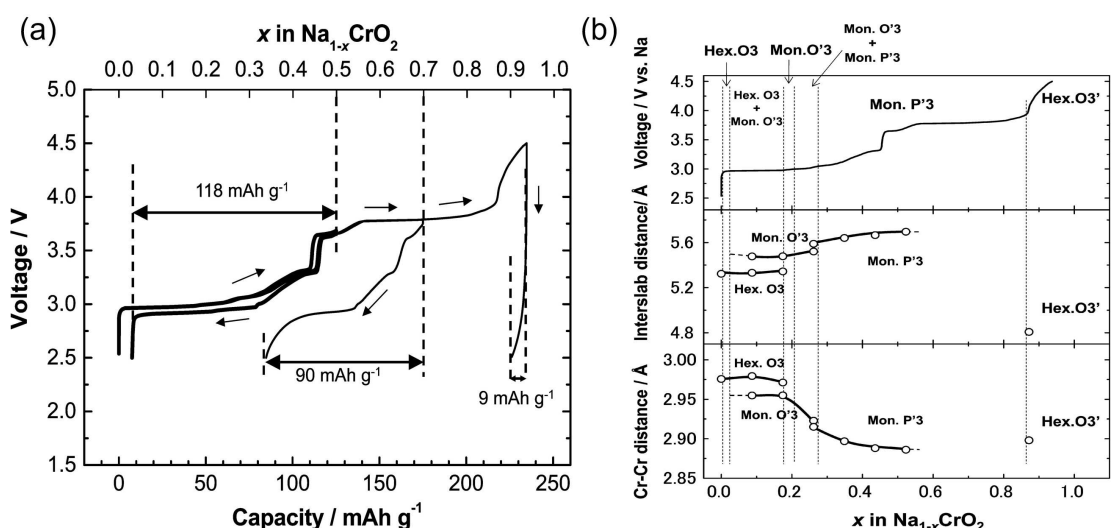


**Figure 4.** (a) Initial charge and discharge curves ( $0.0 \leq x \leq 0.9$ ) in the ranges of 2.5–4.5 V at  $0.05 \text{ C}$ .<sup>[123]</sup> (b) The phase evolution of  $\text{Na}_{1-x}\text{CrO}_2$  with extraction Na content.<sup>[123]</sup>

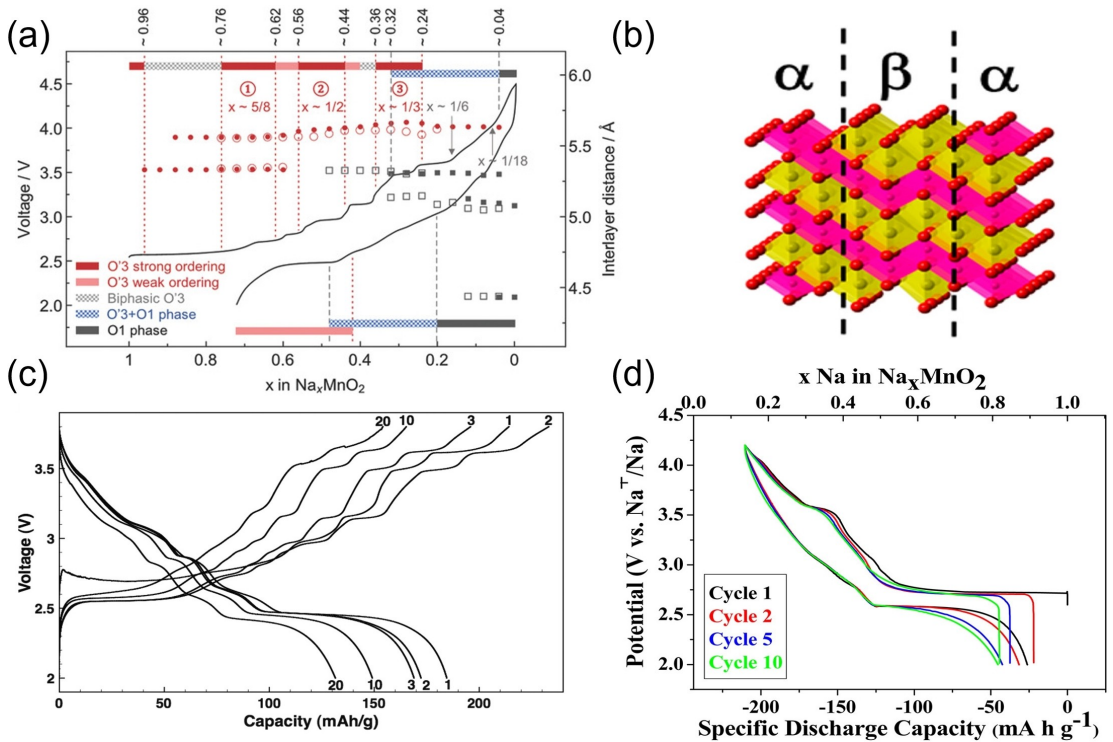


**Figure 5.** (a) Phase transformation evolution for  $\text{NaMnO}_2$  at 0.02 C at 2.0–4.5 V.<sup>[138]</sup> (b)  $\alpha$ - $\text{NaMnO}_2$  and  $\beta$ - $\text{NaMnO}_2$  intergrowth model.<sup>[139]</sup> (c) The electrochemical performance of multiple cycles for  $\alpha$ - $\text{NaMnO}_2$ .<sup>[132]</sup> (d) Charge-discharge curves for  $\beta$ - $\text{NaMnO}_2$  at 0.05 C.<sup>[139]</sup>

100 mAh.g<sup>-1</sup> after 100 cycles at 2 C.<sup>[139]</sup> However, the increased stacking faults and the collapse of long-range structures at low Na content are the main root causes limiting the electrochemical performance.<sup>[139]</sup> Despite this, the intergrown structure of two compatible phases has shown their promising contribution to the electrochemical properties.

### 3.3. O3-NaFeO<sub>2</sub>

$\text{NaFeO}_2$  can be regarded as a standard model of the layered sodium oxide structure, denoted as the O3 phase, with a space group of  $R\text{-}3m$ . Unlike  $\text{LiFeO}_2$ , which has inert chemical properties,  $\text{NaFeO}_2$  has a theoretical capacity of up to 241.8 mAh.g<sup>-1</sup> and is regarded as a promising candidate owing to its cost-effectiveness, abundance, and high redox potential.<sup>[140–145]</sup> Takeada et al. first reported  $\alpha$ - $\text{NaFeO}_2$ , but successful extraction of  $\text{Na}^+$  from  $\alpha$ - $\text{NaFeO}_2$  has not been achieved.<sup>[83]</sup> During charge and discharge, the valence of Fe varies between 3+ and 4+ in  $\text{NaFeO}_2$ , where  $\text{Fe}^{3+}$  ([Ar] 3d<sup>5</sup>) being without J-T distortion and  $\text{Fe}^{4+}$  ([Ar] 3d<sup>4</sup>) exhibiting a strong J-T distortion.<sup>[146]</sup> In octahedral coordination, the ionic radii of Fe differ as 0.645 Å and 0.585 Å, respectively, corresponding to its 3+ and 4+. With the relatively smaller variations between  $\text{Fe}^{3+}$  and  $\text{Fe}^{4+}$ , it is expected to see better structure stability in the Fe-based Na compounds. However, upon Na extraction in the  $\text{NaFeO}_2$  lattice, vacancies are created on the tetrahedra where the  $\text{FeO}_6$  octahedra becomes coplanar as illustrated in Figure 6a. Accordingly,  $\text{Fe}^{3+}$  ions tend to achieve an energetically stable state in the tetrahedral positions, resulting in a preference for the

irreversible migration of  $\text{Fe}^{3+}$  ions from the octahedral positions to the vacant coplanar tetrahedra.<sup>[147,148]</sup> The mean Fe–O bond lengths are significantly different, with 2.07 Å and 1.88 Å at octahedral and tetrahedral coordination, ruining the stability of such an O3 lattice. Moreover,  $\text{Fe}^{4+}$  is unstable in such an environment, and over 40% of  $\text{Fe}^{4+}$  can undergo spontaneous reduction to  $\text{Fe}^{3+}$ .<sup>[149]</sup> As found through in situ synchrotron X-ray diffraction (SXRD) measurements in Figure 6b,  $\alpha$ - $\text{NaFeO}_2$  undergoes a phase transition from O3 to O'3 to O''3 within the voltage range of 2–3.6 V. It is notable that the P3 phase was not observed. However, instead, a new layered hexagonal phase O''3 was generated. This is in stark contrast to most O3 layered oxide materials, such as  $\text{NaCrO}_2$ , O3- $\text{NaMnO}_2$ , and  $\text{NaCoO}_2$ . The new O''3 phase exhibits a non-reversible structural evolution during the charge and discharge processes.<sup>[149]</sup> Yabuuchi et al.<sup>[150]</sup> and Silvan et al.<sup>[151]</sup> reported that, if charging at >3.6 V, the O3 phase rapidly polarizes and undergoes irreversible structural changes (Figure 6c), leading to a rapid decline in reversible performance due to the irreversible migration of Fe from the transition metal layer to the sodium layer and limiting its practical Na extraction and capacity delivery. Moreover, the adverse effect of high-valence  $\text{Fe}^{4+}$  on the stability of the structure is pronounced at high voltage. In 2.5–3.4/3.5 V and at 0.1 C,  $\alpha$ - $\text{NaFeO}_2$  has a voltage plateau at ~3.3 V. It showed a reversible specific capacity of 80/100 mAh.g<sup>-1</sup> (~0.35/0.45 Na), where the  $\text{Na}^+$  ions can reintegrate into the layered structure and facilitate the migration of iron ions back to their initial positions (Figure 6d). Moreover, O3- $\text{NaFeO}_2$  also faces the problem of poor air stability.<sup>[148]</sup>

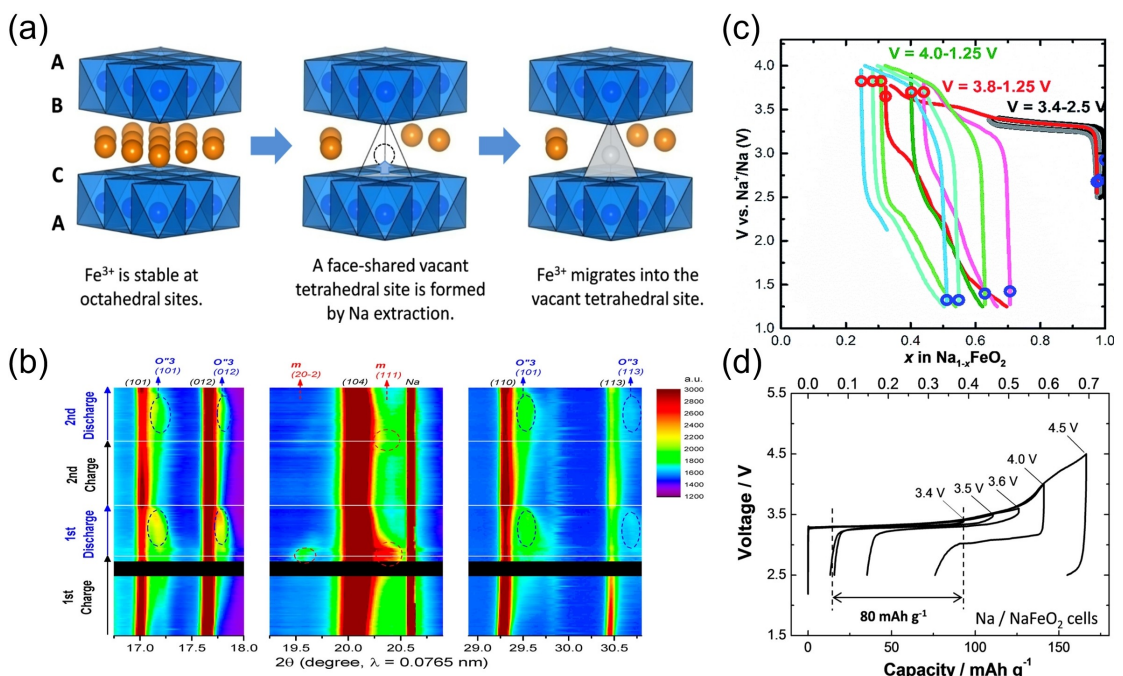


**Figure 6.** (a) Schematic diagram of iron ion migration.<sup>[148]</sup> (b) In-situ SXRD patterns of NaFeO<sub>2</sub> sample during the first cycle.<sup>[149]</sup> (c) Na<sup>+</sup> insertion and extraction content in PITT cycling at different voltage ranges.<sup>[151]</sup> (d) Charge-discharge curves of NaFeO<sub>2</sub> at different voltage ranges.<sup>[150]</sup>

### 3.4. O3-NaCoO<sub>2</sub>

Braconnier et al.<sup>[152]</sup> conducted the first research on the performance of NaCoO<sub>2</sub> as a cathode material for SIBs. Like NaFeO<sub>2</sub>, NaCoO<sub>2</sub> is an O3-type layered oxide material with the space group R3-m. During the charging and discharging process, Co undergoes an oxidation reaction, transitioning from 3+ ([Ar] 3d<sup>6</sup>) to 4+ ([Ar] 3d<sup>5</sup>). Their ionic radii are 0.61 and 0.53 at 3+ and 4+, respectively. Typically, Co<sup>3+</sup> and Co<sup>4+</sup> ions exhibit both lack J-T distortion. Additionally, the mean manganese-oxygen bond lengths for Co<sup>3+</sup> and Co<sup>4+</sup> are 1.908 and 1.874 Å. The theoretical capacity of the material is 235 mAh.g<sup>-1</sup>. However, in experimental studies, it exhibits a significantly poor specific capacity of approximately 40 mAh.g<sup>-1</sup> (~0.2 Na) at a voltage range of 2.5–3.0 V at 70 μA cm<sup>-2</sup>.<sup>[80,114]</sup> This could be attributed to the fact that the complex and irreversible phase transitions during the intercalation or deintercalation process.<sup>[153]</sup> As illustrated in Figure 7a, the O3-Na<sub>x</sub>CoO<sub>2</sub> turns into the O'3 phase occurs at x=0.95, and then the P'3 phase at 0.9>x>0.82.<sup>[80]</sup> These multi-staircase transitions are detrimental to the structure stability, hence limiting the practical capacity of NaCoO<sub>2</sub>. Kaufman and Van der Ven<sup>[153]</sup> further concur the irreversible and complicated phase transitions: O3-O'3-P'3-P3-P'3 by using first-principles calculations.

### 3.5. O'3-NaNiO<sub>2</sub>

NaNiO<sub>2</sub> is a monoclinic lattice system O'3-type layered oxide with a space group of C2/m.<sup>[154,155]</sup> Braconnier et al.<sup>[120]</sup> first reported it as an SIB cathode material in 1982. The Ni valence

varies between 2+ and 4+. Under octahedral coordination, Ni can manifest three distinct sets of ionic radii: 0.69, 0.56, and 0.48 Å, for 2+, 3+, and 4+, respectively. Furthermore, Ni exhibits varying Ni–O average bond lengths, from 2.070 Å to 1.870 Å, when the oxidation state increases from 2+ to 4+. Although Ni-based layered oxide materials are currently considered promising SIB cathodes due to the high redox potential Ni changes from 2+ ([Ar] 3d<sup>8</sup>) to 3+ ([Ar] 3d<sup>7</sup>) to 4+ ([Ar] 3d<sup>7</sup>) ions,<sup>[68]</sup> the large changes in Ni environments can be ruining the lattice structure along the cycling. It has been revealed that the NaNiO<sub>2</sub> undergoes a sequence of irreversible phase transitions during the initial charge and discharge cycles.<sup>[120,154]</sup> These transitions include O'3 (1.0≥x≥0.91 Na)-P'3 (0.91≥x≥0.7 Na)-P''3 (0.84≥x≥0.55 Na)-O''3 (0.81≥x≥0.45 Na)-O'''3 (0.81≥x≥0.79 Na)-O''''3 (0.83≥x≥0 Na)-P''''3 (0.5≥x≥0 Na), as illustrated in Figure 7b. These complicated transitions are detrimental to the cycling stability of such cathodes. Additionally, NaNiO<sub>2</sub> is not stable in air, which is also not conducive to storing and transporting the material.<sup>[156]</sup> Na<sub>x</sub>NiO<sub>2</sub> exhibits a reversible capacity of 123 mAh.g<sup>-1</sup> (~0.52 Na) in 1.25–3.75 V (Figure 7c) and a commendable reversible capacity of 147 mAh.g<sup>-1</sup> (~0.61 Na) within the 2.0–4.5 V range (Figure 7d), specifically at a 0.1 C rate. Nevertheless, with the wider voltage window, the capacity experiences a notable reduction, settling at an approximate value of 100 mAh.g<sup>-1</sup> after 20 cycles.<sup>[155]</sup> The main factor responsible for this phenomenon is the occurrence of gliding in the NiO<sub>2</sub> slabs, leading to the formation of an irreversible phase, P''''3-Na<sub>0.17</sub>NiO<sub>2</sub>, when voltages exceeding 4.0 V. This adversely affects the structural stability of the material and accelerates electrode polarization.<sup>[157]</sup>

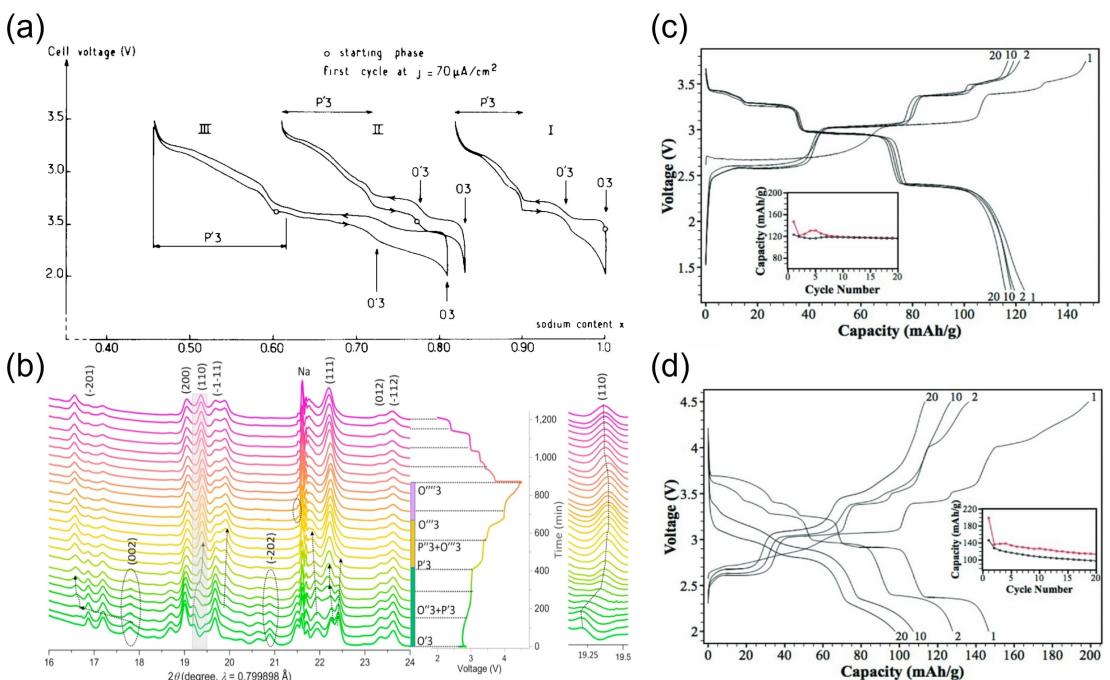


**Figure 7.** (a) Sodium content at different voltage for NaCoO<sub>2</sub>.<sup>[80]</sup> (b) In situ XRD patterns for NaNiO<sub>2</sub> in 1<sup>st</sup> cycle.<sup>[157]</sup> Charge/discharge curve for NaNiO<sub>2</sub> within the voltage range of (c) 1.25–3.75 V and (d) 2.0–4.5 V at 0.1 C.<sup>[155]</sup>

In summary, this chapter provides an overview of five common monovalent metal layered oxide materials. The performance comparison is provided in Table 2. Firstly, Cr and Co are evidently toxic elements. However, the former exhibits outstanding Coulombic efficiency due to the absence or weak J-T effect of Cr<sup>3+</sup> and Cr<sup>4+</sup>. The latter, specifically NaCoO<sub>2</sub>, fails to demonstrate the same energy storage potential as LiCoO<sub>2</sub>, and Co is relatively expensive. Furthermore, considering the strategies of global sustainable development, it is unlikely that Cr and Co based cathode materials will be suitable for large-scale energy storage in the future. Encouragingly, Fe shows tremendous potential due to its abundance in the Earth's crust and low synthesis cost. Nevertheless, it has a lower specific

capacity and instability attributed to the migration of Fe<sup>3+</sup> ions defect. Lastly, Mn- and Ni-based cathode materials in unary-metal systems show excellent energy density and specific capacity compared to other cathode materials. However, as monoclinic structured materials, they possess instability and higher irreversible capacity during cycling due to complex phase transitions.

#### 4. Multi-Metal Systems

The unary metal layered oxide cathode materials, such as O3-NaCrO<sub>2</sub>, O'3-NaMnO<sub>2</sub>, O3-NaFeO<sub>2</sub>, O3-NaCoO<sub>2</sub>, and O'3-NaNiO<sub>2</sub>,

**Table 2.** Electrochemical performance of five unary metal O3-type layered cathode materials in SIB.

Unary metal oxides	Structure	Specific capacity [mAh.g <sup>-1</sup> ]	Voltage range (V)	Average working potential (V)	Electronic configuration at 3+	Phase transition	Advantages	Disadvantages
O3-NaCrO <sub>2</sub> <sup>[123]</sup>	R-3m	120	2.5–3.6	~3.0	[Ar] 3d <sup>3</sup>	O3-O'3-P'3-O3'	low reversible phase transition	Poisonous Cr
O'3- $\alpha$ -NaMnO <sub>2</sub> <sup>[132]</sup> O'3- $\beta$ -NaMnO <sub>2</sub> <sup>[139]</sup>	C2/m or Pmnm	185 and 190	2.0–3.8	~2.8	[Ar] 3d <sup>4</sup>	O'3-O'3 + O1-O1	Inexpensive	Strong J-T effect from Mn <sup>3+</sup>
O3-NaFeO <sub>2</sub> <sup>[150]</sup>	R-3 m	80–100	2.5–3.4	~3.2	[Ar] 3d <sup>5</sup>	O3-O'3-O''3	economic	Fe <sup>3+</sup> migration
O3-NaCoO <sub>2</sub> <sup>+</sup> O'3-NaNiO <sub>2</sub> <sup>[155]</sup>	R-3 m	40	2.0–3.5	~2.7	[Ar] 3d <sup>6</sup>	O3-O'3-P'3-P3	N/A	Expensive and Poisonous Co
	C2/m	120	1.25–3.75	~2.4 (2+–3+); ~3.1 (3+–4+)	[Ar] 3d <sup>7</sup>	O'3-P'3-P''3-O''3-O'''3-P''''3	High voltage	Excessive phase transition

face common challenges associated with complex phase transitions, structural instability, or migration of transition metal ions, so its electrochemical performance is not reliable. It is well-known that introducing new elements is an effective approach that can suppress irreversible phase transitions during  $\text{Na}^+$  icon extraction/insertion. The new element can be a redox-active metal ion, such as Fe, Cr, etc., that can contribute capacity and redox reaction, or can be electrochemically inactive elements, such as Li, Mg, etc., that can act as a pillar to support the O<sub>3</sub> structure against sodium extraction and insertion during cycling. Following the discussion of unary oxides in Section 3, this chapter focuses on conducting in-depth research on O'3 Ni-based and O'3 Mn-based materials, describing the roles of additional redox metal ions and inert pillar ions, as well as their intrinsic structures, in the electrochemical enhancement of such O<sub>3</sub> compounds.

#### 4.1. Ni-Based (C2/m, O'3)

Previous studies have indicated that NaNiO<sub>2</sub> is one of the highly promising cathode materials for SIBs.<sup>[158]</sup> This is attributed to its higher redox potential, which makes it more suitable for operation under high voltage. However, Ni-based O<sub>3</sub> cathode faces numerous challenges, such as rapid capacity decay, poor rate performance, and multiple irreversible phase transitions. In literature, other 3d metal elements, such as Fe, Co, and Ti, were introduced to form new binary or ternary O<sub>3</sub>-type Ni-based cathodes.

When Fe or Co is introduced, the parental O'3 phase will turn into a solid-solution O<sub>3</sub>-type (*R3-m*).<sup>[159]</sup> NaNi<sub>0.5</sub>Co<sub>0.5</sub>O<sub>2</sub> exhibited a reversible capacity of 115 mAh.g<sup>-1</sup> (~0.49 Na) in the

first cycle at 2.0–4.2 V with a 0.1 C rate (Figure 8a), and NaNi<sub>0.5</sub>Fe<sub>0.5</sub>O<sub>2</sub> provided a reversible capacity of 129 mAh.g<sup>-1</sup> (~0.54 Na) in the first cycle at 2.0–3.9 V with a 0.1 C rate (Figure 8b).<sup>[159]</sup> It is noted that Co and Fe are both electrochemically active. In NaNi<sub>0.5</sub>Co<sub>0.5</sub>O<sub>2</sub>, the oxidation of Ni<sup>3+</sup> occurs before Co<sup>3+</sup>, but in NaNi<sub>0.5</sub>Fe<sub>0.5</sub>O<sub>2</sub>, the oxidation of Fe<sup>3+</sup> takes place before Ni<sup>3+</sup>, resulting in a significantly different mechanistic behavior, as revealed in *in-situ* XRD studies (Figure 8c, d). NaNi<sub>0.5</sub>Fe<sub>0.5</sub>O<sub>2</sub> has a smooth sloopy charge-discharge curve, demonstrating a simpler transition, from O<sub>3</sub> (1.0 ≥  $x$  ≥ 0.76 Na), via a two-phase reaction, to P3 (0.64 ≥  $x$  Na). In contrast, NaNi<sub>0.5</sub>Co<sub>0.5</sub>O<sub>2</sub> exhibits a multi-stair charge-discharge profile, corresponding to a highly complex phase transition. O<sub>3</sub>-NaNi<sub>0.5</sub>Co<sub>0.5</sub>O<sub>2</sub> undergoes a short solid-solution reaction (1.0 ≥  $x$  ≥ 0.96 Na), followed several two-phase reactions, turning into O'3 (1.0 ≥  $x$  ≥ 0.96 Na), P'3 (0.72 ≥  $x$  ≥ 0.66 Na), P3 (0.66 ≥  $x$  ≥ 0.58 Na), P''3 (0.58 ≥  $x$  ≥ 0.43 Na), and O''3 (0.39 ≥  $x$  Na). In the NaNi<sub>0.5</sub>Fe<sub>0.5</sub>O<sub>2</sub> system, the Ni<sup>4+</sup>/<sup>3+</sup> oxidation-reduction process makes a significant contribution to the entire capacity and suppresses the formation of unstable J-T Fe<sup>4+</sup>.<sup>[160]</sup> It is believed that the complex phase transition in NaNi<sub>0.5</sub>Co<sub>0.5</sub>O<sub>2</sub> was caused by strong Na–Na interactions leading to Na-vacancy ordering.<sup>[161]</sup> However, in the NaNi<sub>0.5</sub>Co<sub>0.5</sub>O<sub>2</sub> system, the charge density in the transition metal layers is more evenly distributed, stemming from the approximate energy states of Ni<sup>3+</sup> and Co<sup>3+</sup>.<sup>[162,163]</sup> This is because the disturbances caused by the arrangement of Ni and Fe are sufficient to disrupt the long-range order on the Na vacancy sublattice in NaNi<sub>0.5</sub>Fe<sub>0.5</sub>O<sub>2</sub>.<sup>[159]</sup> Furthermore, for NaNi<sub>0.5</sub>Fe<sub>0.5</sub>O<sub>2</sub>, excessive voltage (beyond 3.9 V) leads to the disappearance of the P3 phase, causing structural collapse and irreversible phase transitions, primarily due to the migration of Fe<sup>4+</sup>.<sup>[150,164,165]</sup> Therefore, it is believed that doping

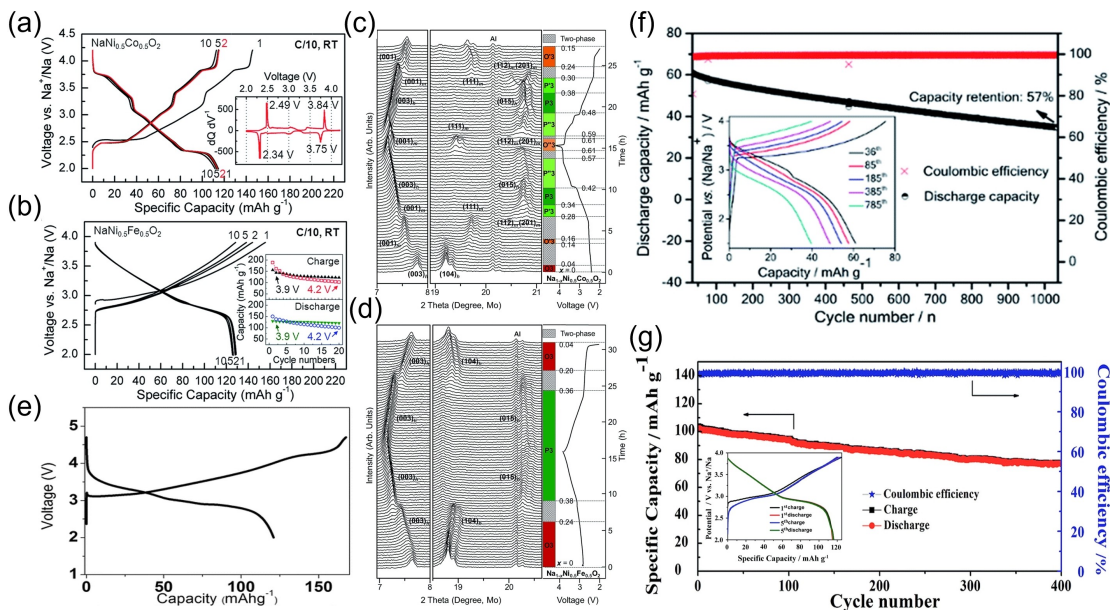


**Figure 8.** (a) Specific capacity of NaNi<sub>0.5</sub>Co<sub>0.5</sub>O<sub>2</sub> in 2.0–4.2 V at 0.1 C.<sup>[159]</sup> (b) Specific capacity of NaNi<sub>0.5</sub>Fe<sub>0.5</sub>O<sub>2</sub> in 2.0–3.9 V at 0.1 C.<sup>[159]</sup> (c) *In-situ* XRD patterns for NaNi<sub>0.5</sub>Co<sub>0.5</sub>O<sub>2</sub> from 2 to 4.2 V at C/24.<sup>[159]</sup> (d) *In-situ* XRD patterns for NaNi<sub>0.5</sub>Fe<sub>0.5</sub>O<sub>2</sub> to 3.9 V at C/24.<sup>[159]</sup> (e) Initial charge-discharge curve for NaFe<sub>1/3</sub>Ni<sub>1/3</sub>Ti<sub>1/3</sub>O<sub>2</sub> at 0.2 C between 2.0–4.7 V.<sup>[166]</sup> (f) Cycle performance at 2 C for NaFe<sub>1/3</sub>Ni<sub>1/3</sub>Ti<sub>1/3</sub>O<sub>2</sub>.<sup>[168]</sup> (g) Cyclic performances and specific capacity of the NaNi<sub>1/4</sub>Co<sub>1/4</sub>Fe<sub>1/4</sub>Ti<sub>1/4</sub>O<sub>2</sub> at 5 C.<sup>[172]</sup>

with inactive tetravalent elements can further enhance the cycling performance of  $\text{NaNi}_{0.5}\text{Fe}_{0.5}\text{O}_2$ .<sup>[159]</sup>

When Ti is introduced, the  $\text{NaNi}_{0.5}\text{Ti}_{0.5}\text{O}_2$  also forms an O3 structure. In the first cycle, the reversible capacity accomplishes 121 mAh.g<sup>-1</sup> (~0.49 Na) within the voltage range of 2.0–4.7 V at 0.2 C, with a Coulombic efficiency of only 70.6% (Figure 8e).<sup>[166]</sup> In  $\text{NaNi}_{0.5}\text{Ti}_{0.5}\text{O}_2$ , Ti is considered electrochemically inactive,<sup>[167,168]</sup> acting as a pillar to support the R-3m structure against sodium extraction and insertion, offering an outstanding cycle performance.<sup>[111,169]</sup> The O3-type  $\text{NaNi}_{0.5}\text{Ti}_{0.5}\text{O}_2$  retains 93% capacity after 100 cycles at 0.2 C and 75% capacity after 300 cycles at 1 C.<sup>[166]</sup> These three examples illustrate how the introduction of additional elements can serve as new redox centers or structural pillars, thereby significantly influencing the mechanistic behavior and, consequently, the electrochemical properties of Ni-based O3 cathodes.

Wang et al.<sup>[168]</sup> synthesized a new ternary O3- $\text{NaFe}_{1/3}\text{Ni}_{1/3}\text{Ti}_{1/3}\text{O}_2$  material using a solid-state reaction method. As shown in Figure 8f,  $\text{NaFe}_{1/3}\text{Ni}_{1/3}\text{Ti}_{1/3}\text{O}_2$  possess a reversible capacity of 117 mAh.g<sup>-1</sup> (~0.48 Na) in the first cycle, with a Coulombic efficiency of 83% at 0.1 C, within a voltage range of 1.5–4.0 V. Moreover, even after 1000 cycles at 2 C, the capacity retention remained as high as 57%. Notably, the Ti remains as pillars, and both Fe and Ni contribute to the redox reactions in  $\text{NaFe}_{1/3}\text{Ni}_{1/3}\text{Ti}_{1/3}\text{O}_2$ . Therefore, it can be expected that  $\text{NaFe}_{1/3}\text{Ni}_{1/3}\text{Ti}_{1/3}\text{O}_2$  heritages the advantages of both  $\text{NaFe}_{0.5}\text{Ni}_{0.5}\text{O}_2$  and  $\text{NaNi}_{0.5}\text{Ti}_{0.5}\text{O}_2$ . It's evident that the charge-discharge curve remains exceptionally smooth throughout the process, resembling that of  $\text{NaNi}_{0.5}\text{Fe}_{0.5}\text{O}_2$ . The presence of only reversible phases of O3 and P3, which is exactly the mechanistic behavior of the  $\text{NaNi}_{0.5}\text{Ti}_{0.5}\text{O}_2$ , during extraction and insertion, without the occurrence of monoclinic distortion, indicates the absence of the O'3 phase. This absence contributes to the outstanding capacity retention and improved structural stability.<sup>[168]</sup>

Undoubtedly, structural stability is gained in the presence of pillar elements, but at the expense of reduced redox centers or capacity performance. Subsequently, a ternary material,  $\text{NaNi}_{1/3}\text{Co}_{1/3}\text{Fe}_{1/3}\text{O}_2$ , was synthesized.<sup>[170]</sup> The  $\text{NaNi}_{1/3}\text{Co}_{1/3}\text{Fe}_{1/3}\text{O}_2$  is an O3-phase with R-3m structure. During the sodium extraction, Co and Fe are oxidized to 4+ before Ni, and all three ions maintain the 4+ state when completely de-sodiated. It possesses a specific capacity of 165 mAh.g<sup>-1</sup> (~0.69 Na) within the voltage range of 2.0–4.2 V at 0.05 C, resulting in an energy density of 500 Wh.kg<sup>-1</sup>, which is comparable to the commercial LiFePO<sub>4</sub>. Additionally, the material demonstrates exceptional rate performance, delivering a capacity of 80 mAh.g<sup>-1</sup> at 30 C. Incorporating Ni and Co effectively inhibits Fe migration within the oxide layers, significantly improving the rate performance and reversible capacity. However, discharge profiles confirm that the influence of Co still leads to complex phase transitions.<sup>[170]</sup> Therefore, the addition of Ni can effectively reduce the consumption of Co while maintaining the same specific capacity as  $\text{NaFe}_{0.5}\text{Co}_{0.5}\text{O}_2$  (160 mAh.g<sup>-1</sup> (~0.67 Na)).<sup>[171]</sup>

Following, a quaternary Ni-based layered oxide cathode material,  $\text{NaNi}_{1/4}\text{Co}_{1/4}\text{Fe}_{1/4}\text{Ti}_{1/4}\text{O}_2$ , has been investigated, and it has been confirmed to possess an O3-type layered oxide structure through XRD analysis. During charging and discharg-

ing, Ni, Co, and Fe ions undergo redox reactions to balance charges, while the oxidation state of Ti ions remains unchanged. In-situ XRD analysis reveals the phase evolution of  $\text{NaNi}_{1/4}\text{Co}_{1/4}\text{Fe}_{1/4}\text{Ti}_{1/4}\text{O}_2$  from O3 to O3 + P3 to P3, highlighting a highly reversible phase transition. It delivered a specific capacity of 116 mAh.g<sup>-1</sup> (~0.47 Na) in the initial cycle within a voltage range of 2.0 to 3.9 V at 0.1 C. Moreover, it demonstrates a relatively high capacity retention of 75% after 400 cycles at 5 C (Figure 8g). The substitution of Ti effectively mitigates the migration of  $\text{Fe}^{3+/4+}$  within the structural layers, resulting in smoother discharge profiles compared to O3-NaNiCoFe during the Na insertion and extraction processes.<sup>[172]</sup>

Owing to the successful example of introducing Co and Al in  $\text{LiNiO}_2$ , Zhou et al.<sup>[156]</sup> synthesized a monoclinic O'3- $\text{NaNi}_{0.8}\text{Co}_{0.15}\text{Al}_{0.05}\text{O}_2$  (Na-NCA) cathode. It is believed that Co improves the electrochemical performance, and Al forms stable Al-O bonds to enhance safety and stability.<sup>[173–181]</sup> It is also noted that the addition of a small amount of  $\text{Al}^{3+}$  and  $\text{Co}^{3+}$  did not change the structure of monoclinic  $\text{NaNiO}_2$ . In Na-NCA, all three elements exist in the 3+, with a small presence of  $\text{Ni}^{2+}$ . O'3- $\text{NaNi}_{0.8}\text{Co}_{0.15}\text{Al}_{0.05}\text{O}_2$  cathode exhibited an initial reversible capacity of 153.4 mAh.g<sup>-1</sup> at 2.0–3.8 V and 0.1 C, and the capacity retention rate was 86.7% after 200 cycles, as shown in Figure 9a. However, as typical Ni-based O'3 cathodes, multiple plateaus were observed in the charge-discharge curves, which were attributed to the phase transition of O'3-O1-P3 caused by the sliding of TMO<sub>2</sub> slabs.<sup>[111,182]</sup> Characterization results using SEM and XRD showed that  $\text{Al}^{3+}$  and  $\text{Co}^{3+}$  effectively alleviated irreversible phase transitions, enhanced structural stability, and provided better pathways for  $\text{Na}^+$  transport.<sup>[156]</sup>

By quenching and slow cooling, Zheng et al.<sup>[183]</sup> modified the structure of Na-NCA into a hexagonal O3 and a monoclinic O'3 structure. The formation of the monoclinic O'3 Na-NCA at room temperature is attributed to the J-T effect of  $\text{Ni}^{3+}$ . The quenching process allows the Na-NCA to retain its high-temperature form, a hexagonal O3 structure at 450 and 500 K.<sup>[120]</sup> Quenched O3 Na-NCA exhibits a higher reversible capacity (162 mAh.g<sup>-1</sup>) in the first cycle at 0.1 C within 1.5–4.5 V window, while the slow-cooled O'3 Na-NCA shows a capacity of 150 mAh.g<sup>-1</sup> (Figure 9b, c). Although O'3 Na-NCA demonstrates higher rate performance than O3 Na-NCA (Figure 9d), O'3 Na-NCA (Figure 9e) exhibits a high irreversible capacity, due to multi-staircase transitions, similar to O'3  $\text{NaNiO}_2$ . Conversely, O3 Na-NCA exhibits enhanced reversibility, which can be attributed to quenching, leading to a higher concentration of oxygen vacancies within the material's oxide layer.<sup>[184,185]</sup> Notwithstanding, several plateaus persist within both O3 Na-NCA and O'3 Na-NCA. This work shed light on utilizing high-temperature thermal motion to overcome the J-T effect of certain elements, enabling the formation of a higher symmetric space group R3-m for cathode materials.

#### 4.2. Mn-Based (C2/m, O'3)

Mn-based layered oxides have been extensively studied due to their relative ease of synthesis, wide-ranging applications, and

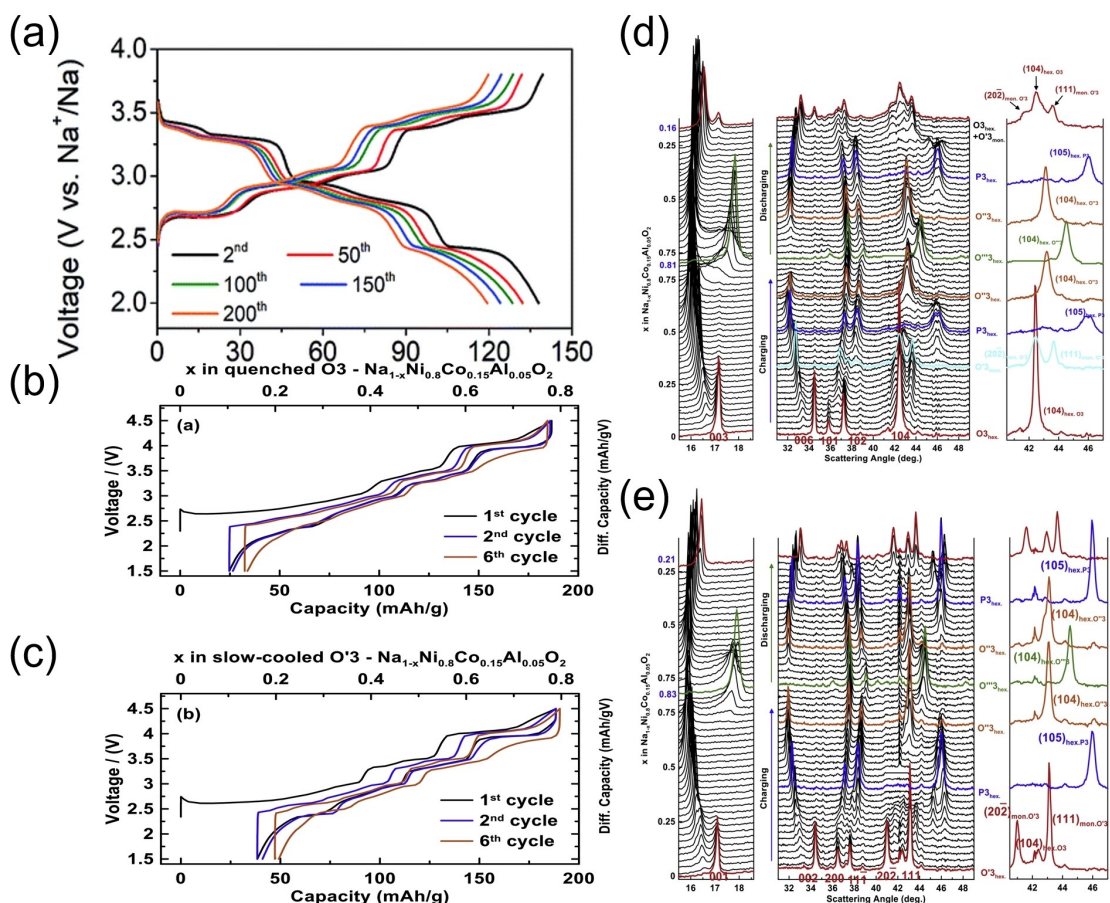


**Figure 9.** (a) Cycle performance for  $\text{NaNi}_{0.8}\text{Co}_{0.15}\text{Al}_{0.05}\text{O}_2$  at 1 C.<sup>[156]</sup> (e) Charge-discharge curve for Quenched O3 Na–NCA and Slow-cooled O'3 Na–NCA.<sup>[183]</sup> (f) In situ XRD patterns for O3 Na-NCA and O'3 Na-NCA.<sup>[183]</sup>

some of the best specific capacities. As mentioned above, the Mn-based O3-type unary layered SIB cathode exhibits the highest discharged capacity. While these materials have not yet achieved the performance of the best SIB materials, this fact offers hope for finding competitive materials from both performance and cost perspectives. Therefore, the research objective is to enhance the electrochemical performance of Mn-based transition metal (TM) layered oxides while maintaining low cost, particularly in compounds rich in inexpensive and abundant TMs such as Fe. In 2015, De Boisse et al.<sup>[110]</sup> studied the O'3-type  $\text{Na}_x\text{Mn}_{1/3}\text{Fe}_{2/3}\text{O}_2$  material as an SIB cathode. After Fe doping, the cathode structure remains in the O'3 form. Within this material, Mn is oxidized preferentially over Fe; therefore, in the preliminary stage of sodium extraction ( $0.96 > x > 0.84$ ), a monoclinic distortion similar to  $\text{NaMnO}_2$  is observed. The overall phase transition process goes from O'3 to O3 to P3 to O3 + O1 to P3 + O'. Such  $\text{Na}_x\text{Mn}_{1/3}\text{Fe}_{2/3}\text{O}_2$  cathode delivers a reversible capacity of  $157.47 \text{ mAh.g}^{-1}$  (~0.65 Na) at a rate of 0.1 C within 1.5–4.2 V during the initial cycles (Figure 10a).<sup>[186]</sup>

While O'3- $\text{Na}_x\text{Fe}_{1-y}\text{Mn}_y\text{O}_2$  has made significant progress in terms of economic cost, its electrochemical performance and air stability are not desirable. Mu et al.<sup>[107]</sup> introduced Cu as second electrochemically active dopant and formed a novel O3- $\text{Na}_{0.9}[\text{Cu}_{0.22}\text{Fe}_{0.30}\text{Mn}_{0.48}]\text{O}_2$  layered oxide material, which exhibits

improved air stability and cost savings. The introduction of Cu turns the O'3- $\text{Na}_x\text{Fe}_{1-y}\text{Mn}_y\text{O}_2$  into a typical O3 structure. As expected, the O3- $\text{Na}_{0.9}[\text{Cu}_{0.22}\text{Fe}_{0.30}\text{Mn}_{0.48}]\text{O}_2$  possessed a reversible capacity of  $100 \text{ mAh.g}^{-1}$  (~0.42 Na) with a Coulombic efficiency of 90.4% and a high-capacity retention of 97% after 100 cycles, within the 2.5–4.05 V voltage window, at 0.1 C (Figure 10b). The O3- $\text{Na}_{0.9}[\text{Cu}_{0.22}\text{Fe}_{0.30}\text{Mn}_{0.48}]\text{O}_2$  also exhibited an excellent cycle performance (nearly 100% retention after 100 cycles) and reversible capacity ( $300 \text{ mAh.g}^{-1}$  at 0.5 C) within a full cell (Figure 10c). The phase transition process of O3- $\text{Na}_{0.9}[\text{Cu}_{0.22}\text{Fe}_{0.30}\text{Mn}_{0.48}]\text{O}_2$  is revealed, with the transition from O3 to O3 + P3 (3.2–3.3 V) to P3 (3.3–3.98 V) to O'3 (>3.98 V) being highly reversible between 2.5 and 4.1 V at a 0.1 C.<sup>[107]</sup> Moreover, experimental data analysis exhibits that  $\text{Cu}^{2+}$  is oxidized to  $\text{Cu}^{3+}$  during Na deintercalation and intercalation.<sup>[187–189]</sup> Therefore, the incorporation of Cu not only prevents material from complex phase transitions, but also enhances the average working voltage, thereby improving the reversibility and energy density of materials.<sup>[190]</sup> Notably, it also demonstrates excellent air stability compared to the O3- $\text{NaFe}_{1/2}\text{Mn}_{1/2}\text{O}_2$  sample.<sup>[107]</sup>

Following, Zhang et al.<sup>[191]</sup> introduced Nb to Mn/Fe-based O'3 cathode and formed O3-type  $\text{NaFe}_{0.55}\text{Mn}_{0.45-x}\text{Nb}_x\text{O}_2$  ( $x=0, 0.01, 0.02, 0.03$ ). It has been revealed that the Nb-doping effectively controls the sliding effect in  $\text{TMO}_2$  as Nb increases

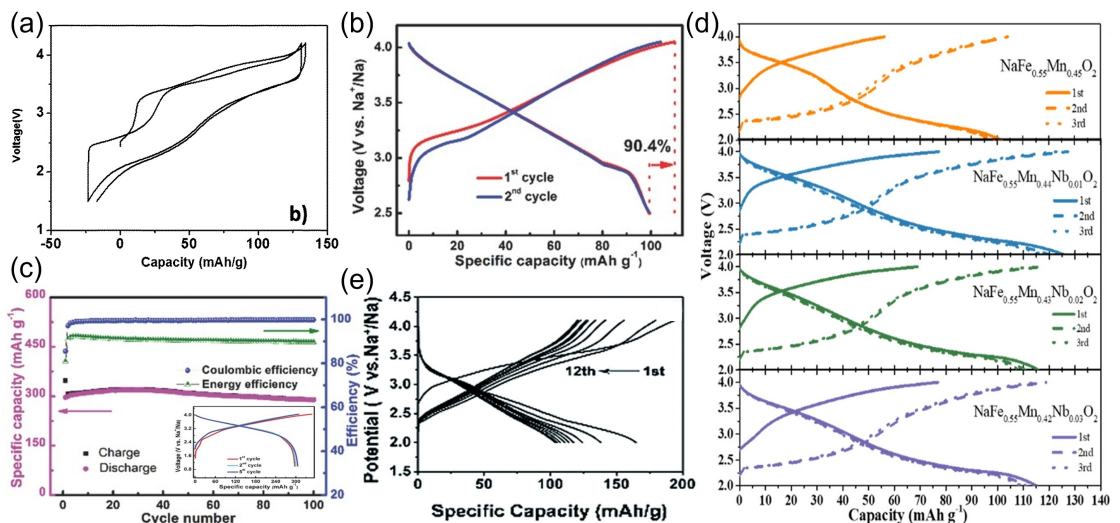


**Figure 10.** (a) Charge-discharge curve for  $\text{NaFe}_{2/3}\text{Mn}_{1/3}\text{O}_2$  within the 1<sup>st</sup> and 2<sup>nd</sup> cycles.<sup>[186]</sup> (b) Charge-discharge curve for  $\text{Na}_0.9[\text{Cu}_{0.22}\text{Fe}_{0.30}\text{Mn}_{0.48}]\text{O}_2$  between 2.5 and 4.05 V at 0.1 C.<sup>[107]</sup> (c) Cycle performance and charge-discharge curves of the full cell for  $\text{Na}_0.9[\text{Cu}_{0.22}\text{Fe}_{0.30}\text{Mn}_{0.48}]\text{O}_2$  within 1–4.05 V at a 0.5 C.<sup>[107]</sup> (d) Charge-discharge curve for  $\text{NaFe}_{0.55}\text{Mn}_{0.45-x}\text{Nb}_x\text{O}_2$  ( $x = 0, 0.01, 0.02, 0.03$ ).<sup>[191]</sup> (e) Cycling curves of the  $\text{NaCr}_{1/3}\text{Fe}_{1/3}\text{Mn}_{1/3}\text{O}_2$  at 0.03 C between 2.0–4.1 V.<sup>[128]</sup>

the interlayer spacing significantly, thus improving the diffusion rate of  $\text{Na}^+$ . A lower diffusion rate of  $\text{Na}^+$  can lead to severe sliding of the  $\text{TMO}_2$  plates during the O3-P3 phase transition.<sup>[192]</sup> The O3-type  $\text{NaFe}_{0.55}\text{Mn}_{0.45-x}\text{Nb}_x\text{O}_2$  cathode material delivered a reversible capacity of  $127.4 \text{ mAh.g}^{-1}$  ( $\sim 0.58 \text{ Na}$ ) within the voltage range of 2.0–4.0 V at 0.1 C and exhibited an excellent rate performance ( $45 \text{ mAh.g}^{-1}$  at 5 C) and more stable cycling (maintaining 65.6% capacity retention after 200 cycles) compared to  $\text{NaFe}_{0.55}\text{Mn}_{0.45}\text{O}_2$  at  $x = 0.01$  (Figure 10d).<sup>[191]</sup> However, when  $x > 0.02$ , the electrochemical performance of  $\text{NaFe}_{0.55}\text{Mn}_{0.45-x}\text{Nb}_x\text{O}_2$  cathodes is slightly declined.<sup>[186,193]</sup> Furthermore, the substitution of Nb effectively suppresses the reduction of  $\text{Mn}^{4+}$  without J-T effect to  $\text{Mn}^{3+}$  with a stronger J-T effect, thereby further enhancing the structural stability.<sup>[194,195]</sup>

Apart from the heavy Cu or Nb, electrochemically active Cr is also introduced as a dopant to form a new type O3-type  $\text{NaCr}_{1/3}\text{Fe}_{1/3}\text{Mn}_{1/3}\text{O}_2$ .<sup>[128]</sup> During the electrochemical reaction, Fe, Mn, and Cr undergo a redox between 3+ and 4+, while, as revealed by XAS,  $\text{Cr}^{4+}$  can be further oxidised into  $\text{Cr}^{4.2+}$ , effectively eliminating the disproportionation reaction during extraction and insertion processes.<sup>[128]</sup> Given the extra  $\text{Cr}^{4++4.2+}$  reaction, the  $\text{NaCr}_{1/3}\text{Fe}_{1/3}\text{Mn}_{1/3}\text{O}_2$  delivered a reversible specific capacity of  $165 \text{ mAh.g}^{-1}$  ( $\sim 0.67 \text{ Na}$ ) (2–4.1 V) and  $186 \text{ mAh.g}^{-1}$  ( $\sim 0.76 \text{ Na}$ ) (1.5–4.2 V) at 0.05 C (Figure 10e). The formation of  $\text{Cr}^{4.2+}$  ions also enables more Cr ions, as stably situated in octahedral positions, to undergo reversible multi-electron redox reactions during cycling. However, in-situ XRD confirmed that O3-type  $\text{NaCr}_{1/3}\text{Fe}_{1/3}\text{Mn}_{1/3}\text{O}_2$  cathode experiences the poorly reversible phase transition processes O3-(O3 + P3)-(P3 + O3'')-O3'', resulting in a less satisfactory cycle performance.<sup>[128]</sup>

### 4.3. Ni/Mn Synergistic System

Combining the both advantages of Ni and Mn redox reactions, nowadays, O3-type Ni/Mn-based binary layered metal oxides have been the most extensively studied in sodium-ion cathode materials. Ni/Mn-based materials have a major imminent advantage compared to others, as the involvement of Ni in redox reactions enables higher operating voltages, while Mn provides higher specific capacity to the material.<sup>[68]</sup> However, in the O3-type cathode, Ni/Mn-based compositions are particularly representative deficient, as they exhibit a complex phase transition that encompasses nearly all structural transformations within the O3 phase because of the J-T effect of  $\text{Mn}^{4+}$ .<sup>[79,104,108,109]</sup> Researchers improved and fine-tuned the electrochemical performance of Ni/Mn-based cathode materials by substituting and doping TM elements, thus alleviating and mitigating the issues above.<sup>[97,104,107,117,196]</sup> Consequently, Ni/Mn-based compositions have become the most popular O3-type sodium-ion cathode materials.

In 2012, Komaba et al.<sup>[197]</sup> reported the electrochemical performance of the O3- $\text{NaNi}_{1/2}\text{Mn}_{1/2}\text{O}_2$  system, which possesses a rhombohedral symmetry (space group:  $R\bar{3}-m$ ). During the sodium extraction/insertion processes, it was observed that in the Ni/Mn-based only  $\text{Ni}^{3+}$  undergoes oxidation-reduction, transitioning between  $\text{Ni}^{2+}$  and  $\text{Ni}^{4+}$ , while the Mn ion is in the +3 state that is inert and does not exhibit electrochemical activity.<sup>[198]</sup> Moreover, a sophisticated structural evolution during the process from O3hex. to O'3mon., P3hex., P'3mon., and P3''hex phases was revealed. At a rate of 0.02 C,  $\text{NaNi}_{1/2}\text{Mn}_{1/2}\text{O}_2$  exhibited a high initial discharge specific capacity of  $185 \text{ mAh.g}^{-1}$  ( $\sim 0.77 \text{ Na}$ ) between 2.2 and 4.5 V, while the initial discharge capacity within the range of 2.2 to 3.8 V was only  $125 \text{ mAh.g}^{-1}$  ( $\sim 0.52 \text{ Na}$ ) (Figure 11a). However, after 50 cycles, capacity retention rates were 75% at 1/30 C with cutoff voltages of 2.2 and 3.8 V. It has been reported that different

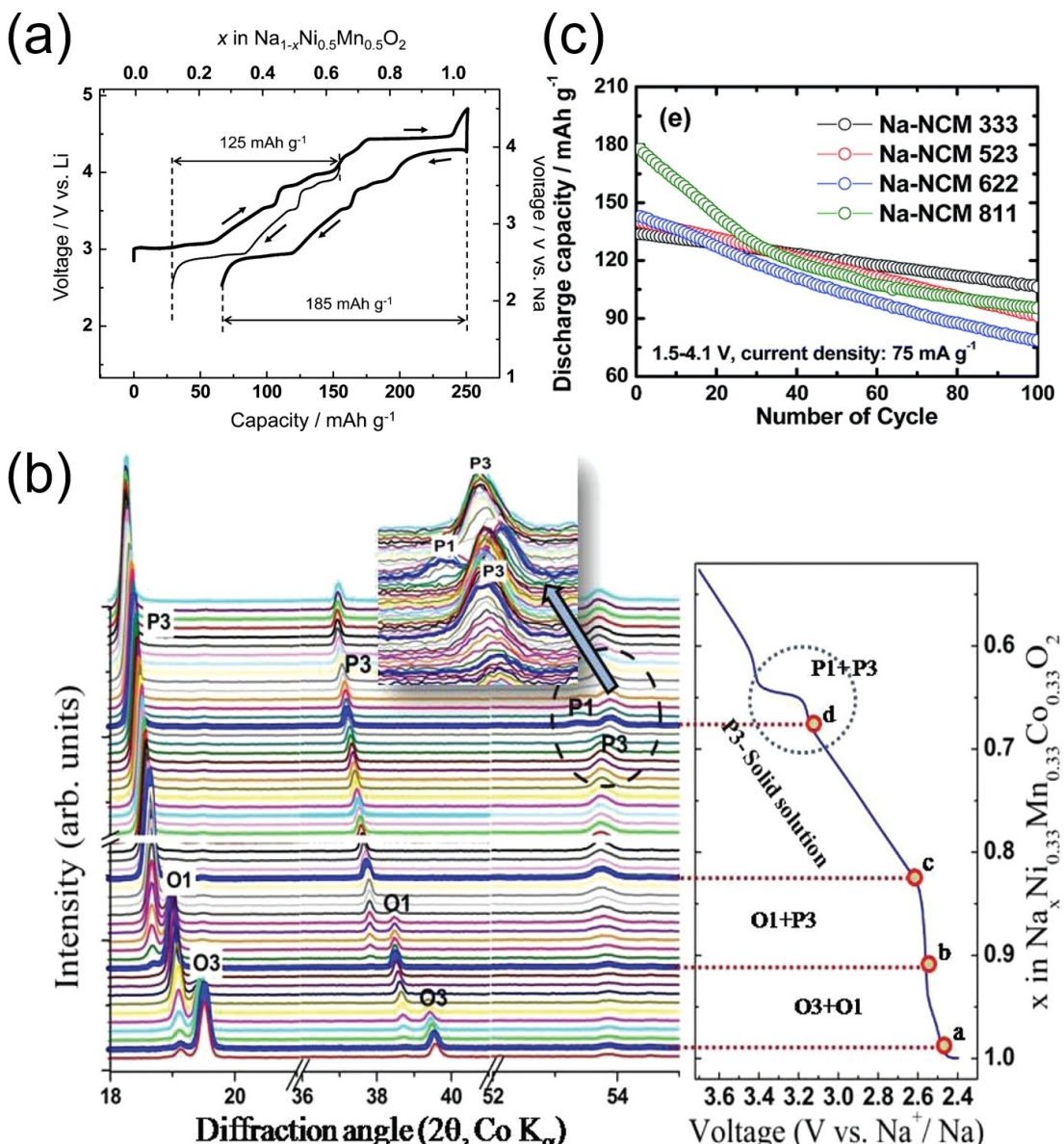


**Figure 11.** (a) Charge-discharge curves of  $\text{NaNi}_{1-x}\text{Mn}_{1/2}\text{O}_2$  in 2.2–3.8 and 2.2–4.5 V at 0.02 C.<sup>[197]</sup> (b) In situ X-ray diffraction patterns for  $\text{NaNi}_{1/3}\text{Mn}_{1/3}\text{Co}_{1/3}\text{O}_2$  within 2.4–3.7 V at 0.05 C.<sup>[182]</sup> (c) Cycling performance for O3-Na $[\text{Ni}_x\text{Co}_y\text{Mn}_z]\text{O}_2$  ( $x = 1/3, 0.5, 0.6, \text{ and } 0.8$ ) within 1.5–4.1 V at 75 mA g<sup>-1</sup>; as Na-NCM 333 for  $x = 1/3$ , Na-NCM 523 for  $x = 0.5$ , Na-NCM 622 for  $x = 0.6$ , and Na-NCM 811 for  $x = 0.8$ .<sup>[206]</sup>

synthesis methods can lead to different performance. For example, Wang et al.<sup>[199]</sup> used a sol-gel method to synthesize O3- $\text{NaNi}_{1/2}\text{Mn}_{1/2}\text{O}_2$ , which exhibits better capacity retention, with 90% of the reversible capacity (127 mAh.g<sup>-1</sup>) still maintained after 100 cycles in the voltage range of 2.0–4.0 V. Similar results have also been reported the sol-gel-prepared  $\text{NaNi}_{0.5}\text{Mn}_{0.5}\text{O}_2$ .<sup>[117,197,200]</sup>

Due to the challenges posed by complex phase transformations during the  $\text{Na}^+$  deintercalation for  $\text{NaNi}_x\text{Mn}_{1-x}\text{O}_2$ , it has been demonstrated that the incorporation of additional redox centers (such as Co, Fe, Ti, Cu, Zn, etc.) and charge carriers or pillars (such as Li and Mg) to form ternary and quaternary O3 cathode is an effective approach to mitigate this issue.<sup>[201–203]</sup>

As heritage from the success of commercial  $\text{LiNi}_{1/3}\text{Mn}_{1/3}\text{Co}_{1/3}\text{O}_2$ ,<sup>[204]</sup> Co is introduced to form a new type of O3-type  $\text{NaNi}_{1/3}\text{Mn}_{1/3}\text{Co}_{1/3}\text{O}_2$ , which combines the cost-effectiveness of  $\text{Na}_x\text{MnO}_2$ , excellent electrochemical performance of  $\text{Na}_x\text{CoO}_2$ , and higher working voltage of  $\text{Na}_x\text{NiO}_2$ <sup>[182,205,206]</sup> for use in SIBs. However, in-situ X-ray diffraction reveals a phase evolution O3 + O1 ( $1.0 \geq x \geq 0.90$ ) to O1 ( $x = 0.90$ ) to O1 + P3 ( $0.90 \geq x \geq 0.82$ ) to P3 ( $0.83 \geq x \geq 0.67$ ) to P1 + P3 ( $0.67 \geq x \geq 0.60$ ), and ultimately to P3 ( $0.60 \geq x$ ) (Figure 11b),<sup>[182]</sup> which is entirely distinct from the phase evolution observed in O'3- $\text{NaNi}_{1/2}\text{Mn}_{1/2}\text{O}_2$ . The different mechanistic behavior signifies the contribution of Co. It exhibits a reversible capacity of 120 mAh.g<sup>-1</sup> (~0.5 Na) in the voltage range of 2–3.75 V at 0.1 C, but it can merely deliver a capacity of 80 mAh.g<sup>-1</sup> (~0.34 Na) at 1 C, which

could be attributed to the relatively poor kinetics of this material. Additionally, it demonstrates that the generated O<sub>1</sub> phase is air sensitive, resulting in the production of NaNi<sub>1/3</sub>Mn<sub>1/3</sub>Co<sub>1/3</sub>O<sub>2</sub>·H<sub>2</sub>O hydrate phase when exposed to air.<sup>[182]</sup> Hwang et al.<sup>[206]</sup> conducted a comprehensive study of O<sub>3</sub>-Na<sub>x</sub>Ni<sub>y</sub>Co<sub>z</sub>Mn<sub>w</sub>O<sub>2</sub> by varying the Ni, Co, and Mn ratio, as the typical LiNi<sub>x</sub>Mn<sub>y</sub>Co<sub>z</sub>O<sub>2</sub> in LIBs. Figure 11c illustrates the charge-discharge voltage curves of Na[Ni<sub>x</sub>Co<sub>y</sub>Mn<sub>z</sub>]O<sub>2</sub> in the range of 1.5–4.1 V. It can be observed that as the Ni content increases,  $x=0.8$  exhibits the highest specific capacity (187.1 mAh.g<sup>-1</sup> (~0.79 Na)). However, the capacity retention is inversely correlation to the Ni content, with  $x=0.8$  merely retaining 50% compared to 76.5% for  $x=1/3$  after 100 cycles. This is due to the fact that a certain amount of Co can improve electronic conductivity and stabilize the layered structure.<sup>[171,207]</sup> Mn, on the other hand, can contribute to better cycling performance and thermal stability of the material. However, an excessive

amount of Ni<sup>4+</sup> ( $x>60\%$ ) can lead to electrolyte decomposition, resulting in a decline in comprehensive electrochemical performance.<sup>[208]</sup> These studies further suggest that the interplay of TM ratios can bring about different electrochemical performance and mechanistic behavior.

Due to the abundance and cost of Fe, it is frequently utilized to partially substitute Ni and Mn, to achieve better electrochemical performance and structural stability. In 2012, it was reported that Na<sub>1-y</sub>(Ni<sub>1/3</sub>Fe<sub>1/3</sub>Mn<sub>1/3</sub>)O<sub>2</sub> maintains a capacity of 100 mAh.g<sup>-1</sup> (~0.42 Na) over 150 cycles between 1.5 and 4.0 V at 0.5 C with a Coulombic efficiency of 99% (Figure 12a).<sup>[209]</sup> Following, the influence of Fe content ( $x=0, 0.1, 0.2, 0.3, 0.4$ , and 1) on electrochemical performance was studied in O<sub>3</sub>-NaFe<sub>x</sub>(Ni<sub>0.5</sub>Mn<sub>0.5</sub>)<sub>1-x</sub>O<sub>2</sub>.<sup>[117]</sup> These materials exhibits better stability in air compared to NaFeO<sub>2</sub>.<sup>[210]</sup> Notably, O<sub>3</sub>-NaFe<sub>0.2</sub>(Ni<sub>0.5</sub>Mn<sub>0.5</sub>)<sub>0.8</sub>O<sub>2</sub> ( $x=0.2$ ) shows the lowest sodium/vacancy ordering. It achieves the best reversible capacity of

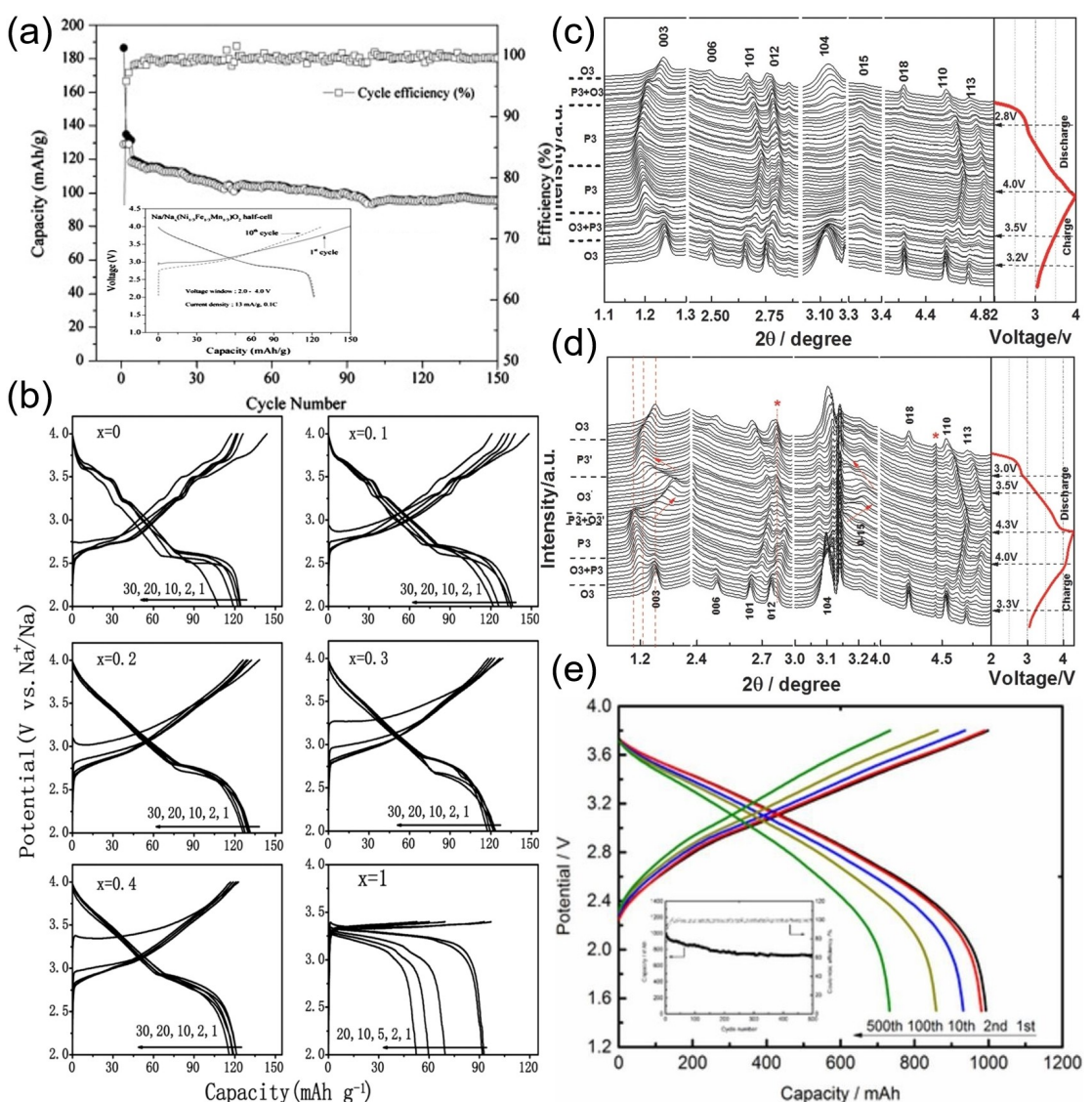


**Figure 12.** (a) Charge-discharge curves and cycling after 150 cycle for Na<sub>1-y</sub>(Ni<sub>1/3</sub>Fe<sub>1/3</sub>Mn<sub>1/3</sub>)O<sub>2</sub> between 1.5 and 4.1 V at 0.5 C.<sup>[209]</sup> (b) Charge-discharge curves of NaFe<sub>x</sub>(Ni<sub>0.5</sub>Mn<sub>0.5</sub>)<sub>1-x</sub>O<sub>2</sub> ( $x=0, 0.1, 0.2, 0.3, 0.4$  and 1) between 2.0 and 4.0 V at 0.05 C.<sup>[117]</sup> In situ XRD of Na<sub>1-y</sub>Ni<sub>1/3</sub>Fe<sub>1/3</sub>Mn<sub>1/3</sub>O<sub>2</sub> (c) within 2.0–4.0 V and (d) within 2.0–4.3 V.<sup>[211]</sup> (e) Cycling performance of NaNi<sub>1/3</sub>Fe<sub>1/3</sub>Mn<sub>1/3</sub>O<sub>2</sub> in soft-packed SIB between 1.5 and 3.8 V at 1 C rate.<sup>[212]</sup>

131 mAh.g<sup>-1</sup> between 2.0 and 4.0 V at 0.05 C (Figure 12b).<sup>[117]</sup> Nevertheless, at high Fe content, O3-NaNi<sub>0.25</sub>Fe<sub>0.5</sub>Mn<sub>0.25</sub>O<sub>2</sub> achieves a higher initial discharge capacity of 140 mAh.g<sup>-1</sup> with a Coulombic efficiency of 93% at a 0.1 C rate in the voltage range of 2.1–3.9 V. Even at a rate of 10 C, it still delivers approximately 85 mAh.g<sup>-1</sup><sup>[210]</sup> and 86 mAh.g<sup>-1</sup><sup>[117]</sup> respectively, which can be attributed to weak electrostatic interactions that promote longer alkali metal-oxygen bonding, enhancing the diffusion capability of Na<sup>+</sup>.

Xie et al.<sup>[211]</sup> conducted further investigations on NaNi<sub>1/3</sub>Fe<sub>1/3</sub>Mn<sub>1/3</sub>O<sub>2</sub>, which revealed that the Na<sub>1-δ</sub>Ni<sub>1/3</sub>Fe<sub>1/3</sub>Mn<sub>1/3</sub>O<sub>2</sub> did not undergo monoclinic phase transition (O3-P3-P3-O3) and is a high reversible during Na<sup>+</sup> extraction/insertion at voltages below 4.0 V (Figure 12c). Nevertheless, in the voltage range of 3.0–4.3 V, two new phases are formed, namely O3' and P3' (Figure 12d). This is mainly due to the fact that below 4.0 V, only Ni is oxidized to a higher valence state of Ni<sup>3+</sup>, whereas under voltages up to 4.3 V, both Ni and Fe are oxidized to 4+. Moreover, through Fe substitution, NaFe<sub>0.2</sub>Mn<sub>0.4</sub>Ni<sub>0.4</sub>O<sub>2</sub> can form a more stable OP2 phase over 4.3 V that had smaller interlayer spacing (5.13 Å) than P3'' phase (5.72 Å), which effectively suppresses both insertions of electrolyte anions and solvent molecules and boost cycling stability.<sup>[114,117]</sup> Moreover, NaFe<sub>0.2</sub>Mn<sub>0.4</sub>Ni<sub>0.4</sub>O<sub>2</sub> delivered a capacity retention rate exceeding 73% (Figure 12e) in soft-packed SIB after 500 cycles at 1 C.<sup>[212]</sup> Overall, the NaNi<sub>1/3</sub>Fe<sub>1/3</sub>Mn<sub>1/3</sub>O<sub>2</sub> is regarded as a highly promising cathode material for practical utilization in SIBs.

Notably, the Fe: Ni: Mn ratio is tricky but key to achieving better performance. For example, the O3-type NaNi<sub>0.6</sub>Fe<sub>0.25</sub>Mn<sub>0.15</sub>O<sub>2</sub> cathode exhibited an initial reversible specific capacity of 190 mAh.g<sup>-1</sup> (~0.8 Na) within 2.0–4.2 V at 0.1 C (Figure 13a) and 81.3% retention capacity (~152 mAh.g<sup>-1</sup>) after 200 cycles within 2.0–4.2 V at 0.5 C. Ni and Fe ions participated in charge compensation, while Mn ions remain at the 4+ oxidation state. The O3-type NaNi<sub>0.6</sub>Fe<sub>0.25</sub>Mn<sub>0.15</sub>O<sub>2</sub> undergoes a phase transition sequence of O3-O'3-P3-O3'' during Na<sup>+</sup> insertion/extraction, where the appearance of the O3'' phase deteriorated electrochemical performance due to its negative impact on Na<sup>+</sup> ion diffusion kinetics and structural stability, resulting in poor rate capability and cycling performance at higher voltages.<sup>[213]</sup> Subsequently, in 2023, NaNi<sub>2/3</sub>Mn<sub>1/6</sub>Fe<sub>1/6</sub>O<sub>2</sub> was fabricated by a high-temperature solid-state method, which demonstrated a well-formed crystalline O3 phase, characterized by hexagonal plate-like particles at 850 °C.<sup>[214]</sup> It exhibited an outstanding initial discharge capacity of 226 mAh.g<sup>-1</sup> (~0.94 Na) at a 0.2 C rate within the voltage range of 1.5–4.2 V, and after 100 cycles, it retained around 76% of its capacity.

Following the Fe introduction, Co is incorporated as the forth redox center and forms a quaternary O3-Na-(Mn<sub>0.25</sub>Fe<sub>0.25</sub>Co<sub>0.25</sub>Ni<sub>0.25</sub>)O<sub>2</sub>, which exhibited a higher specific capacity of 180 mAh.g<sup>-1</sup> (~0.75 Na) within 1.9–4.3 V (average 3.21 V) at 0.1 C (Figure 13b) and an impressive energy density of 578 Wh.kg<sup>-1</sup>.<sup>[69]</sup> Although the performance seems promising, O3-Na(Mn<sub>0.25</sub>Fe<sub>0.25</sub>Co<sub>0.25</sub>Ni<sub>0.25</sub>)O<sub>2</sub> undergoes a more smoothly

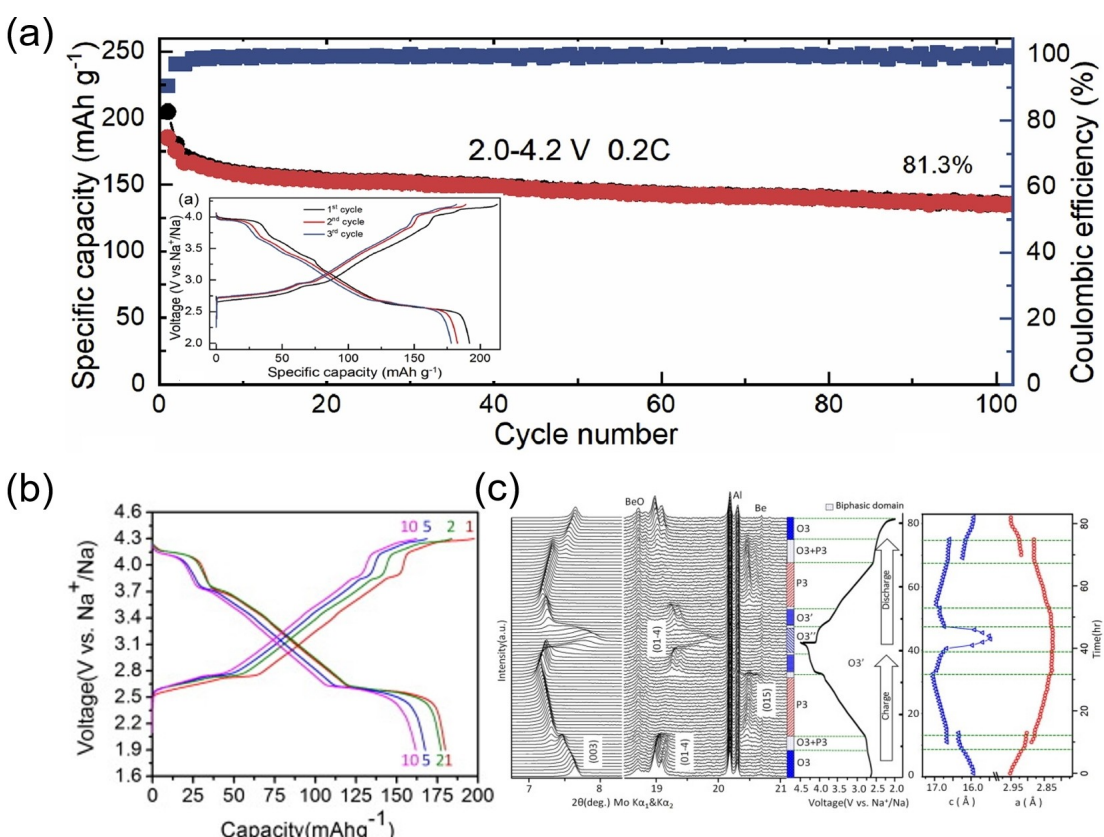


Figure 13. (a) Cycling performance and charge/discharge curves of the NaNi<sub>0.6</sub>Fe<sub>0.25</sub>Mn<sub>0.15</sub>O<sub>2</sub> in 2.0–4.0 V at 0.2 C after 100 cycles.<sup>[213]</sup> (b) Charge-discharge curves of Na(Mn<sub>0.25</sub>Fe<sub>0.25</sub>Co<sub>0.25</sub>Ni<sub>0.25</sub>)O<sub>2</sub> between 1.9 and 4.3 V at 0.1 C.<sup>[69]</sup> (c) In-situ XRD of Na(Mn<sub>0.25</sub>Fe<sub>0.25</sub>Co<sub>0.25</sub>Ni<sub>0.25</sub>)O<sub>2</sub> at 0.02 C.<sup>[69]</sup>

curved electrochemical profile and a phase transition (O3-P3-O3'-O3'') (Figure 13c), whereas the O3'' phase formed at above 4.25 V is not entirely reversible.<sup>[69]</sup> Therefore, in-depth investigations into phase transition mechanisms at high voltages will contribute to improving the reversible capacity and cycling stability of the material.

Apart from Fe, Ti<sup>4+</sup> also offers the advantages of abundant resources and low cost. Guo et al.<sup>[111]</sup> studied the O3-NaNi<sub>0.5</sub>Mn<sub>0.5-x</sub>Ti<sub>x</sub>O<sub>2</sub> ( $x=0, 0.1, 0.2, 0.3, 0.4$ , and  $0.5$ ) and reported that NaNi<sub>0.5</sub>Mn<sub>0.2</sub>Ti<sub>0.3</sub>O<sub>2</sub> ( $x=0.3$ ) exhibited a best reversible capacity of approximately 135 mAh.g<sup>-1</sup> (~0.55 Na) within 2.0-

4.0 V at 0.5 C (Figure 14a). After 200 cycles at a 1 C rate, NaNi<sub>0.5</sub>Mn<sub>0.2</sub>Ti<sub>0.3</sub>O<sub>2</sub> showed a capacity retention rate of 85%, compared to only 11% for NaNi<sub>0.5</sub>Mn<sub>0.5</sub>O<sub>2</sub>. Even at a high rate of 5 C, it still delivered an impressive reversible capacity of 93 mAh.g<sup>-1</sup>.<sup>[111]</sup> Due to the slightly larger ionic radius of Ti<sup>4+</sup> (0.605 Å) compared to Mn<sup>4+</sup> (0.53 Å), it results in a longer bond length in the TMO, thereby increasing the interlayer spacing. Accordingly, this effectively suppresses the complex and irreversible multiphase transition of the O3 phase.<sup>[215]</sup>

Cu<sup>2+</sup> can act as a stabilizer in Na<sub>x</sub>MnO<sub>2</sub> by inhibiting the J-T distortion. This is because Cu<sup>2+</sup> can reduce the energy differ-

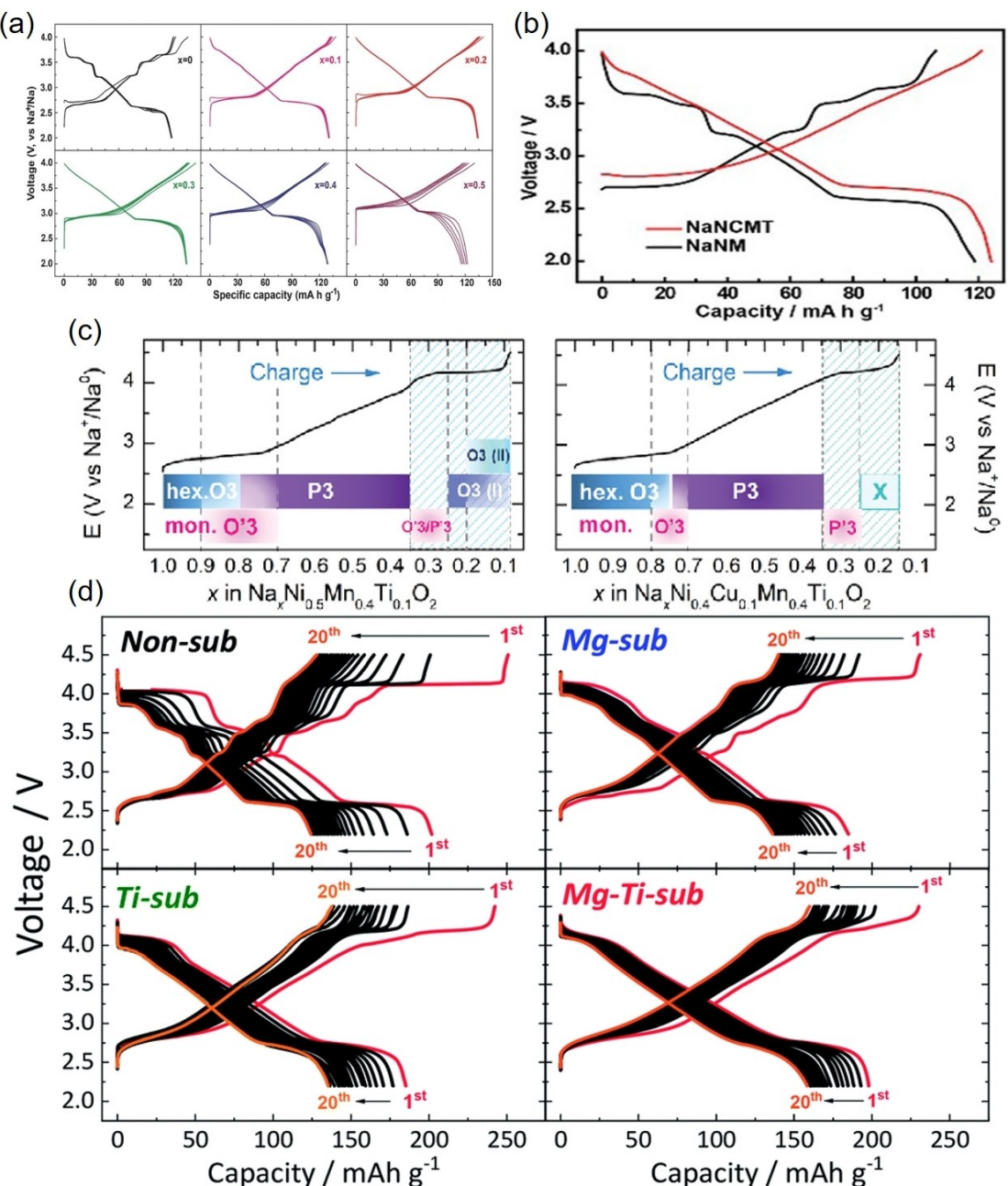


**Figure 14.** (a) Charge/discharge curves for O3-NaNi<sub>0.5</sub>Mn<sub>0.5-x</sub>Ti<sub>x</sub>O<sub>2</sub> ( $x=0, 0.1, 0.2, 0.3, 0.4$ , and  $0.5$ ) within 2.0–4.0 V at 0.5 C.<sup>[111]</sup> (b) First charge/discharge curves for O3-NaNi<sub>0.45</sub>Cu<sub>0.05</sub>Mn<sub>0.4</sub>Ti<sub>0.1</sub>O<sub>2</sub> and NaNi<sub>1/2</sub>Mn<sub>1/2</sub>O<sub>2</sub> between 2.0 and 4.0 V at 0.1 C.<sup>[218]</sup> (c) Phase transition and evolution of lattice parameters of NaNi<sub>0.5</sub>Mn<sub>0.4</sub>Ti<sub>0.1</sub>O<sub>2</sub> and NaNi<sub>0.4</sub>Cu<sub>0.1</sub>Mn<sub>0.4</sub>Ti<sub>0.1</sub>O<sub>2</sub>.<sup>[219]</sup> (d) Charge-discharge curve of Non-sub, Mg-sub, Ti-sub, and Mg-Ti-sub in voltage range of 2.2–4.5 V at a rate of 0.045 C.<sup>[220]</sup>

ence between the stacking of O and P.<sup>[216,217]</sup> Yao et al.<sup>[218]</sup> added Cu as the additional dopant and synthesized O<sub>3</sub>-NaNi<sub>0.45</sub>Cu<sub>0.05</sub>Mn<sub>0.4</sub>Ti<sub>0.1</sub>O<sub>2</sub> cathode material and found that the electrochemical performance of the substituted samples was significantly improved due to the inhibition of charge ordering and complex phase transitions (O<sub>3</sub>-P<sub>3</sub>) during cycling, achieving an initial discharge capacity of 124 mAh.g<sup>-1</sup> (~0.52 Na) between 2.0 and 4.0 V at 0.1 C (Figure 14b) and a 9-fold higher capacity retention rate compared to NaNi<sub>0.5</sub>Mn<sub>0.5</sub>O<sub>2</sub> after 500 cycles. Additionally, NaNi<sub>0.45</sub>Cu<sub>0.05</sub>Mn<sub>0.4</sub>Ti<sub>0.1</sub>O<sub>2</sub> shows an approximately 20-fold increase in air stability compared to NaNi<sub>0.5</sub>Mn<sub>0.5</sub>O<sub>2</sub> cathode material.

Afterward, comparative research on NaNi<sub>0.5-y</sub>Cu<sub>y</sub>Mn<sub>0.5-z</sub>Ti<sub>z</sub>O<sub>2</sub> ( $z=0.1\text{--}0.5$ ) was conducted<sup>[219]</sup> and it was found that the material ( $z=0.2$  and  $y=0.05$ ) achieves the highest specific capacity of 200 mAh.g<sup>-1</sup> (~0.83 Na) between 2 and 4.5 V at 0.1 C rate.<sup>[219]</sup> The in-situ XRD revealed only 3% contraction in lattice parameters/interlayer spacing, demonstrating the highest structure stability. It is noted that Ti addition doesn't prevent phase formation with significant lattice contraction during Na ion extraction/insertion<sup>[219]</sup> and Cu introduction smoothes charge-discharge curves (Figure 14c); no new O<sub>3</sub> phase was observed.

An electrochemically-inert Mg<sup>2+</sup> ion has also been explored as a substitution.<sup>[88]</sup> Kubota et al.<sup>[220]</sup> prepared O<sub>3</sub>-Na[Ni<sub>4/9</sub>Mn<sub>1/3</sub>Mg<sub>1/18</sub>Ti<sub>1/6</sub>]O<sub>2</sub> by doping Mg and Ti into the O<sub>3</sub>-type NaNi<sub>1/2</sub>Mn<sub>1/2</sub>O<sub>2</sub>, which showed a reversible capacity of 198 mAh.g<sup>-1</sup> (~0.75 Na) in voltage range of 2.2–4.5 V at a rate of 0.045 C. Nonetheless, after 50 cycles, the O<sub>3</sub>-Na[Ni<sub>4/9</sub>Mn<sub>1/3</sub>Mg<sub>1/18</sub>Ti<sub>1/6</sub>]O<sub>2</sub> cathode retained 70% of its capacity, while the Mg-substituted, Ti-substituted and non-substituted materials had retention rates of 60%, 60% and 43% (Figure 14d). The substitution of Ti<sup>4+</sup> ions and Mg<sup>2+</sup> ions led to the formation of a coexisting P-Oe phase (P<sub>3</sub>-OP<sub>2</sub> and OP<sub>2</sub>-O<sub>3</sub>) between P<sub>3</sub>-O<sub>3</sub> in Na[Ni<sub>4/9</sub>Mn<sub>1/3</sub>Mg<sub>1/18</sub>Ti<sub>1/6</sub>]O<sub>2</sub>, which enlarge TM-TM distance to delay the O<sub>3</sub>-O'<sub>3</sub> transition.<sup>[220]</sup> Moreover, in XRD analysis, it indicates that the phase composition of the NaNi<sub>1/2</sub>Mn<sub>1/2</sub>O<sub>2</sub> cathode is predominantly in the P<sub>3</sub> phase, indicating a highly irreversible phase transition. In contrast, the XRD of the NMMT displays two peaks that are (003) O<sub>3</sub> and (003) P<sub>3</sub>, with the (104) O<sub>3</sub> peak of the O<sub>3</sub> phase being notably pronounced, demonstrating a distinct single-phase transition (O<sub>3</sub>-P<sub>3</sub>) (Figure 15a).<sup>[221]</sup> The co-doping of Mg and Ti has proven advantageous that absorb micro-strain and alleviate distortion to improve structural stability and integrity. Furthermore, adding Mg as an effective HF scavenger prevented surface particle degradation from electrolyte attack.<sup>[222]</sup>

Subsequently, building upon prior research that demonstrated improved cycling stability in P<sub>2</sub>/P<sub>3</sub>/O<sub>3</sub> sodium layered oxides through the substitution of Cu<sup>2+</sup>, Mg<sup>2+</sup>, and Zn<sup>2+</sup>,<sup>[88,223–225]</sup> a team has conducted a comparative study utilizing Cu<sup>2+</sup>, Mg<sup>2+</sup>, and Zn<sup>2+</sup> as replacements for O<sub>3</sub>-NaNi<sub>0.5</sub>Mn<sub>0.5-x</sub>Ti<sub>x</sub>O<sub>2</sub>. Zn<sup>2+</sup> (0.73 Å) and Cu<sup>2+</sup> (0.74 Å) have the same ionic radius, but the former lacks redox and J-T activity. NaNi<sub>0.45</sub>Zn<sub>0.05</sub>Mn<sub>0.4</sub>Ti<sub>0.1</sub>O<sub>2</sub> exhibited a slightly lower reversible capacity of 165 mAh.g<sup>-1</sup> (~0.69 Na) in the voltage range of 1.2–4.4 V at 0.1 C<sup>[226]</sup> but showed superior cycling stability (approximately 85%) compared to O<sub>3</sub>-NaNi<sub>0.5</sub>Mn<sub>0.5-x</sub>Ti<sub>x</sub>O<sub>2</sub> (about 65%)

after 100 cycles (Figure 15b). In this comparative experiment, it can be demonstrated that Cu<sup>2+</sup> is involved in oxidation-reduction, whereas Zn<sup>2+</sup> behaves similarly to Mg<sup>2+</sup> as a pillar to support the structure against lattice strains due to the lack of oxidation-reduction activity. The phase transition process for NaNi<sub>0.45</sub>Zn<sub>0.05</sub>Mn<sub>0.4</sub>Ti<sub>0.1</sub>O<sub>2</sub> is as follows: O<sub>3</sub> to O'<sub>3</sub> to P<sub>3</sub> (2.5–4.0 V), the coexistence of P<sub>3</sub> and O<sub>1</sub> (4.0–4.5 V), and only O<sub>1</sub> phase (> 4.5 V). The two-phase stage of P<sub>3</sub>-O<sub>1</sub> with the delayed O<sub>1</sub> presence limits the metal ion migration and mitigated volume reduction during Na extraction/insertion, ensuring stability.<sup>[226]</sup>

It has been found that the introduction of a small amount of Li<sup>+</sup> can effectively enhance the electrochemical performance of O<sub>3</sub> cathode materials in terms of cycling performance over a wider voltage range. The role of introducing Li<sup>+</sup> into O<sub>3</sub>-type materials is considered to be a stabilizing pillar for the structure.<sup>[104,227,228]</sup> Liu et al.<sup>[229]</sup> prepared O<sub>3</sub>-Na<sub>0.78</sub>Li<sub>0.18</sub>Ni<sub>0.25</sub>Mn<sub>0.583</sub>O<sub>w</sub> by electrochemically ion exchange method with Li<sub>1.167</sub>Ni<sub>0.25</sub>Mn<sub>0.583</sub>O<sub>2</sub> as starting material. The O<sub>3</sub>-Na<sub>0.78</sub>Li<sub>0.18</sub>Ni<sub>0.25</sub>Mn<sub>0.583</sub>O<sub>w</sub> retains the O<sub>3</sub> structure up to 4.2 V, with 0.8 Na being extracted. The excellent structure stability of this material may be related to the tetrahedral Li formed during the initial lithiation, allowing the material to bypass the phase transition mechanisms observed in most O<sub>3</sub> compounds.<sup>[229]</sup> It demonstrated excellent initial charge/discharge capacity in the voltage range of 1.5–4.5 V, delivering 240 mAh.g<sup>-1</sup> (~0.92 Na) at 0.5 C (Figure 15c). It is noteworthy that, by incorporating a small amount of Li, the O<sub>3</sub> cathode surpassed the energy density of LiCoO<sub>2</sub> (560 Wh.kg<sup>-1</sup>) and LiFePO<sub>4</sub> (560 Wh.kg<sup>-1</sup>), reaching 675 Wh.kg<sup>-1</sup>, which remained high at 430 Wh.kg<sup>-1</sup> even in a full-cell SIB, making it the highest-performing sodium-ion battery reported to date.<sup>[230–232]</sup>

Following this, Zheng et al.<sup>[233]</sup> studied the O<sub>3</sub>-NaLi<sub>0.1</sub>Ni<sub>0.35</sub>Mn<sub>0.55</sub>O<sub>2</sub>, which undergoes a phase transition from O<sub>3</sub>, via a two-phase reaction of O<sub>3</sub>-O'<sub>3</sub>, to P<sub>3</sub>. Although the incorporation of Li<sup>+</sup> in O<sub>3</sub>-NaLi<sub>0.1</sub>Ni<sub>0.35</sub>Mn<sub>0.55</sub>O<sub>2</sub> can result in smoother charge-discharge curves, it appears that the function of Li<sup>+</sup> in O<sub>3</sub>-NaLi<sub>0.1</sub>Ni<sub>0.35</sub>Mn<sub>0.55</sub>O<sub>2</sub> does not prevent the phase transition of the O<sub>3</sub> structure into P<sub>3</sub> structure. O<sub>3</sub>-NaLi<sub>0.1</sub>Ni<sub>0.35</sub>Mn<sub>0.55</sub>O<sub>2</sub> can deliver an initial reversible capacity of 128 mAh.g<sup>-1</sup> (~0.51 Na) at 2.0–4.2 V under 0.1 C rate, maintaining an 85% capacity retention after 100 cycles (Figure 15d).<sup>[233]</sup> With an expanded voltage range (1.5–4.3 V), it could provide a specific capacity of 160 mAh.g<sup>-1</sup> (~0.56 Na). The extraction of Li<sup>+</sup> primarily occurs after the potential is reached to 3.6 V. During the Na<sup>+</sup> insertion process, some of the Li<sup>+</sup> is reinserted to the oxide layer. As the number of cycles increases, the amount of Li<sup>+</sup> continues to decrease, but the residual Li<sup>+</sup> amount does not affect the cycling stability of the material. Besides, the substitution of Li in the material led to the formation of a new phase called O'<sub>3</sub>, effectively mitigating the irreversibility of the phase transition between O<sub>3</sub> and P<sub>3</sub> and significantly enhancing electrochemistry performance, especially at wider working potential regions.<sup>[233]</sup>

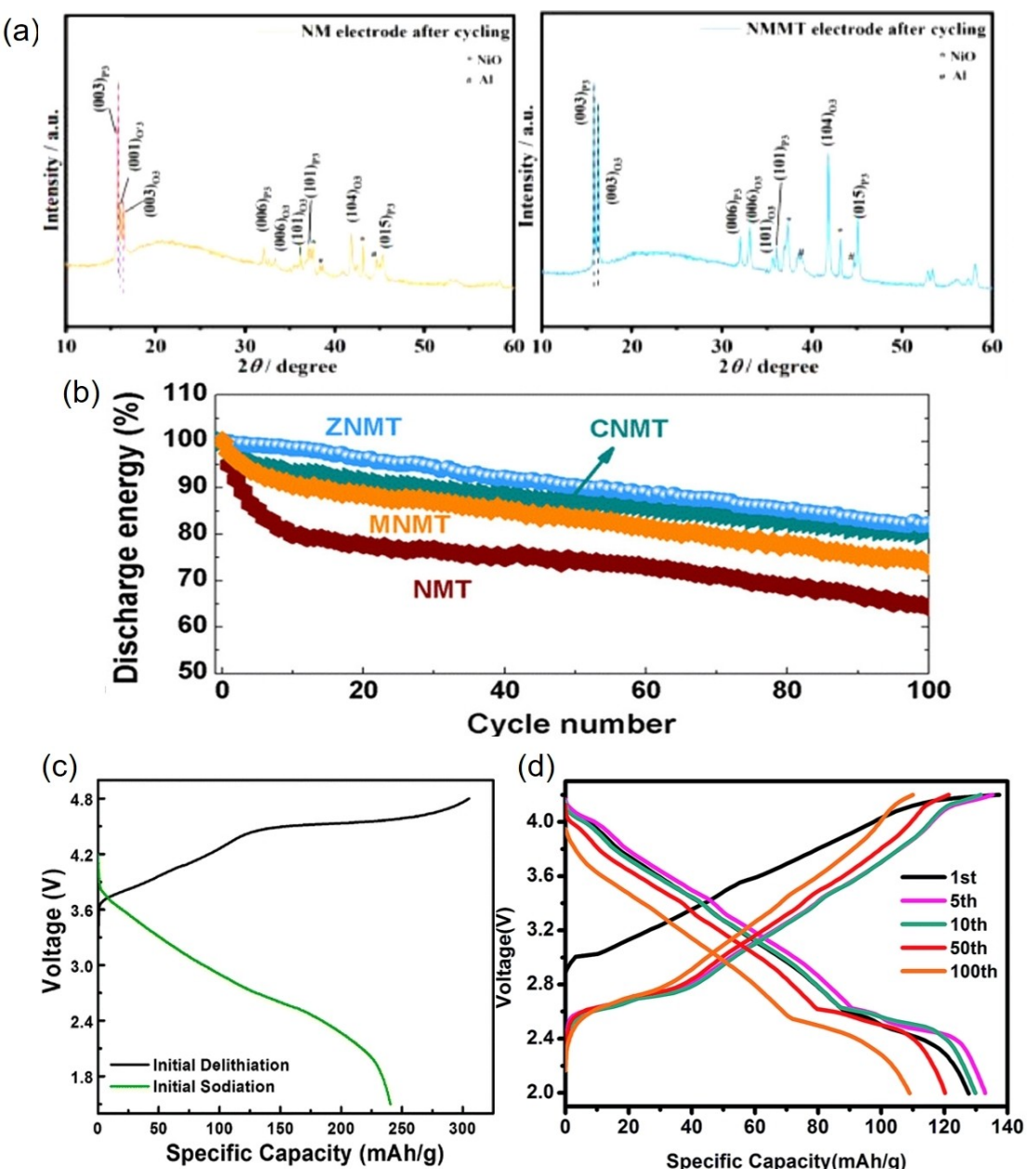


**Figure 15.** (a) the XRD pattern for NM and NMMT electrode.<sup>[221]</sup> (b) Comparison of  $Zn^{2+}$  (ZNMT:  $NaNi_{0.45}Zn_{0.05}Mn_{0.4}Ti_{0.1}O_2$ ),  $Mg^{2+}$  (MNMT:  $NaNi_{0.45}Mg_{0.05}Mn_{0.4}Ti_{0.1}O_2$ ), and  $Cu^{2+}$  (CNMT:  $NaNi_{0.45}Cu_{0.05}Mn_{0.4}Ti_{0.1}O_2$ ) substituents and No-sub (NMT:  $NaNi_{0.5}Mn_{0.4}Ti_{0.1}O_2$ ) in cycling stability within 1.2–4.4 V at a 0.1 C.<sup>[226]</sup> (c) Initial charge-discharge curve for  $Na_{0.78}Li_{0.18}Ni_{0.25}Mn_{0.583}O_w$  in 1.5–4.5 V at 0.5 C.<sup>[229]</sup> (d) Charge-discharge curve for  $O_3-NaLi_{0.1}Ni_{0.35}Mn_{0.55}O_2$  in 2.0–4.2 V at 0.1 C.<sup>[233]</sup>

#### 4.4. High-Entropy $Na_xTMO_2$

High-entropy oxides (HEOs), a novel class of compounds, have shown great promise for energy storage applications. Their unique properties, often unachievable in conventional materials with single or a few principal elements, have attracted considerable attention from the scientific community.<sup>[234,235]</sup> Layered O3-type HEOs exhibits excellent long-term cycling stability and rate performance as an intercalation-type cathode for SIBs, thanks to the entropy stabilization of the host matrix.<sup>[239,236]</sup> HEOs are considered a new class of multicompo-

nent metal oxide systems that can exist in different crystal structures, including spinel, rock salt, and perovskite structures.<sup>[237]</sup> In typical crystal structures, HEOs have five or more major elements sharing the same atomic sites, allowing for the formation of stable solid solutions (Figure 16).<sup>[119]</sup> Due to the extremely complex compositions of these materials, they often exhibit excellent properties such as better structural stability, high retention capacity, good high-temperature/low-temperature performance, and good energy storage capabilities.<sup>[238–240]</sup>

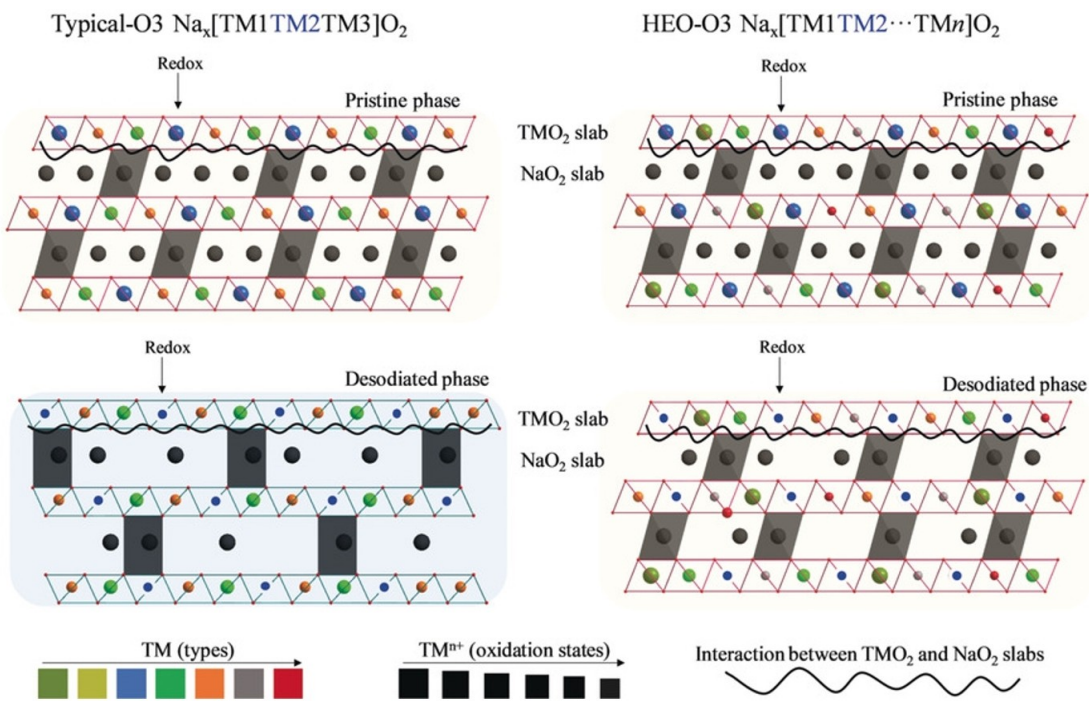


Figure 16. Schematic diagram for TMO of typical-O3 and HEO-O3.<sup>[119]</sup>

To further suppress the monoclinic phase transitions ( $O'3$  and  $P'3$ ) occurring during  $\text{Na}^+$  insertion and extraction, Guo et al.<sup>[241]</sup> have developed a five-component O3-type layered oxide cathode material,  $\text{Na}_{0.94}\text{Ni}_{0.29}\text{Cu}_{0.1}\text{Fe}_{0.16}\text{Mn}_{0.3}\text{Ti}_{0.15}\text{O}_2$  that exhibits only the O3-P3 phase transition during the deintercalation, without the occurrence of monoclinic phases such as  $O'3$ , and demonstrates a highly reversible capacity of 122 mAh.g<sup>-1</sup>.

(~0.5 Na) at 0.1 C (Figure 17a) within 2–4 V window, with a capacity retention of 79% after 300 cycles at 0.5 C (Figure 17b). Furthermore, Tripathi et al.<sup>[242]</sup> utilized O3- $\text{Na}_{0.9}\text{Cu}_{0.12}\text{Ni}_{0.1}\text{Fe}_{0.30}\text{Mn}_{0.43}\text{Ti}_{0.05}\text{O}_2$  as a cathode material in 18650 batteries. In 18650 batteries, O3- $\text{Na}_{0.9}\text{Cu}_{0.12}\text{Ni}_{0.1}\text{Fe}_{0.30}\text{Mn}_{0.43}\text{Ti}_{0.05}\text{O}_2$  achieved an energy density of 62 Wh.kg<sup>-1</sup>, with a specific capacity of 80 mAh.g<sup>-1</sup> in the voltage range of 1–4 V at 1 C rate.

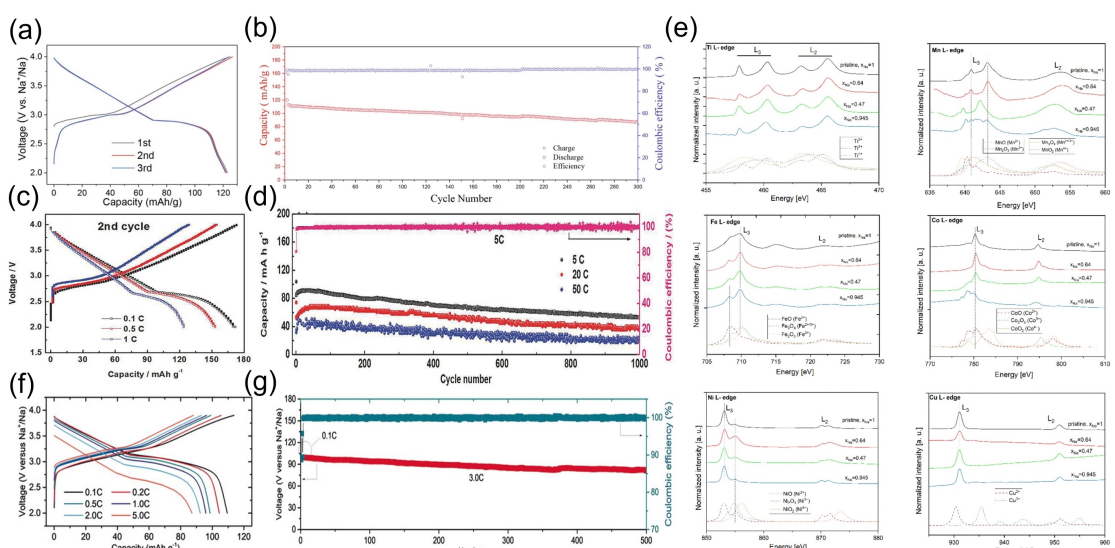


Figure 17. (a) Charge-discharge profiles for NNCFMTO within 2.0–4.0 V at 0.1 C.<sup>[241]</sup> (b) Cycle performance for NNCFMTO within 2.0–4.0 V at 0.5 C.<sup>[241]</sup> (c) Charge and discharge curves for  $\text{Na}[\text{Li}_{0.05}\text{Mn}_{0.50}\text{Ni}_{0.30}\text{Cu}_{0.10}\text{Mg}_{0.05}] \text{O}_2$  within 2.0–4.0 V at 0.1 C, 0.5 C and 1 C.<sup>[24]</sup> (d) Cycling performance for  $\text{Na}[\text{Li}_{0.05}\text{Mn}_{0.50}\text{Ni}_{0.30}\text{Cu}_{0.10}\text{Mg}_{0.05}] \text{O}_2$  within 2.0–4.0 V at 5, 20, and 50 C.<sup>[24]</sup> (e)  $L_{2,3}$  edge XAS spectra of Ti, Mn, Fe, Co, Ni, and Cu for  $\text{NaTi}_{1/6}\text{Mn}_{1/6}\text{Fe}_{1/6}\text{Co}_{1/6}\text{Ni}_{1/6}\text{Cu}_{1/6}\text{O}_2$ .<sup>[251]</sup> (f) Charge-discharge curves from 0.1 to 5.0 C for  $\text{NaNi}_{0.12}\text{Cu}_{0.12}\text{Mg}_{0.12}\text{Fe}_{0.15}\text{Co}_{0.15}\text{Mn}_{0.1}\text{Ti}_{0.1}\text{Sn}_{0.1}\text{Sb}_{0.04}\text{O}_2$  between 2.0–3.9 V.<sup>[119]</sup> (g) Cycle performance for  $\text{NaNi}_{0.12}\text{Cu}_{0.12}\text{Mg}_{0.12}\text{Fe}_{0.15}\text{Co}_{0.15}\text{Mn}_{0.1}\text{Ti}_{0.1}\text{Sn}_{0.1}\text{Sb}_{0.04}\text{O}_2$  between 2.0–3.9 V at 3.0 C.<sup>[119]</sup>

It exhibited a Coulombic efficiency of over 99.5% and 80% capacity retention after 80 cycles.<sup>[242]</sup> In  $\text{Na}_{0.9}\text{Cu}_{0.12}\text{Ni}_{0.10}\text{Fe}_{0.30}\text{Mn}_{0.43}\text{Ti}_{0.05}\text{O}_2$  and  $\text{Na}_{0.9}\text{Cu}_{0.12}\text{Ni}_{0.10}\text{Fe}_{0.30}\text{Mn}_{0.43}\text{Ti}_{0.05}\text{O}_2$ , although Ti and Cu do not participate in the redox reactions, they contribute significantly to stabilizing the structure and reducing phase transitions.<sup>[111,243]</sup> Furthermore, the electrostatic interactions between Na and O was facilitated through the doping of  $\text{Cu}^{2+}$ , resulting in heightened conductivity.<sup>[244]</sup> This increase in conductivity hinders the rearrangement of  $\text{Na}^+$ /vacancy at high voltage and reinforces the structural stability during the insertion and extraction of  $\text{Na}^+$ . As a consequence, the P3-O3' phase transition is effectively suppressed.<sup>[244]</sup> Previous studies have also shown similar effects for  $\text{Li}^+$ ,  $\text{Zn}^{2+}$ ,  $\text{Mg}^{2+}$ , and  $\text{Sn}^{4+}$  in SIBs.<sup>[226,244–248]</sup>

Based on the excellent performance achieved by the partial Li and Mg substitution in O3- $\text{NaNi}_{1/2}\text{Mn}_{1/2}\text{O}_2$ , a novel air-stable O3-type  $\text{Na}[\text{Li}_{0.05}\text{Mn}_{0.50}\text{Ni}_{0.30}\text{Cu}_{0.10}\text{Mg}_{0.05}]\text{O}_2$  cathode material was tested and characterized by Deng et al.<sup>[24]</sup> It exhibits reversible capacity of  $172.0 \text{ mAh.g}^{-1}$  ( $\sim 0.69 \text{ Na}$ ) at 0.1 C (Figure 17c) and  $49.0 \text{ mAh.g}^{-1}$  at 50 C within a voltage range of 2.0–4.0 V. Remarkably, it demonstrates high-capacity retention rates of 82% and 70.4% after 400 cycles at a 1 C and 1000 cycles at a 20 C (Figure 17d), respectively. In the full cell system, based on the entire amount of cathode and anode (hard carbon), it offers an energy density of up to  $215 \text{ Wh.kg}^{-1}$  at 0.1 C.<sup>[24]</sup> The authors attribute the improved electronic conductivity and  $\text{Na}^+$  diffusion kinetics to incorporating  $\text{Li}^+$  and  $\text{Mg}^{2+}$  ions. Additionally, the structural stability is enhanced by the presence of  $\text{Mn}^{4+}$  oxidation states,<sup>[68,104]</sup> while the irreversible phase transition is suppressed by the  $\text{Cu}^{2+}/\text{Cu}^{3+}$  redox couple,<sup>[249,250]</sup> thus improving the material's rate performance and long-term cycling stability.<sup>[250]</sup> Nonetheless, the content of  $\text{Mn}^{3+}$  gradually increases with the cycles, leading to the resurgence of the J-T effect and causing capacity degradation.<sup>[24]</sup> Furthermore, this material can be synthesized through an industrially viable coprecipitation method, indicating that it can be relatively easily produced on a large scale.

Following, Molenda et al.<sup>[251]</sup> reported that a HEO O3- $\text{NaTi}_{1/6}\text{Mn}_{1/6}\text{Fe}_{1/6}\text{Co}_{1/6}\text{Ni}_{1/6}\text{Cu}_{1/6}\text{O}_2$ , exhibited a simple phase transition (O3-P3). The oxidation states of Ti, Mn, Fe, Co, Ni, and Cu were revealed through  $\text{L}_{2,3}$  edge XAS spectra (Figure 17e) and found that only Ti and Cu consistently remained in the 4+ and 2+ states, respectively, during cycling. While Fe did not exhibit a clear redox change, it maintained a mixed valence state (2+ and 3+). Mn remained in the 4+ state as the battery charged up to 3.9 V ( $\sim 0.47 \text{ Na}$ ) and only showed the emergence of 2+ and 3+ states as it discharged to 1.5 V. Co displayed active chemical behavior, varying between 4+ and 2+. In the case of HEO, the oxidation states of Ni were limited to 2+ and 3+, without the appearance of 4+.<sup>[251]</sup>

Recently, a highly complex HEO O3-type  $\text{NaNi}_{0.12}\text{Cu}_{0.12}\text{Mg}_{0.12}\text{Fe}_{0.15}\text{Co}_{0.15}\text{Mn}_{0.1}\text{Ti}_{0.1}\text{Sn}_{0.1}\text{Sb}_{0.04}\text{O}_2$  (NNCMFCMTSSO)<sup>[119]</sup> was reported and the nine ions appear various oxidation states ranging from divalent to pentavalent. Among these elements,  $\text{Ni}^{2+}$ ,  $\text{Cu}^{2+}$ ,  $\text{Co}^{3+}$ , and  $\text{Fe}^{3+}$  provide charge compensation for capacity by redox, while  $\text{Mg}^{2+}$ ,  $\text{Mn}^{4+}$ ,

and  $\text{Ti}^{4+}$  can offer structural support as pillars to the cathode material, and  $\text{Sn}^{4+}$  and  $\text{Sb}^{5+}$  can provide higher operating voltages for the battery.<sup>[154,248,252–256]</sup> Consequently, the O3 phase region exhibits only about 60% of the theoretical discharge capacity. Such NNCMFCMTSSO undergoes an O3-O3'-P3-O3'-P3-O3' phase transition in the first cycle, but a highly reversible and simple phase transitions from the O3' phase to the P3 phase in the second and following cycles. This material can provide a reversible capacity of  $110 \text{ mAh.g}^{-1}$  ( $\sim 0.47 \text{ Na}$ ) at a rate of 0.1 C in the voltage range of 2.0–3.9 V (Figure 17f), with a capacity retention of approximately 83% after 500 cycles at 3.0 C (Figure 17g).<sup>[119]</sup> Overall, HEO engineering contributes to achieving a highly stable state in the O3-type structure, maintaining a high-capacity retention during long-term cycling. The concept of high-entropy configuration will provide a new avenue for enhancing the electrochemical performance of SIBs.

## 5. Discussion and Perspective

Among the spectrum of cathode materials suitable for SIBs, O3-type layered oxide materials have displayed exceptional energy density characteristics, primarily attributable to advanced engineering approaches such as doping and substitution. These methods have enabled O3-type layered oxides to rival the performance of commercially available  $\text{LiFePO}_4$  cathodes used in LIBs. For example, the extensively studied O3-type compound,  $\text{NaNi}_{0.5}\text{Mn}_{0.5}\text{O}_2$ , demonstrates a notable reversible capacity of  $185 \text{ mAh.g}^{-1}$  within the voltage window spanning from 2.2 to 4.5 V. Nonetheless, the increased ionic radius of  $\text{Na}^+$  compared to  $\text{Li}^+$  becomes evident during the sodium-ion deintercalation process, resulting in more pronounced chemical interactions within the layered oxide materials. These reactions include the occurrences of  $\text{Na}^+$ /vacancy re-ordering, layered oxide sliding, and J-T effects, leading to the formation of up to four distinct phase transition products: O'3, P3, P'3, and P3'.<sup>[11]</sup> As a result, most O3-type materials undergo complex phase transitions and exhibit multiple voltage plateaus, significantly impacting their irreversible capacity, cycling stability, and rate performance.<sup>[40,257]</sup> Ni-based and Mn-based O3-type layered oxide materials have been re-examined to reveal and explore these phase transition defects. In O3-type layered oxides, unlike the P2-type structure,  $\text{TMO}_2$  plays an important role, where its layer slides without breaking the TM–O bonds forms the P3 phase with prismatic positions. For example, the monoclinic distortion in Ni-based monovalent materials is due to the reduced negative charge on oxygen atoms by Ni–O bonds, inhibiting the Coulombic attraction between Na and O ions and increasing the interlayer spacing of the oxide layers to slide in the oxide layer.<sup>[160]</sup> Cationic substitution effectively generates new TM–O bonds to mitigate such complex chemical behaviors.

Firstly, even Ni-based and Mn-based with the J-T effect are associated together, such as  $\text{NaNi}_{0.5}\text{Mn}_{0.5}\text{O}_2$ , a reduction in atomic spacing and a decrease in Fourier transform (FT) amplitude have been observed, effectively suppressing monoclinic distortion.<sup>[197]</sup> The incorporation of Cu is regarded as a

**Table 3** Electrochemical performance of different O3-type layered cathode materials in SIBs.

	Multi-metal oxides	Structure	Specific capacity [mAh·g <sup>-1</sup> ]	Voltage range (V)	Cycle performance [mAh·g <sup>-1</sup> ]	Phase transitions
Ni-based	NaNi <sub>0.5</sub> Co <sub>0.5</sub> O <sub>2</sub> <sup>[159]</sup>	R-3m	115 (0.1 C)	2.0–4.2	0.4 % decay per cycle	O3-O'3-P'3-P3-P3-O''3
	NaNi <sub>0.5</sub> Fe <sub>0.5</sub> O <sub>2</sub> <sup>[159]</sup>	R-3m	129 (0.1 C)	2.0–3.9	0.3 % decay per cycle	O3-P3
	NaNi <sub>0.7</sub> Fe <sub>0.3</sub> O <sub>2</sub> <sup>[160]</sup>	R-3m	135 (0.2 C)	2.5–3.8	100 mA·h·g <sup>-1</sup> (30 cycles)	O3-P3
	NaNi <sub>0.5</sub> Fe <sub>0.5</sub> O <sub>2</sub> <sup>[160]</sup>	R-3m	112 (0.2 C)	2.5–3.8	62 mA·h·g <sup>-1</sup> (30 cycles)	O3-P3
	NaTi <sub>0.5</sub> Ni <sub>0.5</sub> O <sub>2</sub> <sup>[166]</sup>	R-3m	121 (0.2 C)	2.0–4.7	93.2% (100 cycles at 0.2 C) and 75% (300 cycles at 1 C)	O3-P3
	Na[Fe <sub>1/3</sub> Ni <sub>1/3</sub> Ti <sub>1/3</sub> ]O <sub>2</sub> <sup>[168]</sup>	R3m	117 (0.1 C)	1.5–4.0	57% (1000 cycles at 2 C)	O3-O3+P3-P3
	NaNi <sub>1/3</sub> Co <sub>1/3</sub> Fe <sub>1/3</sub> O <sub>2</sub> <sup>[170]</sup>	R-3m	165 (0.05 C)	2.0–4.0	90% (20 cycles at 0.2 C)	N/A
	NaNi <sub>1/4</sub> Co <sub>1/4</sub> Fe <sub>1/4</sub> Ti <sub>1/4</sub> O <sub>2</sub> <sup>[172]</sup>	R-3m	116 (0.1 C)	2.0–3.9	75% (400 cycles at 5 C)	O3-O3+P3-P3
	NaNi <sub>0.8</sub> Co <sub>0.15</sub> Al <sub>0.05</sub> O <sub>2</sub> <sup>[156]</sup>	C2/m	153.9 (0.1 C)/137.7 (1 C)	2.0–3.8	86.7% (200 cycles at 0.1 C)	O3-O1-P3
	Hexagonal NaNi <sub>0.8</sub> Co <sub>0.15</sub> Al <sub>0.05</sub> O <sub>2</sub> <sup>[183]</sup>	R-3m	162 (0.1 C)	1.5–4.5	90% (120 cycles)	O3-O'3-P3-O''3-O'''3
Mn-based	Monoclinic NaNi <sub>0.8</sub> Co <sub>0.15</sub> Al <sub>0.05</sub> O <sub>2</sub> <sup>[183]</sup>	C2/m	150 (0.1 C)	1.5–4.5	90% (120 cycles at 0.1 C)	O3-P3-O'3-O''3
	NaMn <sub>1/3</sub> Fe <sub>2/3</sub> O <sub>2</sub> <sup>[186]</sup>	R-3m	157 (0.1 C)	1.5–4.2	80% (15 cycles at 0.1 C)	O3-O'3-O3-p3-O3+O1-O3+O'
	Na <sub>0.9</sub> [Cu <sub>0.22</sub> Fe <sub>0.30</sub> Mn <sub>0.48</sub> ]O <sub>2</sub> <sup>[107]</sup>	R-3m	100 (0.1 C)	2.5–4.05	97% (100 cycles at 0.1 C)	O3-P3+O3-P3-O'3
	NaFe <sub>0.55</sub> Mn <sub>0.45</sub> , <sub>x</sub> Nb <sub>x</sub> O <sub>2</sub> <sup>[191]</sup>	R-3m	127 (0.1 C)	2.0–4.0	65.6% (200 cycles at 0.1 C)	O3-P3
	NaCr <sub>1/3</sub> Fe <sub>1/3</sub> Mn <sub>1/3</sub> O <sub>2</sub> <sup>[178]</sup>	R-3m	186 (0.05 C)	1.5–4.2	N/A	O3-O3+P3-P3+O3''-O3''
Mn-Ni based	NaNi <sub>0.5</sub> Mn <sub>0.5</sub> O <sub>2</sub> <sup>[197]</sup>	R-3m	185 (0.02 C)	2.2–4.5	75% (50 cycles at 0.2 C)	O3-O3-P3-P3-P3''
	NaNi <sub>0.5</sub> Mn <sub>0.5</sub> O <sub>2</sub> (sol-gel method) <sup>[198]</sup>	R-3m	141(0.05 C)	2.0–4.0	90% (100 cycles at 0.05 C)	O3-O'3-P3-P3-P3''
	Co					
	NaNi <sup>1/3</sup> Mn <sup>1/3</sup> Co <sup>1/3</sup> O <sub>2</sub> <sup>[182]</sup>	R-3m	120 (0.1 C)	2.0–3.75	N/A	O3+O1-O1-O1+P3-P3-P1+P3-P3
Fe	Na[Ni <sub>x</sub> Co <sub>y</sub> Mn <sub>2</sub> ]O <sub>2</sub> ( $x=1/3$ ) <sup>[206]</sup>	R-3m	141.1(0.06 C)	1.5–4.1	76.5% (100 cycles at 0.3 C)	O3+O1-O1-O1+P3-P3-P1+P3-P3
	Na[Ni <sub>x</sub> Co <sub>y</sub> Mn <sub>2</sub> ]O <sub>2</sub> ( $x=0.5$ ) <sup>[206]</sup>	R-3m	146.1(0.06 C)	1.5–4.1	69% (100 cycles at 0.3 C)	O3+O1-O1-O1+P3-P3-P1+P3-P3
	Na[Ni <sub>x</sub> Co <sub>y</sub> Mn <sub>2</sub> ]O <sub>2</sub> ( $x=0.6$ ) <sup>[206]</sup>	R-3m	150 (0.06 C)	1.5–4.1	73% (100 cycles at 0.3 C)	O3+O1-O1-O1+P3-P3-P1+P3-P3
	Na[Ni <sub>x</sub> Co <sub>y</sub> Mn <sub>2</sub> ]O <sub>2</sub> ( $x=0.8$ ) <sup>[206]</sup>	R-3m	187.1(0.06 C)	1.5–4.1	50% (100 cycles at 0.3 C)	O3+O1-O1-O1+P3-P3-P1+P3-P3
	Fe					
	NaNi <sub>1/3</sub> Fe <sub>1/3</sub> Mn <sub>1/3</sub> O <sub>2</sub> <sup>[209]</sup>	R-3m	120 (0.5 C)	1.5–4.0	83% (150 cycles at 0.5 C)/73% (500 cycles at 1 C) as soft-packed sodium ion battery <sup>[212]</sup>	O3-O3+P3-P3
	NaFe <sub>x</sub> (Ni <sub>0.5</sub> Mn <sub>0.5</sub> ) <sub>1-x</sub> O <sub>2</sub> ( $x=0.2$ ) <sup>[177]</sup>	R-3m	131 (0.05 C)	2.0–4.0	95.2% (30 cycles at 0.05 C)	O3-O3+P3-P3
	NaNi <sub>0.25</sub> Fe <sub>0.5</sub> Mn <sub>0.25</sub> O <sub>2</sub> <sup>[210]</sup>	R-3m	140 (0.1 C)	2.1–3.9	76.1% (150 cycles at 1 C)	O3-O3+P3-P3
	Ni-rich O3-Na[Ni <sub>0.66</sub> Fe <sub>0.23</sub> Mn <sub>0.11</sub> ]O <sub>2</sub> <sup>[213]</sup>	R-3m	190 (0.05 C)	2.0–4.2	84% (200 cycles at 2 C)	O3-O'3-P3-O3''
	NaNi <sub>2/3</sub> Mn <sub>1/6</sub> Fe <sub>1/6</sub> O <sub>2</sub> <sup>[214]</sup>	R-3m	226 (0.2 C)	1.5–4.2	76% (100 cycles at 0.2 C)	

<b>Ti</b>	Na(Mn <sub>0.25</sub> Fe <sub>0.25</sub> Co <sub>0.25</sub> Ni <sub>0.25</sub> )O <sub>2</sub> <sup>[69]</sup>	R-3m	180 (0.1 C)	1.9–4.3	89% (20 cycles at 0.1 C)	O3-P3-O3'-O3''
	NaNi <sub>0.5</sub> Mn <sub>0.2</sub> Ti <sub>0.3</sub> O <sub>2</sub> <sup>[111]</sup>	R-3m	135 (0.05 C)	2.0–4.0	85% (200 cycles at 1 C)	O3-P3
	NaNi <sub>0.45</sub> Cu <sub>0.05</sub> Mn <sub>0.4</sub> Ti <sub>0.1</sub> O <sub>2</sub> <sup>[218]</sup>	R-3m	124 (0.1 C)	2.0–4.0	70.2% (500 cycles at 1 C)	O3-P3
	NaNi <sub>0.5-y</sub> Cu <sub>y</sub> Mn <sub>0.5-z</sub> Ti <sub>z</sub> O <sub>2</sub> ( $z=2$ ) <sup>[219]</sup>	R-3m	200 (0.1 C)	2.4–4.5/ average 3.1	80% (100 cycles at 0.05 C)	O3-O'3-P3-
<b>Li</b>	Na[Ni <sub>4/9</sub> Mn <sub>1/3</sub> Mg <sub>1/18</sub> Ti <sub>1/6</sub> ]O <sub>2</sub> <sup>[220]</sup>	R-3m	198 (0.045 C)	2.2–4.5	86% (50 cycles at 0.045 C)	O3-O'3-P3-OP2-O3
	NaNi <sub>0.45</sub> Zn <sub>0.05</sub> Mn <sub>0.4</sub> Ti <sub>0.1</sub> O <sub>2</sub> <sup>[226]</sup>	R-3m	152 (0.1 C)	1.2–4.4	85% (100 cycles at 0.1 C)	O3-O'3-P3-
	Na <sub>0.78</sub> Li <sub>0.18</sub> Ni <sub>0.23</sub> Mn <sub>0.58</sub> O <sub>w</sub> <sup>[229]</sup>	R-3m	240 (0.5 C)	1.5–4.5	80% (30 cycles at 0.5 C)	O3-O'3-P3
	NaLi <sub>0.1</sub> Ni <sub>0.35</sub> Mn <sub>0.55</sub> O <sub>2</sub> <sup>[233]</sup>	R-3m	128 (0.1 C)/160 (0.1 C)	2.0–4.2/1.5–4.3	85% (100 cycles at 0.1 C)	O3-O'3-P3
<b>High-entropy oxides (HEOs)</b>						
	Na <sub>0.94</sub> Ni <sub>0.29</sub> Cu <sub>0.1</sub> Fe <sub>0.16</sub> Mn <sub>0.3</sub> Ti <sub>0.15</sub> O <sub>2</sub> <sup>[241]</sup>	R-3m	122 (0.1 C)	2.0–4.0	79% (300 cycles at 0.5 C)	O3-O3+P3-P3
	Na <sub>0.9</sub> Cu <sub>0.12</sub> Ni <sub>0.10</sub> Fe <sub>0.3</sub> Mn <sub>0.43</sub> Ti <sub>0.05</sub> O <sub>2</sub> <sup>[242]</sup>	R-3m	105 (0.2 C)	2.5–4.2	90% (200 cycles at 0.2 C)	O3-O3+P3-P3
	Na[Li <sub>0.05</sub> Mn <sub>0.5</sub> Ni <sub>0.30</sub> Cu <sub>0.10</sub> Mg <sub>0.05</sub> ]O <sub>2</sub> <sup>[24]</sup>	R-3m	172 (0.1 C)	2.0–4.0	70.4% (1000 cycles at 20 C)	O3-P3
	NaTi <sub>1/6</sub> Mn <sub>1/6</sub> Fe <sub>1/6</sub> Co <sub>1/6</sub> Ni <sub>1/6</sub> Cu <sub>1/6</sub> O <sub>2</sub> <sup>[251]</sup>	R-3m	129 (0.1 C)	2.0–4.1	N/A	O3-P3
NaNi <sub>0.12</sub> Cu <sub>0.12</sub> Mg <sub>0.12</sub> Fe <sub>0.15</sub> Co <sub>0.15</sub> Mn <sub>0.1</sub> Ti <sub>0.1</sub> Sn <sub>0.1</sub> Sb <sub>0.04</sub> O <sub>2</sub> <sup>[19]</sup>						
1 <sup>st</sup> O3 (R-3m) 2 <sup>nd</sup> O'3 (C2/m)						
2.0–3.9 83% (500 cycles at 3 C)						

practical and effective approach to improve the sodium storage capabilities of O<sub>3</sub>-type Ni/Mn-based transition metal oxides.<sup>[258,259]</sup> Moreover, among numerous cation substitutions and doping, materials with Ti<sup>4+</sup> substitution exhibit significantly reduced complex phase transitions, simplifying the phase transition products and smoothing the voltage profiles. Ti<sup>4+</sup> is difficult to oxidize to a higher valence state and can provide stronger Ti–O bonds, which can suppress the disorder caused by Cu–O and Ni–O bonds, such as the formation of an O–Cu–O–Ti–O sequence, reducing the possibility of interlayer disorder in TMO.<sup>[260]</sup> The Ti–O bonds can also reduce the number of active J–T ions (e.g., Ni–O).<sup>[69]</sup> This enables materials containing both Ni and Cu to not only possess higher working voltage and electronic conductivity but also achieve more stable cycling performance. Furthermore, titanium (Ti) can generate more stable Ti–TM interactions between two adjacent edges of the Ti–O<sub>6</sub> octahedra,<sup>[261]</sup> which can effectively mitigate the migration of Fe<sup>3+</sup> ions, thereby suppressing the formation of the O'3 phase that would typically occur in NaFeO<sub>2</sub>. This significantly improves the long-term cycling performance of iron-containing layered cathode materials. However, it is worth noting that Ti<sup>4+</sup> substitution can also lead to instability in phase transitions in the high-voltage region. Studies have shown that the substitution of Zn<sup>2+</sup> is an effective approach to address the instability of phase transitions in the high-voltage region.<sup>[262–264]</sup> Additionally, although quaternary-metal and high-entropy materials offer relatively good cycling performance (Table 3), as the number of dopants increases, it is observed that TMO bonds exhibit more complex phenomena and tendencies in those system compositions, and the effects and interactions of each minor cation bond are more challenging to analyze.

## 6. Conclusions

In the context of the exponential expansion within the non-fossil energy sector, particularly concerning large-scale energy storage solutions, there has been a notable redirection of research efforts towards the pursuit of economically viable and high-performing rechargeable battery systems in recent years. Notably, SIBs have experienced significant progress due to their similarities with LIBs in terms of electrochemical reaction mechanisms, as well as their advantage of abundant sodium resources and intrinsic safety features. Given their suitability for applications in large-scale energy storage, SIBs are positioned to play a pivotal role in promoting sustainability within the rapidly growing new energy industry.

The optimization of cathode materials holds paramount importance in facilitating the commercialization and realization of the maximum performance potential of SIBs. O<sub>3</sub>-type layered transition metal oxide cathode materials have garnered substantial attention due to their notable advantages in practical applications compared to alternative materials. Nonetheless, these O<sub>3</sub>-type layered oxides still face challenges such as limited cycling stability, relatively low resistance to environmental factors, and somewhat inferior rate performance. Consequently, this article offers a comprehensive review of

recent advancements in the domain of layered transition metal oxide cathode materials for SIBs, with a specific focus on elucidating the sodium storage mechanism, examining structural evolution, and assessing the electrochemical performance of O<sub>3</sub>-type layered oxide materials.

Integrating transition metal elements (such as Cu, Ti, Zn, Mg, Li) in Ni- and Mn-based oxides has yielded substantial improvements in the cycling stability and rate capability of SIBs. Nonetheless, uncertainties persist regarding the precise roles and enhancement mechanisms of doping and substitution elements, encompassing variations in their compositional attributes, oxidation states, electrochemical reactivity, types of substituted atoms, and manufacturing methodologies, particularly within the context of quaternary-metal systems and beyond. Additionally, it is noteworthy that no linear correlation is observed between the energy density and the number of incorporated doping or substitution elements. For instance, although high-entropy metal oxides may offer relatively moderate capacities and cycling stability, they fall short of meeting the stringent requirements of mobile battery applications.

Hence, in the process of conceiving a new O<sub>3</sub>-type cathode material, it is imperative to recognize that a straightforward strategy involving element substitution and doping may not necessarily result in the most advantageous cathode material. Rather, what is required is a systematic research approach that delves deeper into elucidating how the introduced doping elements exert their influence on the crystal structure and the local electronical environments. In this regard, it becomes crucial to take into account the inherent attributes of the material in question and to delicately manage the physical and chemical interactions among the various transition metal elements, all the while giving due consideration to their respective roles and contributions.

## Acknowledgements

The authors are grateful to the financial support by the Australian Research Council through a Discovery Project (DP230100198). Open Access publishing facilitated by University of Wollongong, as part of the Wiley - University of Wollongong agreement via the Council of Australian University Librarians.

## Conflict of Interests

The authors declare no competing financial interest.

**Keywords:** Sodium-ion batteries • O<sub>3</sub>-layered oxide cathode materials • Ni/Mn systems • element substitution • element doping

- [1] T. Kober, H.-W. Schiffer, M. Densing, E. Panos, *Energy Strategy Rev.* 2020, 31, 100523.
- [2] W. Zuo, M. Luo, X. Liu, J. Wu, H. Liu, J. Li, M. Winter, R. Fu, W. Yang, Y. Yang, *Energy Environ. Sci.* 2020, 13, 4450.
- [3] W. Li, B. Song, A. Manthiram, *Chem. Soc. Rev.* 2017, 46, 3006.

- [4] Y. X. Yin, S. Xin, Y. G. Guo, L. J. Wan, *Angew. Chem. Int. Ed.* **2013**, *52*, 13186.
- [5] M. Armand, J.-M. Tarascon, *Nature* **2008**, *451*, 652.
- [6] Y. Yan, Y. Yin, Y. Guo, L.-J. Wan, *Sci. China Chem.* **2014**, *57*, 1564.
- [7] T. Nagaura, *Prog. Batteries Sol. Cells* **1990**, *9*, 209.
- [8] C. Julien, A. Mauger, A. Vijh, K. Zaghib, C. Julien, A. Mauger, A. Vijh, K. Zaghib, *Lithium batteries*. Springer, 2016.
- [9] B. Scrosati, J. Garche, *J. Power Sources* **2010**, *195*, 2419.
- [10] A. B. Yaroslavtsev, T. Kulova, A. M. Skundin, *Russ. Chem. Rev.* **2015**, *84*, 826.
- [11] C. Vaalma, D. Buchholz, M. Weil, S. Passerini, *Nat. Rev. Mater.* **2018**, *3*, 1.
- [12] A. Fu-qiang, Z. Hong-liang, C. Zhi, Q. J. Yi-cheng, Z. Wei-nan, L. Ping, *Chinese Journal of Engineering* **2019**, *41*, 22.
- [13] X. Wu, Y. Li, Y. Xiang, Z. Liu, Z. He, X. Wu, Y. Li, L. Xiong, C. Li, J. Chen, *J. Power Sources* **2016**, *336*, 35.
- [14] S. Park, D. Kim, H. Ku, M. Jo, S. Kim, J. Song, J. Yu, K. Kwon, *Electrochim. Acta* **2019**, *296*, 814.
- [15] J. Yan, X. Liu, B. Li, *RSC Adv.* **2014**, *4*, 63268.
- [16] H. Yu, H. Zhou, *J. Phys. Chem. Lett.* **2013**, *4*, 1268.
- [17] R. S. Carmichael, *Practical handbook of physical properties of rocks and minerals* (1988). CRC press, 2017.
- [18] M. C. Summaries, *Mineral commodity summaries*. vol 200. US Geological Survey: Reston, VA, USA. 2019.
- [19] H. Pan, Y.-S. Hu, L. Chen, *Energy Environ. Sci.* **2013**, *6*, 2338.
- [20] S. W. Kim, D. H. Seo, X. Ma, G. Ceder, K. Kang, *Adv. Energy Mater.* **2012**, *2*, 710.
- [21] M. D. Slater, D. Kim, E. Lee, C. S. Johnson, *Adv. Funct. Mater.* **2013**, *23*, 947.
- [22] G. Berckmans, M. Messagie, J. Smekens, N. Omar, L. Vanhaverbeke, J. Van Mierlo, *Energies* **2017**, *10*, 1314.
- [23] K. Kubota, N. Yabuuchi, H. Yoshida, M. Dahbi, S. Komaba, *MRS Bull.* **2014**, *39*, 416.
- [24] J. Deng, W. B. Luo, X. Lu, Q. Yao, Z. Wang, H. K. Liu, H. Zhou, S. X. Dou, *Adv. Energy Mater.* **2018**, *8*, 1701610.
- [25] T. Jin, X. Ji, P. F. Wang, K. Zhu, J. Zhang, L. Cao, L. Chen, C. Cui, T. Deng, S. Liu, *Angew. Chem. Int. Ed.* **2021**, *60*, 11943.
- [26] C. Shi, L. Wang, X. Chen, J. Li, S. Wang, J. Wang, H. Jin, *Nanoscale Horiz.* **2022**, *7*, 338.
- [27] N. F. Mahamad Yusoff, N. H. Idris, L. Noerochim, *Int. J. Energy Res.* **2022**, *46*, 667.
- [28] P. K. Nayak, L. Yang, W. Brehm, P. Adelhelm, *Angew. Chem. Int. Ed.* **2018**, *57*, 102.
- [29] F. Wei, Q. Zhang, P. Zhang, W. Tian, K. Dai, L. Zhang, J. Mao, G. Shao, *J. Electrochem. Soc.* **2021**, *168*, 050524.
- [30] T. Zhang, J. Mao, X. Liu, M. Xuan, K. Bi, X. L. Zhang, J. Hu, J. Fan, S. Chen, G. Shao, *RSC Adv.* **2017**, *7*, 41504.
- [31] Z. Jian, C. Bommier, L. Luo, Z. Li, W. Wang, C. Wang, P. A. Greaney, X. Ji, *Chem. Mater.* **2017**, *29*, 2314.
- [32] C. Bin, X. Li, *Acta Phys. Chim. Sin.* **2020**, *36*, 1905003.
- [33] K. C. Wasalathilake, H. Li, L. Xu, C. Yan, *J. Energy Chem.* **2020**, *42*, 91.
- [34] S. Zhu, A. Huang, Q. Wang, Y. Xu, *Nanotechnology* **2021**, *32*, 165401.
- [35] T. Wang, K. Yang, J. Shi, S. Zhou, L. Mi, H. Li, W. Chen, *J. Energy Chem.* **2020**, *46*, 71.
- [36] Z.-J. Zhang, W.-J. Li, S.-L. Chou, C. Han, H.-K. Liu, S.-X. Dou, *J. Mater. Sci. Technol.* **2021**, *68*, 140.
- [37] Z. Lin, Q. Xia, W. Wang, W. Li, S. Chou, *InfoMat.* **2019**, *1*, 376.
- [38] Y. Huang, L. Zhao, L. Li, M. Xie, F. Wu, R. Chen, *Adv. Mater.* **2019**, *31*, 1808393.
- [39] A. Ponrouch, E. Marchante, M. Courty, J.-M. Tarascon, M. R. Palacin, *Energy Environ. Sci.* **2012**, *5*, 8572.
- [40] Y.-J. Fang, Z.-X. Chen, X.-P. Ai, H.-X. Yang, Y.-L. Cao, *Acta Phys. Chim. Sin.* **2017**, *33*, 211.
- [41] Q. Liu, Z. Hu, M. Chen, C. Zou, H. Jin, S. Wang, S. L. Chou, S. X. Dou, *Small* **2019**, *15*, 1805381.
- [42] K. Kubota, S. Komaba, *J. Electrochem. Soc.* **2015**, *162*, A2538.
- [43] Z. Hu, Q. Liu, S. L. Chou, S. X. Dou, *Adv. Mater.* **2017**, *29*, 1700606.
- [44] S. Komaba, T. Ishikawa, N. Yabuuchi, W. Murata, A. Ito, Y. Ohsawa, *ACS Appl. Mater. Interfaces* **2011**, *3*, 4165.
- [45] M. Dahbi, N. Yabuuchi, K. Kubota, K. Tokiwa, S. Komaba, *Phys. Chem. Chem. Phys.* **2014**, *16*, 15007.
- [46] X. Wu, W. Deng, J. Qian, Y. Cao, X. Ai, H. Yang, *J. Mater. Chem. A* **2013**, *1*, 10130.
- [47] D. Yang, X.-Z. Liao, J. Shen, Y.-S. He, Z.-F. Ma, *J. Mater. Chem. A* **2014**, *2*, 6723.
- [48] C. Wang, L. Liu, S. Zhao, Y. Liu, Y. Yang, H. Yu, S. Lee, G.-H. Lee, Y.-M. Kang, R. Liu, *Nat. Commun.* **2021**, *12*, 2256.
- [49] E. Gabriel, C. Ma, K. Graff, A. Conrado, D. Hou, H. Xiong, *eScience* **2023**, *5*, 100139.
- [50] Z.-Y. Gu, Y.-L. Heng, J.-Z. Guo, J.-M. Cao, X.-T. Wang, X.-X. Zhao, Z.-H. Sun, S.-H. Zheng, H.-J. Liang, B. Li, *Nano Res.* **2023**, *16*, 439.
- [51] Y. Liu, J. Li, Q. Shen, J. Zhang, P. He, X. Qu, Y. Liu, *eScience* **2022**, *2*, 10.
- [52] H.-R. Yao, W.-J. Lv, X.-G. Yuan, Y.-J. Guo, L. Zheng, X.-A. Yang, J. Li, Y. Huang, Z. Huang, P.-F. Wang, *Nano Energy* **2022**, *97*, 107207.
- [53] D. Kundu, E. Talaie, V. Duffort, L. F. Nazar, *Angew. Chem. Int. Ed.* **2015**, *54*, 3431.
- [54] Y. Wang, R. Chen, T. Chen, H. Lv, G. Zhu, L. Ma, C. Wang, Z. Jin, J. Liu, *Energy Storage Mater.* **2016**, *4*, 103.
- [55] X. Xiang, K. Zhang, J. Chen, *Adv. Mater.* **2015**, *27*, 5343.
- [56] F. Wei, Q. Zhang, P. Zhang, W. Tian, K. Dai, L. Zhang, J. Mao, G. Shao, *J. Electrochem. Soc.* **2021**, *168*, 050524.
- [57] Y. Liu, C. Wang, M. Ren, H. Fang, Z. Jiang, F. Li, *J. Energy Chem.* **2021**, *63*, 351.
- [58] Z.-X. Huang, X.-L. Zhang, X.-X. Zhao, H.-Y. Lü, X.-Y. Zhang, Y.-L. Heng, H. Geng, X.-L. Wu, *J. Mater. Sci. Technol.* **2023**, *160*, 9.
- [59] Y.-F. Zhu, Y. Xiao, S.-X. Dou, Y.-M. Kang, S.-L. Chou, *eScience* **2021**, *1*, 13.
- [60] J. Xiao, X. Li, K. Tang, D. Wang, M. Long, H. Gao, W. Chen, C. Liu, H. Liu, G. Wang, *Mater. Chem. Front.* **2021**, *5*, 3735.
- [61] P. Barpanda, L. Lander, S. Nishimura, A. Yamada, *Adv. Energy Mater.* **2018**, *8*, 1703055.
- [62] Y. Qi, Z. Tong, J. Zhao, L. Ma, T. Wu, H. Liu, C. Yang, J. Lu, Y.-S. Hu, *Joule* **2018**, *2*, 2348.
- [63] Q. Ni, Y. Bai, F. Wu, C. Wu, *Adv. Sci.* **2017**, *4*, 1600275.
- [64] C. Fang, Y. Huang, W. Zhang, J. Han, Z. Deng, Y. Cao, H. Yang, *Adv. Energy Mater.* **2016**, *6*, 1501727.
- [65] W. Luo, M. Allen, V. Raju, X. Ji, *Adv. Energy Mater.* **2014**, *4*, 1400554.
- [66] Q. Liu, Z. Hu, M. Chen, C. Zou, H. Jin, S. Wang, S. L. Chou, Y. Liu, S. X. Dou, *Adv. Funct. Mater.* **2020**, *30*, 1909530.
- [67] E. Goikolea, V. Palomares, S. Wang, I. R. de Larramendi, X. Guo, G. Wang, T. Rojo, *Adv. Energy Mater.* **2020**, *10*, 2002055.
- [68] J.-Y. Hwang, S.-T. Myung, Y.-K. Sun, *Chem. Soc. Rev.* **2017**, *46*, 3529.
- [69] X. Li, D. Wu, Y.-N. Zhou, L. Liu, X.-Q. Yang, G. Ceder, *Electrochem. Commun.* **2014**, *49*, 51.
- [70] I. Hasa, D. Buchholz, S. Passerini, B. Scrosati, J. Hassoun, *Adv. Energy Mater.* **2014**, *4*, 1400083.
- [71] R. Qiao, K. Dai, J. Mao, T.-C. Weng, D. Sokaras, D. Nordlund, X. Song, V. S. Battaglia, Z. Hussain, G. Liu, *Nano Energy* **2015**, *16*, 186.
- [72] K. Dai, J. Mao, X. Song, V. Battaglia, G. Liu, *J. Power Sources* **2015**, *285*, 161.
- [73] H. Kim, H. Kim, Z. Ding, M. H. Lee, K. Lim, G. Yoon, K. Kang, *Adv. Energy Mater.* **2016**, *6*, 1600943.
- [74] J. Deng, W. B. Luo, S. L. Chou, H. K. Liu, S. X. Dou, *Adv. Energy Mater.* **2018**, *8*, 1701428.
- [75] F. Sen, H. Göksu, *Materials Research Foundations* **2020**, *76*, 183.
- [76] Y. Xie, E. Gabriel, L. Fan, I. Hwang, X. Li, H. Zhu, Y. Ren, C. Sun, J. Pipkin, M. Dustin, *Chem. Mater.* **2021**, *33*, 4445.
- [77] P. F. Wang, Y. You, Y. X. Yin, Y. S. Wang, L. J. Wan, L. Gu, Y. G. Guo, *Angew. Chem.* **2016**, *128*, 7571.
- [78] H.-R. Yao, P.-F. Wang, Y. Wang, X. Yu, Y.-X. Yin, Y.-G. Guo, *Adv. Energy Mater.* **2017**, *7*, 1700189. doi: 10.1002/aenm.201700189.
- [79] A. Mendiboure, C. Delmas, P. Hagenmuller, *J. Solid State Chem.* **1985**, *57*, 323.
- [80] C. Delmas, J.-J. Braconnier, C. Fouassier, P. Hagenmuller, *Solid State Ionics* **1981**, *3*, 165.
- [81] S. Kikkawa, S. Miyazaki, M. Koizumi, *J. Power Sources* **1985**, *14*, 231.
- [82] L. Shacklette, T. Jow, L. Townsend, *J. Electrochem. Soc.* **1988**, *135*, 2669.
- [83] Y. Takeda, K. Nakahara, M. Nishijima, N. Imanishi, O. Yamamoto, M. Takano, R. Kanno, *Mater. Res. Bull.* **1994**, *29*, 659.
- [84] C. Didier, M. Guignard, C. Denage, O. Szajwaj, S. Ito, I. Saadoune, J. Darriet, C. Delmas, *Electrochim. Solid-State Lett.* **2011**, *14*, A75.
- [85] M. Jia, Y. Qiao, X. Li, K. Jiang, H. Zhou, *J. Mater. Chem. A* **2019**, *7*, 20405.
- [86] D. Wu, X. Li, B. Xu, N. Twu, L. Liu, G. Ceder, *Energy Environ. Sci.* **2015**, *8*, 195.
- [87] Y. Ono, Y. Yui, M. Hayashi, K. Asakura, H. Kitabayashi, K. I. Takahashi, *ECS Trans.* **2014**, *58*, 33.
- [88] C. Zhang, R. Gao, L. Zheng, Y. Hao, X. Liu, *ACS Appl. Mater. Interfaces* **2018**, *10*, 10819.
- [89] C. Delmas, D. Carlier, M. Guignard, *Adv. Energy Mater.* **2021**, *11*, 2001201.

- [90] X. Gao, F. Jiang, Y. Yang, Y. Zhang, G. Zou, H. Hou, Y. Hu, W. Sun, X. Ji, *ACS Appl. Mater. Interfaces* **2019**, *12*, 2432.
- [91] C. Delmas, C. Fouassier, P. Hagenmuller, *Physica B+C* **1980**, *99*, 81.
- [92] K. Jiang, X. Zhang, H. Li, X. Zhang, P. He, S. Guo, H. Zhou, *ACS Appl. Mater. Interfaces* **2019**, *11*, 14848.
- [93] S. Birgisson, T. L. Christiansen, B. B. Iversen, *Chem. Mater.* **2018**, *30*, 6636. doi: 10.1021/acs.chemmater.8b01566.
- [94] Q.-C. Wang, J.-K. Meng, X.-Y. Yue, Q.-Q. Qiu, Y. Song, X.-J. Wu, Z.-W. Fu, Y.-Y. Xia, Z. Shadike, J. Wu, *J. Am. Chem. Soc.* **2018**, *141*, 840.
- [95] Y. Xiao, Y. F. Zhu, H. R. Yao, P. F. Wang, X. D. Zhang, H. Li, X. Yang, L. Gu, Y. C. Li, T. Wang, *Adv. Energy Mater.* **2019**, *9*, 1803978.
- [96] C. Fouassier, C. Delmas, P. Hagenmuller, *Mater. Res. Bull.* **1975**, *10*, 443.
- [97] M. Keller, D. Buchholz, S. Passerini, *Adv. Energy Mater.* **2016**, *6*, 1501555.
- [98] Y. Fang, X. Y. Yu, X. W. Lou, *Angew. Chem. Int. Ed.* **2017**, *56*, 5801.
- [99] P. Zhou, Z. Che, F. Ma, J. Zhang, J. Weng, X. Wu, Z. Miao, H. Lin, J. Zhou, S. Zhuo, *Chem. Eng. J.* **2021**, *420*, 127667.
- [100] J. Zhang, W. Wang, W. Wang, S. Wang, B. Li, *ACS Appl. Mater. Interfaces* **2019**, *11*, 22051.
- [101] W. Xu, G. Zou, H. Hou, X. Ji, *Small* **2019**, *15*, 1804908.
- [102] P. K. Nayak, E. M. Erickson, F. Schipper, T. R. Penki, N. Munichandraiah, P. Adelhelm, H. Sclar, F. Amalraj, B. Markovsky, D. Aurbach, *Adv. Energy Mater.* **2018**, *8*, 1702397.
- [103] Y.-K. Sun, *ACS Energy Lett.* **2020**, *5*, 1278.
- [104] S.-M. Oh, S.-T. Myung, J.-Y. Hwang, B. Scrosati, K. Amine, Y.-K. Sun, *Chem. Mater.* **2014**, *26*, 6165.
- [105] J. Liu, W. H. Kan, C. D. Ling, *J. Power Sources* **2021**, *481*, 229139.
- [106] R.-M. Gao, Z.-J. Zheng, P.-F. Wang, C.-Y. Wang, H. Ye, F.-F. Cao, *Energy Storage Mater.* **2020**, *30*, 9.
- [107] L. Mu, S. Xu, Y. Li, Y. S. Hu, H. Li, L. Chen, X. Huang, *Adv. Mater.* **2015**, *27*, 6928.
- [108] S. Guo, H. Yu, P. Liu, Y. Ren, T. Zhang, M. Chen, M. Ishida, H. Zhou, *Energy Environ. Sci.* **2015**, *8*, 1237.
- [109] C.-Y. Yu, J.-S. Park, H.-G. Jung, K.-Y. Chung, D. Aurbach, Y.-K. Sun, S.-T. Myung, *Energy Environ. Sci.* **2015**, *8*, 2019.
- [110] B. M. De Boisse, J.-H. Cheng, D. Carlier, M. Guignard, C.-J. Pan, S. Bordere, D. Filimonov, C. Drathen, E. Suard, B.-J. Hwang, *J. Mater. Chem. A* **2015**, *3*, 10976.
- [111] P. F. Wang, H. R. Yao, X. Y. Liu, J. N. Zhang, L. Gu, X. Q. Yu, Y. X. Yin, Y. G. Guo, *Adv. Mater.* **2017**, *29*, 1700210.
- [112] X. G. Yuan, Y. J. Guo, L. Gan, X. A. Yang, W. H. He, X. S. Zhang, Y. X. Yin, S. Xin, H. R. Yao, Z. Huang, *Adv. Funct. Mater.* **2022**, *32*, 2111466.
- [113] T. Risthaus, L. Chen, J. Wang, J. Li, D. Zhou, L. Zhang, D. Ning, X. Cao, X. Zhang, G. Schumacher, *Chem. Mater.* **2019**, *31*, 5376.
- [114] P. F. Wang, Y. You, Y. X. Yin, Y. G. Guo, *Adv. Energy Mater.* **2018**, *8*, 1701912.
- [115] T.-Y. Yu, Y.-K. Sun, *J. Electrochem. Soc.* **2021**, *6*, 361.
- [116] Y.-J. Guo, P.-F. Wang, Y.-B. Niu, X.-D. Zhang, Q. Li, X. Yu, M. Fan, W.-P. Chen, Y. Yu, X. Liu, *Nat. Commun.* **2021**, *12*, 5267.
- [117] D. D. Yuan, Y. X. Wang, Y. L. Cao, X. P. Ai, H. X. Yang, *ACS Appl. Mater. Interfaces* **2015**, *7*, 8585.
- [118] Y. Fan, W. Zhang, Y. Zhao, Z. Guo, Q. Cai, *Energy Storage Mater.* **2021**, *40*, 51.
- [119] C. Zhao, F. Ding, Y. Lu, L. Chen, Y. S. Hu, *Angew. Chem. Int. Ed.* **2020**, *59*, 264.
- [120] J. Braconnier, C. Delmas, P. Hagenmuller, *Mater. Res. Bull.* **1982**, *17*, 993.
- [121] S. Komaba, C. Takei, T. Nakayama, A. Ogata, N. Yabuuchi, *Electrochim. Commun.* **2010**, *12*, 355.
- [122] X. Xia, J. Dahn, *Electrochim. Solid-State Lett.* **2011**, *15*, A1.
- [123] K. Kubota, I. Ikeuchi, T. Nakayama, C. Takei, N. Yabuuchi, H. Shiiba, M. Nakayama, S. Komaba, *J. Phys. Chem. C* **2015**, *119*, 166.
- [124] J.-J. Ding, Y.-N. Zhou, Q. Sun, Z.-W. Fu, *Electrochim. Commun.* **2012**, *22*, 85.
- [125] S.-H. Bo, X. Li, A. J. Toumar, G. Ceder, *Chem. Mater.* **2016**, *28*, 1419.
- [126] F. Geng, Q. Yang, C. Li, B. Hu, C. Zhao, M. Shen, B. Hu, *J. Phys. Chem. Lett.* **2021**, *12*, 781.
- [127] M. Cao, T. Wang, Z. Shadike, K. Nam, Y. Zhou, Z. Fu, *J. Electrochim. Soc.* **2018**, *165*, A565. doi: 10.1149/2.0631803jes.
- [128] M.-H. Cao, Y. Wang, Z. Shadike, J.-L. Yue, E. Hu, S.-M. Bak, Y.-N. Zhou, X.-Q. Yang, Z.-W. Fu, *J. Mater. Chem. A* **2017**, *5*, 5442.
- [129] Y. Cao, M. Xiao, X. Sun, W. Dong, F. Huang, *Chem. Eur. J.* **2023**, *29*, e202202997.
- [130] J.-P. Parant, R. Olazcuaga, M. Devalette, C. Fouassier, P. Hagenmuller, *J. Solid State Chem.* **1971**, *3*, 1.
- [131] Y. Shao-Horn, S. Hackney, A. Armstrong, P. Bruce, R. Gitzendanner, C. Johnson, M. Thackeray, *J. Electrochim. Soc.* **1999**, *146*, 2404.
- [132] X. Ma, H. Chen, G. Ceder, *J. Electrochim. Soc.* **2011**, *158*, A1307.
- [133] A. R. Armstrong, N. Dupre, A. J. Paterson, C. P. Grey, P. G. Bruce, *Chem. Mater.* **2004**, *16*, 3106.
- [134] J. Reed, G. Ceder, A. Van Der Ven, *Electrochim. Solid-State Lett.* **2001**, *4*, A78.
- [135] J. Reed, G. Ceder, *Chem. Rev.* **2004**, *104*, 4513.
- [136] E. J. Wu, P. D. Tepesch, G. Ceder, *Philos. Mag. B* **1998**, *77*, 1039.
- [137] T. Hewston, B. Chamberland, *J. Phys. Chem. Solids* **1987**, *48*, 97.
- [138] X. Chen, Y. Wang, K. Wiaderek, X. Sang, O. Borkiewicz, K. Chapman, J. LeBeau, J. Lynn, X. Li, *Adv. Funct. Mater.* **2018**, *28*, 1805105.
- [139] J. Billaud, R. J. Clément, A. R. Armstrong, J. Canales-Vázquez, P. Rozier, C. P. Grey, P. G. Bruce, *J. Am. Chem. Soc.* **2014**, *136*, 17243.
- [140] T. Ohzuku, A. Ueda, *Solid State Ionics* **1994**, *69*, 201.
- [141] Y. Li, Y. Gao, X. Wang, X. Shen, Q. Kong, R. Yu, G. Lu, Z. Wang, L. Chen, *Nano Energy* **2018**, *47*, 519.
- [142] P. Barpanda, *Chem. Mater.* **2016**, *28*, 1006.
- [143] J. Xu, Z. Han, K. Jiang, P. Bai, Y. Liang, X. Zhang, P. Wang, S. Guo, H. Zhou, *Small* **2020**, *16*, 1904388.
- [144] Y. Kawabe, N. Yabuuchi, M. Kajiyama, N. Fukuhara, T. Inamasu, R. Okuyama, I. Nakai, S. Komaba, *Electrochemistry* **2012**, *80*, 80.
- [145] S. Komaba, T. Mikumo, A. Ogata, *Electrochim. Commun.* **2008**, *10*, 1276.
- [146] K. Kubota, T. Asari, H. Yoshida, N. Yaabuuchi, H. Shiiba, M. Nakayama, S. Komaba, *Adv. Funct. Mater.* **2016**, *26*, 6047.
- [147] N. Yabuuchi, K. Kubota, M. Dahbi, S. Komaba, *Chem. Rev.* **2014**, *114*, 11636.
- [148] N. Yabuuchi, S. Komaba, *Sci. Technol. Adv. Mater.* **2014**, *15*, 043501.
- [149] E. Lee, D. E. Brown, E. E. Alp, Y. Ren, J. Lu, J.-J. Woo, C. S. Johnson, *Chem. Mater.* **2015**, *27*, 6755.
- [150] N. Yabuuchi, H. Yoshida, S. Komaba, *Electrochemistry* **2012**, *80*, 716.
- [151] B. Silvan, E. Gonzalo, L. Djuandhi, N. Sharma, F. Fauth, D. Saurel, *J. Mater. Chem. A* **2018**, *6*, 15132.
- [152] J.-J. Braconnier, C. Delmas, C. Fouassier, P. Hagenmuller, *Mater. Res. Bull.* **1980**, *15*, 1797.
- [153] J. L. Kaufman, A. Van der Ven, *Phys. Rev. Mater.* **2019**, *3*, 015402.
- [154] M. H. Han, E. Gonzalo, M. Casas-Cabanas, T. Rojo, *J. Power Sources* **2014**, *258*, 266.
- [155] P. Vassilaras, X. Ma, X. Li, G. Ceder, *J. Electrochim. Soc.* **2012**, *160*, A207.
- [156] P. Zhou, X. Liu, J. Weng, L. Wang, X. Wu, Z. Miao, J. Zhao, J. Zhou, S. Zhuo, *J. Mater. Chem. A* **2019**, *7*, 657.
- [157] L. Wang, J. Wang, X. Zhang, Y. Ren, P. Zuo, G. Yin, J. Wang, *Nano Energy* **2017**, *34*, 215.
- [158] Y. Lyu, Y. Liu, Z.-E. Yu, N. Su, Y. Liu, W. Li, Q. Li, B. Guo, B. Liu, *Sustainable MaterTechnol.* **2019**, *21*, e00098.
- [159] P. Vassilaras, D.-H. Kwon, S. T. Dacek, T. Shi, D.-H. Seo, G. Ceder, J. C. Kim, *J. Mater. Chem. A* **2017**, *5*, 4596.
- [160] X. Wang, G. Liu, T. Iwao, M. Okubo, A. Yamada, *J. Phys. Chem. C* **2014**, *118*, 2970.
- [161] A. J. Toumar, S. P. Ong, W. D. Richards, S. Dacek, G. Ceder, *Phys. Rev. Appl.* **2015**, *4*, 064002.
- [162] C. Delmas, M. Menetrier, L. Croguennec, I. Saadoune, A. Rougier, C. Pouillerie, G. Prado, M. Grüne, L. Fournes, *Electrochim. Acta* **1999**, *45*, 243.
- [163] B. Hwang, Y. Tsai, D. Carlier, G. Ceder, *Chem. Mater.* **2003**, *15*, 3676.
- [164] I. Saadoune, A. Maazaz, M. Menetrier, C. Delmas, *J. Solid State Chem.* **1996**, *122*, 111.
- [165] J. Thorne, S. Chowdhury, R. Dunlap, M. Obrovac, *J. Electrochim. Soc.* **2014**, *161*, A1801.
- [166] H. Yu, S. Guo, Y. Zhu, M. Ishida, H. Zhou, *Chem. Commun.* **2014**, *50*, 457.
- [167] T. Hwang, J.-H. Lee, S. H. Choi, R.-G. Oh, D. Kim, M. Cho, W. Cho, M.-S. Park, *ACS Appl. Mater. Interfaces* **2019**, *11*, 30894.
- [168] J. Wang, X. He, D. Zhou, F. Schappacher, X. Zhang, H. Liu, M. C. Stan, X. Cao, R. Kloepsch, *J. Mater. Chem. A* **2016**, *4*, 3431.
- [169] S. Maletti, A. Sarapulova, A. Schökel, D. Mikhailova, *ACS Appl. Mater. Interfaces* **2019**, *11*, 33923.
- [170] P. Vassilaras, A. J. Toumar, G. Ceder, *Electrochim. Commun.* **2014**, *38*, 79.
- [171] H. Yoshida, N. Yabuuchi, S. Komaba, *Electrochim. Commun.* **2013**, *34*, 60.
- [172] J.-L. Yue, Y.-N. Zhou, X. Yu, S.-M. Bak, X.-Q. Yang, Z.-W. Fu, *J. Mater. Chem. A* **2015**, *3*, 23261.

- [173] Q. Deng, F. Zheng, W. Zhong, Q. Pan, Y. Liu, Y. Li, Y. Li, J. Hu, C. Yang, M. Liu, *Chem. Eng. J.* **2021**, *404*, 126446.
- [174] V. K. Kumar, S. Ghosh, S. Biswas, S. K. Martha, *J. Electrochem. Soc.* **2020**, *167*, 080531.
- [175] V. K. Kumar, S. Ghosh, S. Ghosh, P. S. Behera, S. Biswas, S. K. Martha, *J. Alloys Compd.* **2022**, *924*, 166444.
- [176] I. Hasa, S. Passerini, J. Hassoun, *J. Mater. Chem. A* **2017**, *5*, 4467.
- [177] W.-L. Pang, X.-H. Zhang, J.-Z. Guo, J.-Y. Li, X. Yan, B.-H. Hou, H.-Y. Guan, X.-L. Wu, *J. Power Sources* **2017**, *356*, 80.
- [178] E. Zhecheva, R. Stoyanova, *Solid State Ionics* **1993**, *66*, 143.
- [179] T. Ohzuku, A. Ueda, M. Kouguchi, *J. Electrochem. Soc.* **1995**, *142*, 4033.
- [180] H. Arai, S. Okada, Y. Sakurai, J. Yamaki, *J. Electrochem. Soc.* **1997**, *144*, 3117.
- [181] G. Wang, S. Zhong, D. Bradhurst, S. Dou, H. Liu, *Solid State Ionics* **1999**, *116*, 271.
- [182] M. Sathiya, K. Hemalatha, K. Ramesha, J.-M. Tarascon, A. Prakash, *Chem. Mater.* **2012**, *24*, 1846.
- [183] L. Zheng, R. Fielden, J. C. Bennett, M. Obrovac, *J. Power Sources* **2019**, *433*, 226698.
- [184] A. Yamada, K. Miura, K. Hinokuma, M. Tanaka, *J. Electrochem. Soc.* **1995**, *142*, 2149.
- [185] P. Strobel, F. Le Cras, L. Seguin, M. Anne, J. Tarascon, *J. Solid State Chem.* **1998**, *135*, 132.
- [186] E. Gonzalo, M. Han, J. L. Del Amo, B. Acebedo, M. Casas-Cabanas, T. Rojo, *J. Mater. Chem. A* **2014**, *2*, 18523.
- [187] S.-Y. Xu, X.-Y. Wu, Y.-M. Li, Y.-S. Hu, L.-Q. Chen, *Chin Phys B* **2014**, *23*, 118202.
- [188] J. Zhao, L. Mu, Y. Qi, Y.-S. Hu, H. Liu, S. Dai, *Chem. Commun.* **2015**, *51*, 7160.
- [189] P. Liu, Y. Li, Y.-S. Hu, H. Li, L. Chen, X. Huang, *J. Mater. Chem. A* **2016**, *4*, 13046.
- [190] J. L. Wang, L. R. Wu, H. X. Zhang, H. R. Wang, D. Zhang, X. C. Duan, *Chemistry – A European Journal* **2023**, *29*, e202301014.
- [191] L. Zhang, T. Yuan, L. Soule, H. Sun, Y. Pang, J. Yang, S. Zheng, *ACS Appl. Energ. Mater.* **2020**, *3*, 3770.
- [192] R. Li, Y. Liu, Z. Wang, J. Li, *Electrochim. Acta* **2019**, *318*, 14.
- [193] M. Sathiya, J. Thomas, D. Batuk, V. Pimenta, R. Gopalan, J.-M. Tarascon, *Chem. Mater.* **2017**, *29*, 5948.
- [194] M. Leng, J. Bi, Z. Xing, W. Wang, X. Gao, J. Wang, Z. Qian, *Chem. Eng. J.* **2021**, *413*, 127824.
- [195] Y. Fan, E. Olsson, G. Liang, Z. Wang, A. M. D'Angelo, B. Johannessen, L. Thomsen, B. Cowie, J. Li, F. Zhang, *Angew. Chem.* **2023**, *135*, e202213806.
- [196] Y. Wang, R. Xiao, Y.-S. Hu, M. Avdeev, L. Chen, *Nat. Commun.* **2015**, *6*, 6954.
- [197] S. Komaba, N. Yabuuchi, T. Nakayama, A. Ogata, T. Ishikawa, I. Nakai, *Inorg. Chem.* **2012**, *51*, 6211.
- [198] R. Fielden, M. Obrovac, *J. Electrochem. Soc.* **2015**, *162*, A453.
- [199] P.-F. Wang, Y. You, Y.-X. Yin, Y.-G. Guo, *J. Mater. Chem. A* **2016**, *4*, 17660.
- [200] N. Yabuuchi, M. Yano, H. Yoshida, S. Kuze, S. Komaba, *J. Electrochem. Soc.* **2013**, *160*, A3131.
- [201] Y. Gao, J. Dahn, *J. Electrochem. Soc.* **1996**, *143*, 100.
- [202] J.-S. Kim, C. S. Johnson, J. T. Vaughey, M. M. Thackeray, S. A. Hackney, W. Yoon, C. P. Grey, *Chem Mater.* **2004**, *16*, 1996.
- [203] N. Yabuuchi, K. Yoshii, S.-T. Myung, I. Nakai, S. Komaba, *J. Am. Chem. Soc.* **2011**, *133*, 4404.
- [204] N. Yabuuchi, T. Ohzuku, *J. Power Sources* **2003**, *119*, 171.
- [205] C. Ruhatiya, S. Singh, A. Goyal, X. Niu, T. N. Hanh Nguyen, V. H. Nguyen, V. M. Tran, M. L. Phung LE, A. Garg, L. Gao, *J. Electrochem. Energy Convers. Storage.* **2020**, *17*, 011009.
- [206] J.-Y. Hwang, C. S. Yoon, I. Belharouak, Y.-K. Sun, *J. Mater. Chem. A* **2016**, *4*, 17952.
- [207] H.-J. Noh, S. Youn, C. S. Yoon, Y.-K. Sun, *J. Power Sources* **2013**, *233*, 121.
- [208] Y.-K. Sun, Z. Chen, H.-J. Noh, D.-J. Lee, H.-G. Jung, Y. Ren, S. Wang, C. S. Yoon, S.-T. Myung, K. Amine, *Nat. Mater.* **2012**, *11*, 942.
- [209] D. Kim, E. Lee, M. Slater, W. Lu, S. Rood, C. S. Johnson, *Electrochem. Commun.* **2012**, *18*, 66.
- [210] S.-M. Oh, S.-T. Myung, C. S. Yoon, J. Lu, J. Hassoun, B. Scrosati, K. Amine, Y.-K. Sun, *Nano Lett.* **2014**, *14*, 1620.
- [211] Y. Xie, H. Wang, G. Xu, J. Wang, H. Sheng, Z. Chen, Y. Ren, C. J. Sun, J. Wen, J. Wang, *Adv. Energy Mater.* **2016**, *6*, 1601306.
- [212] H. Wang, X.-Z. Liao, Y. Yang, X. Yan, Y.-S. He, Z.-F. Ma, *J. Electrochem. Soc.* **2016**, *163*, A565.
- [213] F. Ding, C. Zhao, D. Zhou, Q. Meng, D. Xiao, Q. Zhang, Y. Niu, Y. Li, X. Rong, Y. Lu, *Energy Storage Mater.* **2020**, *30*, 420.
- [214] M. Li, X. Qiu, Y. Yin, T. Wei, Z. Dai, *J. Alloys Compd.* **2023**, *969*, 172406.
- [215] L. Tan, Q. Wu, Z. Liu, Q. Chen, H. Yi, Z. Zhao, L. Song, S. Zhong, X. Wu, L. Li, *J. Colloid Interface Sci.* **2022**, *622*, 1037.
- [216] S. Kumakura, Y. Tahara, S. Sato, K. Kubota, S. Komaba, *Chem. Mater.* **2017**, *29*, 8958.
- [217] S. Wang, C. Sun, N. Wang, Q. Zhang, *J. Mater. Chem. A* **2019**, *7*, 10138.
- [218] H.-R. Yao, P.-F. Wang, Y. Gong, J. Zhang, X. Yu, L. Gu, C. OuYang, Y.-X. Yin, E. Hu, X.-Q. Yang, *J. Am. Chem. Soc.* **2017**, *139*, 8440.
- [219] Q. Wang, S. Mariyappan, J. Vergnet, A. M. Abakumov, G. Rousse, F. Rabuel, M. Chakir, J. M. Tarascon, *Adv. Energy Mater.* **2019**, *9*, 1901785.
- [220] K. Kubota, N. Fujitani, Y. Yoda, K. Kuroki, Y. Tokita, S. Komaba, *J. Mater. Chem. A* **2021**, *9*, 12830.
- [221] S. Zhao, Q. Shi, W. Feng, Y. Liu, X. Yang, X. Zou, X. Lu, Y. Zhao, *Chin. Chem. Lett.* **2023**, *35*, 108606.
- [222] J.-Y. Hwang, T.-Y. Yu, Y.-K. Sun, *J. Mater. Chem. A* **2018**, *6*, 16854.
- [223] Y. Zhang, S. Kim, G. Feng, Y. Wang, L. Liu, G. Ceder, X. Li, *J. Electrochem. Soc.* **2018**, *165*, A1184.
- [224] J. Wang, Z. Zhou, Y. Li, M. Li, F. Wang, Q. Yao, Z. Wang, H. Zhou, J. Deng, *J. Alloys Compd.* **2019**, *792*, 1054.
- [225] M. D. Radin, A. Van der Ven, *Chem. Mater.* **2016**, *28*, 7898.
- [226] S. Mariyappan, T. Marchandier, F. Rabuel, A. Iadecola, G. Rousse, A. V. Morozov, A. M. Abakumov, J.-M. Tarascon, *Chem. Mater.* **2020**, *32*, 1657.
- [227] E. Lee, J. Lu, Y. Ren, X. Luo, X. Zhang, J. Wen, D. Miller, A. DeWahl, S. Hackney, B. Key, *Adv. Energy Mater.* **2014**, *4*, 1400458.
- [228] J. Xu, H. Liu, Y. S. Meng, *Electrochim. Commun.* **2015**, *60*, 13.
- [229] H. Liu, J. Xu, C. Ma, Y. S. Meng, *Chem. Commun.* **2015**, *51*, 4693.
- [230] J.-M. Tarascon, M. Armand, *Nature* **2001**, *414*, 359.
- [231] J. B. Goodenough, Y. Kim, *Chem. Mater.* **2010**, *22*, 587.
- [232] B. L. Ellis, K. T. Lee, L. F. Nazar, *Chem. Mater.* **2010**, *22*, 691.
- [233] S. Zheng, G. Zhong, M. J. McDonald, Z. Gong, R. Liu, W. Wen, C. Yang, Y. Yang, *J. Mater. Chem. A* **2016**, *4*, 9054.
- [234] Y. Ma, Y. Ma, Q. Wang, S. Schweidler, M. Botros, T. Fu, H. Hahn, T. Brezesinski, B. Breitung, *Energy Environ. Sci.* **2021**, *14*, 2883.
- [235] A. Sarkar, L. Velasco, D. Wang, Q. Wang, G. Talasila, L. de Biasi, C. Kübel, T. Brezesinski, S. S. Bhattacharya, H. Hahn, *Nat. Commun.* **2018**, *9*, 3400.
- [236] N. Qiu, H. Chen, Z. Yang, S. Sun, Y. Wang, Y. Cui, *J. Alloys Compd.* **2019**, *777*, 767.
- [237] A. Salian, S. Mandal, *Crit. Rev. Solid State Mater. Sci.* **2022**, *47*, 142.
- [238] C. M. Rost, E. Sachet, T. Borman, A. Moballegh, E. C. Dickey, D. Hou, J. L. Jones, S. Curtarolo, J.-P. Maria, *Nat. Commun.* **2015**, *6*, 8485.
- [239] J.-W. Yeh, S.-J. Lin, *J. Mater. Res.* **2018**, *33*, 3129.
- [240] J. Gild, Y. Zhang, T. Harrington, S. Jiang, T. Hu, M. C. Quinn, W. M. Mellor, N. Zhou, K. Vecchio, J. Luo, *Sci. Rep.* **2016**, *6*, 1.
- [241] H. Guo, M. Avdeev, K. Sun, X. Ma, H. Wang, Y. Hu, D. Chen, *Chem. Eng. J.* **2021**, *412*, 128704.
- [242] A. Tripathi, A. Rudola, S. R. Gajjela, S. Xi, P. Balaya, *J. Mater. Chem. A* **2019**, *7*, 25944.
- [243] S. Mariyappan, Q. Wang, J. M. Tarascon, *J. Electrochem. Soc.* **2018**, *165*, A3714.
- [244] Z. Liang, M. Ren, Y. Guo, T. Zhang, X. Gao, H. Ma, F. Li, *Inorg. Chem. Front.* **2023**, *10*, 7187.
- [245] C. Ma, X.-L. Li, X.-Y. Yue, J. Bao, R.-J. Luo, Y.-N. Zhou, *Chem. Eng. J.* **2022**, *432*, 134305.
- [246] H. R. Yao, P. F. Wang, Y. Wang, X. Yu, Y. X. Yin, Y. G. Guo, *Adv. Energy Mater.* **2017**, *7*, 1700189.
- [247] Y. You, S. Xin, H. Y. Asl, W. Li, P.-F. Wang, Y.-G. Guo, A. Manthiram, *Chem.* **2018**, *4*, 2124.
- [248] M. Sathiya, Q. Jacquet, M. L. Doublet, O. M. Karakulina, J. Hadermann, J. Tarascon, *Adv. Energy Mater.* **2018**, *8*, 1702599.
- [249] Y. Li, Z. Yang, S. Xu, L. Mu, L. Gu, Y. S. Hu, H. Li, L. Chen, *Adv. Sci.* **2015**, *2*, 1500031.
- [250] W. Kang, Z. Zhang, P.-K. Lee, T.-W. Ng, W. Li, Y. Tang, W. Zhang, C.-S. Lee, D. Y. W. Yu, *J. Mater. Chem. A* **2015**, *3*, 22846.
- [251] J. Molenda, A. Milewska, W. Zająć, K. Walczak, M. Wolczko, A. Komenda, J. Tobola, *J. Mater. Chem. A* **2023**, *11*, 4248.
- [252] T. Yuan, S. Li, Y. Sun, J.-H. Wang, A.-J. Chen, Q. Zheng, Y. Zhang, L. Chen, G. Nam, H. Che, *ACS Nano* **2022**, *16*, 18058.
- [253] X. Rong, E. Hu, Y. Lu, F. Meng, C. Zhao, X. Wang, Q. Zhang, X. Yu, L. Gu, Y.-S. Hu, *Joule* **2019**, *3*, 503.
- [254] Z.-Y. Li, R. Gao, J. Zhang, X. Zhang, Z. Hu, X. Liu, *J. Mater. Chem. A* **2016**, *4*, 3453.

- [255] X. Bai, M. Sathiya, B. Mendoza-Sánchez, A. Iadecola, J. Vergnet, R. Dedryvère, M. Saubanère, A. M. Abakumov, P. Rozier, J. M. Tarascon, *Adv. Energy Mater.* **2018**, *8*, 1802379.
- [256] D. Yuan, X. Liang, L. Wu, Y. Cao, X. Ai, J. Feng, H. Yang, *Adv. Mater.* **2014**, *26*, 6301.
- [257] T.-R. Chen, T. Sheng, Z.-G. Wu, J.-T. Li, E.-H. Wang, C.-J. Wu, H.-T. Li, X.-D. Guo, B.-H. Zhong, L. Huang, *ACS Appl. Mater. Interfaces* **2018**, *10*, 10147.
- [258] M. Kouthaman, K. Kannan, R. Subadevi, M. Sivakumar, *Journal of the Taiwan Institute of Chemical Engineers* **2022**, *140*, 104565.
- [259] Y.-M. Zheng, X.-B. Huang, X.-M. Meng, S.-D. Xu, L. Chen, S.-B. Liu, D. Zhang, *ACS Appl. Mater. Interfaces* **2021**, *13*, 45528.
- [260] K. Mukai, Y. Kishida, H. Nozaki, K. Dohmae, *Chem. Mater.* **2013**, *25*, 2828.
- [261] S. Xu, H. Chen, C. Li, R. Nie, Y. Yang, M. Zhou, X. Zhang, H. Zhou, *J. Alloys Compd.* **2023**, *962*, 171199.
- [262] X. Meng, D. Zhang, Z. Zhao, Y. Li, S. Xu, L. Chen, X. Wang, S. Liu, Y. Wu, *J. Alloys Compd.* **2021**, *887*, 161366.
- [263] W. Qin, Y. Liu, J. Liu, Z. Yang, Q. Liu, *Electrochim. Acta* **2022**, *418*, 140357.
- [264] K. Zhang, D. Kim, Z. Hu, M. Park, G. Noh, Y. Yang, J. Zhang, V. W.-H Lau, S.-L. Chou, M. Cho, *Nat. Commun.* **2019**, *10*, 5203.
- [265] L. P. Wang, L. Yu, X. Wang, M. Srinivasan, Z. J. Xu, *J. Mater. Chem. A* **2015**, *3*, 9353.
- [266] E. Gabriel, D. Hou, E. Lee, H. Xiong, *Energy Sci Eng.* **2022**, *10*, 1672.
- [267] D. Fei-Xiang, R. Xiao-Hui, W. Hai-Bo, Y. Yang, H. Zi-Lin, D. Rong-Bin, L. Ya-Xiang, H. Yong-Sheng, *ACTA PHYSICA SINICA* **2022**, *71*, 108801.
- [268] C. Zhao, Q. Wang, Z. Yao, J. Wang, B. Sánchez-Lengeling, F. Ding, X. Qi, Y. Lu, X. Bai, B. Li, *Science* **2020**, *370*, 708.

---

Manuscript received: February 20, 2024

Accepted manuscript online: February 22, 2024

Version of record online: March 19, 2024

---